AD-A059 016 BOEING AEROSPACE CO SEATTLE WA NAVY SYSTEMS AND ADVA--ETC F/G 14/2
FEASIBILITY DEMONSTRATION OF FIBER OPTIC DIGITAL STATUS MONITOR--ETC(U)
MAR 78 G E MILLER, T A LINDSAY N00019-77-C-0039

UNCLASSIFIED D296-10048-1 NL

1 OF 2
AD
A059016

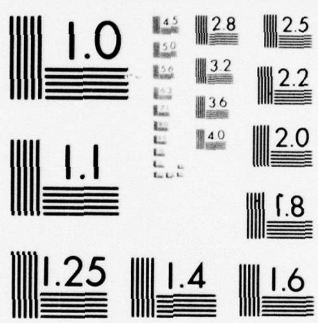

MICROCOPY RESOLUTION TEST CHART
NATIONAL BUREAU OF STANDARDS-1963-A

AD A059016

DDC FILE COPY

LEVEL II

FEASIBILITY DEMONSTRATION OF FIBER-OPTIC DIGITAL STATUS MONITORING DEVICES

FINAL REPORT

D296-10048-1

Approved for public release; distribution unlimited.

The work described in this report was performed under contract N00019-77-C-0039 for the Naval Air Systems Command, Washington, D.C. The program manager for this effort was Mr. A. Glista of Code Air-52022.

Publication of this report does not constitute approval by the Naval Air System Command of the findings or conclusions herein. It is published for the exchange and stimulation of ideas.

BOEING AEROSPACE COMPANY
Naval Systems and Advanced Projects Division
Seattle, Washington 98124

UNCLASSIFIED

SECURITY CLASSIFICATION OF THIS PAGE (When Data Entered)

REPORT DOCUMENTATION PAGE

READ INSTRUCTIONS BEFORE COMPLETING FORM

1. REPORT NUMBER

2. GOVT ACCESSION NO.

9

3. RECIPIENT'S CATALOG NUMBER

4. TITLE (and Subtitle)

6 FEASIBILITY DEMONSTRATION OF FIBER OPTIC DIGITAL STATUS MONITORING DEVICES.

5. TYPE OF REPORT & PERIOD COVERED

FINAL ENGINEERING rept.

JAN [redacted]77 [redacted]-MAR [redacted]78

14

6. PERFORMING ORG. REPORT NUMBER

D296-10048-1

7. AUTHOR(s)

10 GLEN E. MILLER
THOMAS A. LINDSAY

15

8. CONTRACT OR GRANT NUMBER(s)

N00019-77-C-0039 new

9. PERFORMING ORGANIZATION NAME AND ADDRESS

BOEING AEROSPACE COM~~PANY~~
NAVY SYSTEMS AND ADVANCED PROJECTS DIVI~~SION~~
P. O. BOX 3999, SEATTLE, WA 98124

10. PROGRAM ELEMENT, PROJECT, TASK AREA & WORK UNIT NUMBERS

62762N

17 WF54582603

11. CONTROLLING OFFICE NAME AND ADDRESS

NAVAL AIR SYSTEMS COMMAND
CODE AIR 52022
WASHINGTON, D.C. 20361 16 F54582

12. REPORT DATE

11 MAR [redacted]78 12 137p.

13. NUMBER OF PAGES

121

14. MONITORING AGENCY NAME & ADDRESS (if different from Controlling Office)

15. SECURITY CLASS. (of this report)

UNCLASSIFIED

15a. DECLASSIFICATION/DOWNGRADING SCHEDULE

N/A

16. DISTRIBUTION STATEMENT (of this Report)

Approved for public release; distribution unlimited.

17. DISTRIBUTION STATEMENT (of the abstract entered in Block 20, if different from Report)

18. SUPPLEMENTARY NOTES

NONE

19. KEY WORDS (Continue on reverse side if necessary and identify by block number)

FIBER OPTICS	SENSOR	FUEL LEVEL SENSOR
DIGITAL STATUS MONITOR	STRAIN	TEMPERATURE
MEASUREMENT	DISPLACEMENT	
TRANSDUCER	FLOW RATE	
PRESSURE	EVENT COUNTER	

20. ABSTRACT (Continue on reverse side if necessary and identify by block number)

This report covers the development and testing of feasibility models of a family of inherently digital fiber optic status-monitoring sensors which sense liquid level, linear displacement, fluid flow rate, strain, pressure and temperature as well as count physical events. In all cases, the sensors are electrically passive. All excitation is in the form of optical power supplied via fiber optics. All response signals are in the form of optical power transmitted via fiber optics. All response signals are inherently

DD FORM 1 JAN 73 1473 EDITION OF 1 NOV 65 IS OBSOLETE

UNCLASSIFIED

SECURITY CLASSIFICATION OF THIS PAGE (When Data Entered)

410 379 78 09 06 024

20. ABSTRACT (Continued)

digital, i.e. they do not employ analog/digital conversion. Design considerations, performance data and recommendations for further investigation are included.

Optical fibers, because of their very small geometry, offer a whole new approach to the precise sensing of small changes in various physical parameters. Sensors employing fiber optics enjoy the many inherent advantages of fiber optics, which include interference immunity, resistance to environmental conditions, small physical size and light weight. Digital fiber optic sensors are a natural adjunct to digital data systems for the above reasons and because no analog/digital conversion is required.

Distribution List

Office of the Undersecretary of Defense
Research and Engineering
Electronics and Physical Sciences
Pentagon, Room 3D 1079
Washington, DC 20301
Attn: L. Weisberg (1)
T. Walsh (1)
E. Myers (1)

Advisory Group on Electron Devices
201 Varick St.
New York, NY 10014

Air Force Office of Scientific Research
Dept. of the Air Force
Washington, DC 20333

Naval Electronic System Command
Washington, DC 20361
Attn: Code 304

Naval Sea Systems Command
Washington, DC 20560
Attn: SEA 0341

Naval Material Command
Washington, DC 20360
Attn: MAT 08E4 (1)
MAT 08T243
MAT 04T1

Naval Air Development Center
Warminster, PA 18974
Attn: Mr. Leon Smith

Naval Air Systems Command
Washington, DC 20361
Attn: AIR-360A
AIR-310B
AIR-340D
AIR-533
AIR-5204
AIR-52025C

Defense Documentation Center for
Scientific and Technical Information
Cameron Station, Bldg No. 5
Alexandria, VA 22314

Naval Ocean Systems Center
San Diego, CA 92152
Attn: R. Lubduska
W. Tinston
T. Meador
D. Williams

Office of Naval Research
800 N. Quincy St.
Arlington, VA 22217
Attn: Dr. J. Dimmock, Code 427

Defense Advanced Research Projects
Agency
1400 Wilson Blvd.
Arlington, VA 22209
Attn: Dr. Harry Windsor

Distribution List (continued)

Valtec Corp.
Electro-Fiberoptics Division
99 Hartwell Street
West Boylston, MA 01583

Ishwar D. Aggarwal
Galileo Electro-Optic Corp.
Sturbridge, MA 01566

G. S. Anderson
Belden Wire
2000 S. Batavia Avenue
Geneva, IL 60134

Rod Anderson
Galileo Electro Optics Corp.
Galileo Park
Sturbridge, MA 01518

Rudolf R. August
Rockwell International
3400 East Anaheim
Anaheim, CA 92803

Franz Auracher
Siemens AG
D8000 Munich
GERMANY

Albert A. Ballman
Bell Telephone Laboratories
Murray Hill, NJ 07974

Michael K. Barnowski
Hughes Research Laboratories
3011 Malibu Canyon Road
Malibu, CA 90265

R. J. Baumbick
Project Manager
NASA-Lewis Research Center
Cleveland, OH 44135

Robert Bellino
Brand Rex Co.
Willimantic, CT 06226

Robert Biard
Spectronics, Inc.
830 E. Arapaho
Richardson, TX 75080

Gary Bickel
ITT EOPD
P. O. Box 7065
Roanoke, VA 25018

Fred A. Blum
Science Center
Rockwell International
Thousand Oaks, CA 91360

Gerard M. Blum
Philips Laboratories
Briarcliff Manor, NY 10510

Gerald B. Brandt
Westinghouse Research
Pittsburgh, PA 15219

Dr. Robert E. Brooks
TRW Systems Group
One Space Park (Bldg. R1)
Redondo Beach, CA 90278

Distribution List (continued)

Dr. Rudolf G. Buser
U.S. Army Electronics Command
Fort Monmouth, NJ 07703

Gary C. Bjorklund
Bell Laboratories
Holmdel, NJ 07733

R. A. Cerny
Valtec Corp.
Electro Fiber Optics Division
99 Hartwell Street
West Boylston, MA 01583

William S. C. Chang
Washington University
St. Louis, MO 63130

Di Chen
Honeywell Research
10701 Lyndale Avenue South
Bloomington, MN 55420

Peter Cheo
United Technologies Research Center
East Hartford, CT 06108

Alfred Y. Cho
Bell Laboratories
Murray Hill, NJ 07974

Roy Clapper
IBM Corporation
Owego, NY 13827

William Coderre
Bell-Northern Research
P. O. Box 3511, Station C
Ottawa, Ontario, CANADA K1Y 4HY

William H. Culver
Optelecom Inc.
2841 Chesapeak St. NW
Washington, DC 20008

Gary D. Cummings
Simmonds Precision
Norwich Oxford Rd.
Norwich, NY 13815

Philip Currier
General Dynamics
P. O. Box 748
Fort Worth, TX 76101

David G. Dalgoutte
Standard Telecommunication Labs.
Harlow
ENGLAND

Philip Dann
Mail Stop 102A366
IBM Corporation
Owego, NY 13827

Robert R. Ferguson
Bell Northern
P. O. Box 3511 Sta C
Ottawa, Ontario, CANADA K1Y4H7

Richard L. Foley
RCA Laboratories
Princeton, NJ 08654

Distribution List (continued)

Louis J. Frisco
Raychem Corp.
300 Constitution Drive
Menlo Park, CA 94025

Robert L. Gallawa
U.S. Department of Commerce
OT/ITS, Boulder Laboratories
Boulder, CO 80302

Thomas G. Giallorenzi
Naval Research Laboratory
Washington, DC 20375

Robert Gill
Laser Diode Labs
205 Forrest St.
Metuchen, NJ 08840

James E. Goell
ITT
Box 7065
Roanoke, VA 25018

Milton Gottlieb
Westinghouse Research Labs
Pittsburgh, PA 15219

Jacob M. Hammer
RCA Laboratories
Princeton, NJ 08654

Dell Hanson
H. P. Corp.
1501 Page Mill Road
Palo Alto, CA 94304

Jay M. Harris
National Science Foundation
1800 G Street, N.W.
Washington, DC 20006

Charles Husbands
Mitre Corp
P. O. Box 208
Bedford, MA 01730

Frank F. Johnson
Vought Corporation Systems Div.
Group 2-51742
P. O. Box 5907
Dallas, TX 75222

Kenneth Kamm
E.I. DuPont de Nemours
Plastic Dept.
1007 Market Street
Wilmington, DE 19898

George Kaposhilin
Hewlett-Packard Company
640 Page Mill Road
Palo Alto, CA 94304

Felix P. Kapron
Bell Northern
P.O. Box 3511 Sta C
Ottawa, Ontario, CANADA K1Y4H7

Rod Katz, D/813
Naval Avionics Facility
6000 E. 21st Street
Indianapolis, IN 46218

Donald B. Keck
Corning Glass Works
Corning, NY 14830

Distribution List (continued)

Jim Kellogg
Dept 11-22, Bldg 152, Plant B-1
Lockheed California Co.
P.O. Box 551
Burbank, CA 91520

H. Kogelnik
Bell Laboratories
Holmdel, NJ 07733

Henry Kressel
RCA Laboratories
Princeton, NJ 08654

John A. Laurent
General Electric Co. (GEOS)
100 Plastics Avenue
Pittsfield, MA 01201

Eric G. Lean
IBM Research
Yorktown Heights, NY 10598

Robert Lebduska, Code 4400
Naval Electronics Laboratory Center
271 Catalina Blvd
San Diego, CA 92152

Dennis Lieurance
General Dynamics/Convair
P. O. Box 80847
San Diego, CA 92199

Roy Love
Corning Glass Works, C-7
Corning, NY 14830

P. B. Macedo
Vitreous State Laboratory
The Catholic University of America
Washington, DC 20017

Gary E. Marx
Westinghouse Electric Corp.
Baltimore, MD 21233

Ivars M Ingailis
MIT Lincoln Laboratory
244 Wood Street
Lexington, MA 02173

F. Ray McDevitt
Harris ESD
P.O. Box 37
Melborne, FL 32901

R. D. McDonald
Canada Wire
240 Hymus Boulevard
Ponte Claire, Quebec
CANADA

Henry T. Minden
Sperry Rand Research Center
Sudbury, MA 01742

Peter G. Mockel
Siemens AG Research Labs
Hofmannstr. 51
München 70,
GERMANY

Ronald L. Ohlhaber
IIT Research Institute
10 West 35th Street
Chicago, IL 60616

Distribution List (continued)

Dan B. Ostrowsky
Thomson CSF
Domaine de Corbeville
Orsay, FRANCE

John M. Pankratz
Texas Instruments
P.O. Box 5936
Dallas, TX 75222

Michael Papuchon
Thomson CSF
Domaine de Corbeville
Orsay 91401
FRANCE

David R. Porter
Boeing
P. O. Box 3707
Seattle, WA 98124

Frederick Scholl
Exxon Enterprises
350 Executive Blvd
Elmsford, NY 10523

Don R. Scieres
Xerox Palo Alto
Palo Alto, CA 94304

Manhar L. Shah
Harris Corporation
Melbourne, FL 32901

M. C. Shoquist
Sperry Univac
Box 3525
St. Paul, MN 55116

Walter P. Siegmund
American Optical Corp.
14 Mechanic Street
Southbridge, MA 01550

Peter W. Smith
Bell Laboratories
Holmdel, NJ 07733

Ron Soloman
McDonnell-Douglas Corp.
P. O. Box 515, Dept 354
Bldg. 33, Post 405
St. Louis, MO 63166

Thomas E. Stockton
Laser Diode Laboratories
205 Forrest Street
Metuchen, NJ 08840

Times Wire & Cable Co.
358 Hall Avenue
Wallingford, CT 06492

Chen S. Tsai
Carnegie-Mellon University
Electrical Engineering Dept.
Pittsburgh, PA 15213

Roger Uhlhorn
McDonnell Aircraft Co.
St. Louis, MO 63166

Shyh Wang
Department of Electrical
Engineering
University of California
Berkeley, CA 94720

Distribution List (continued)

Gus Weinstock
McDonnell Aircraft Company
St. Louis Airport
St. Louis, MO 63166

Amnon Yariv
California Institute of Technology
Electrical Engineering Dept.
Pasadena, CA 91125

Jack A. York
Boeing Commercial Airplane Co.
P. O. Box 3707, Stop 47-18
Seattle, WA 98124

David A. Zann
Air Force Avionics Lab/AAT
Wright-Patterson AFB
Dayton, OH 45433

Charlotte Zelon
Rockwell International
Los Angeles, CA 90052

Frits Zernike
Philips Laboratories
345 Scarsborough Road
Briarcliff Manor, NY 10510

Larry F. Zimmerman
Naval Avionics Center
6000 E. 21st St.
Indianapolis, IN 46218

Peter Zory
IBM Research Center
P.O. Box 218
Yorktown Heights, NY 10598

Foreign Distribution List

Mr. P. Gardner
ASA-7 Room 842
The Adelphi
John Adams St.
London, United Kingdom
WC2-N6BB

Hellermann Deutsch
East Grinstead
Sussex, United Kingdom
RH19 1RW
Attn: S. S. Pearce

Plessey Company Ltd.
South Leigh Park House
East Leigh Road
Havant Hants. PO9 2PE
Attn: J. P. Dakin, United Kingdom

Belling Lee
Great Cambridge Rd.
Endfield Middlesex
EN1 3RY United Kingdom
Attn: Mr. Chris Castro

Philips Research Laboratories
Natuurkundig Laboratorium
Endhoven, The Netherlands
Attn: Mr. J. H. C. van Heuven

Quartz et Silice
54, Avenue Hoche
75365 Paris Cedex 08 FRANCE
Attn: Christian Dambrine

Hallaudse Signaalapparaten B.V.
Hengelo, The Netherlands
P.O. Box 42
Attn: F. Dijkshoorn

Fort Fibores Optiques
Z.I. "La Gaudree"
5 Rue Lambert 91410 Dourdan
FRANCE
Attn: S. Lucas

Marconi Avionics Ltd.
Airport Works
Rochester
Kent Mel 2xx United Kingdom
Attn: R. P. G. Collison

Laboratoires De Marcoussis
Centre De Recherches De La Compagnie
Generale D'Electricite
Route De Nozay
91460 Marcouissis, France
Attn: Jaques Ernest

Thomson - CSF
Laboratoire Central De Recherches
Domaine de Corbeville BP10
91401 Orsay FRANCE
Attn: M. Desomiere

TRT
5, Avenue Riamur
92350 Le Plessis - Robinson - BP21
Attn: Daniel Capoaossi,France

Siemans AG
Zentrale Forschung und Entwicklung
Forschungslaboratorien - Abteilung
Optik
Otto-Hahn-Ring 6 Postfach 832729
D8000 München 83 GERMANY
Attn: Mr. Mettler, Dr. Heywant

Cables Cortaillod
CH 2016 Cortaillod
Switzerland
Attn: Jean Marie Chaveau

JM Decaudin
Direction des Recherches Studes et
Techniques
2639 Victor
45015
Paris, France

THE BOEING COMPANY

TABLE OF CONTENTS

TABLE OF CONTENTS (continued)

LIST OF ILLUSTRATIONS

LIST OF ILLUSTRATIONS (continued)

LIST OF ILLUSTRATIONS (continued)

1.0 INTRODUCTION

Ever since the advent of the digital data system, there has been a need for a family of inherently digital sensors --- as opposed to inherently analog sensors which can interface with a digital data system only through an analog/digital converter. Traditionally, direct digital sensing has been limited largely to sensing of gross events which could be made to actuate switches, alter magnetic circuits or interrupt light beams. A classic example of the latter is the optical shaft position encoder which uses an optically-encoded disc to interrupt light beams which are then sensed usually by phototransistors.

An intermediate form of sensor produces an output frequency which is proportional to the measured parameter and which, by means of a time-gated counter, is converted into a digital output.

Optical fibers, because of their very small geometry, open a whole new avenue to the precise sensing of small changes in various physical parameters. The small geometry permits digital sensing of proportionally small quantum changes without resorting to complex and inconveniently bulky optical systems. Modern fiber optical fibers provide a convenient low-loss means for transmitting excitation to, and respose signals from, remote sensors. The resultant sensors and all associated "wiring" then enjoy the many inherent advantages of fiber optics:

1. EMI immunity
2. EMP immunity
3. Potential resistance to gamma and neutron radiation
4. Potential resistance to high and low temperature
5. Resistance to attack by acids, alkalies, oils, fuels and solvents
6. High reliability
7. Light weight and small size
8. Safety in flammable and explosive atmospheres
9. Eventual low cost

The scope of this research and development effort was to design, develop, fabricate and test feasibility models of a family of fiber optic digital status-monitoring sensors to:

1. Measure liquid fuel level
2. Measure linear displacement
3. Count physical events
4. Measure liquid flow rate
5. Measure strain (or small linear displacement)
6. Measure gas or liquid pressure
7. Measure temperature

In all cases, the status-monitoring sensors are electrically passive. All excitation is in the form of optical power supplied via fiber optics. All response signals are in the form of optical power transmitted via fiber optics. All response signals are inherently digital

The various sensor models were developed in the above order and, in several instances, derived benefit from those which were previously developed and evaluated.

In general, all feasibility-model sensors successfully demonstrated feasibility and, in most cases, clearly identified areas in which possible future effort might most profitably be applied to eventually produce first-generation devices suitable for field-testing and evaluation.

Digital fiber optic sensors are a natural adjunct to digital data systems, and particularly to those digital data systems which employ fiber optic data transmission lines or buses for any one of the several good reasons. It is not difficult to envision an avionic system of the future, in which subsystems might be interconnected by a digital fiber optic data bus, and in which subsystems such as the air data package and the engine data package might employ digital fiber optic sensors exclusively.

2.0 SCANNER/RECEIVER (SR-1100)

2.1 FUNCTION

The SR-1100Scanner/Receiver was designed specifically to function as a complete electrical/optical and optical/electrical interface for the Fuel Level, Linear Displacement, Strain, Temperature, and Pressure Sensors investigated during this study effort. Interfacing is accomplished through two fiber optic connectors, one of which couples a series of eight sequential optical interrogation pulses to a sensor via one bundle of optical fibers, and one of which couples a resultant series of eight sequential optical response pulses from the sensor back to an optical receiver via a second bundle of optical fibers.

The SR-1100provides three means for mointoring the output of a sensor:

1. A front-panel display of eight LED binary indicators.
2. An eight-line parallel NRZ binary output.
3. An eight-bit serial NRZ binary output with a separate line for word sync.

When operating with internal clock, the bit rate is 10KB/S. Provisions are also made for operating with an externally - supplied clock.

It was intended that the SR-1100 might eventually serve as a universal fiber optic interface for a broad family of electrically-passive fiber optically-coupled digital status-monitoring sensors. The universal fiber optical interface greatly simplifies the task of multiplexing a number of sensors into a single integrated data system.

2.2 DESCRIPTION

A simplified functional block diagram of the SR-1100 Scanner/Receiver is shown in Figure 2.2.1.

Basically, the SR-1100 contains the following functional blocks which perform the indicated functions:

Timing Section - Generates an internal 10-KHz clock or accepts an externally supplied clock. The clock drives both the commutator and the decommutator and supplies delayed clocks required by the coherent receiver and decommutator.

Commutator - Commutates the current drive to an array of solid state emitters (in this case, eight) which sequentially excite groups of fibers within a fiber optic bundle to provide excitation to a sensor.

Coherent Receiver - Detects the optical response from each interrogration of the sensor.

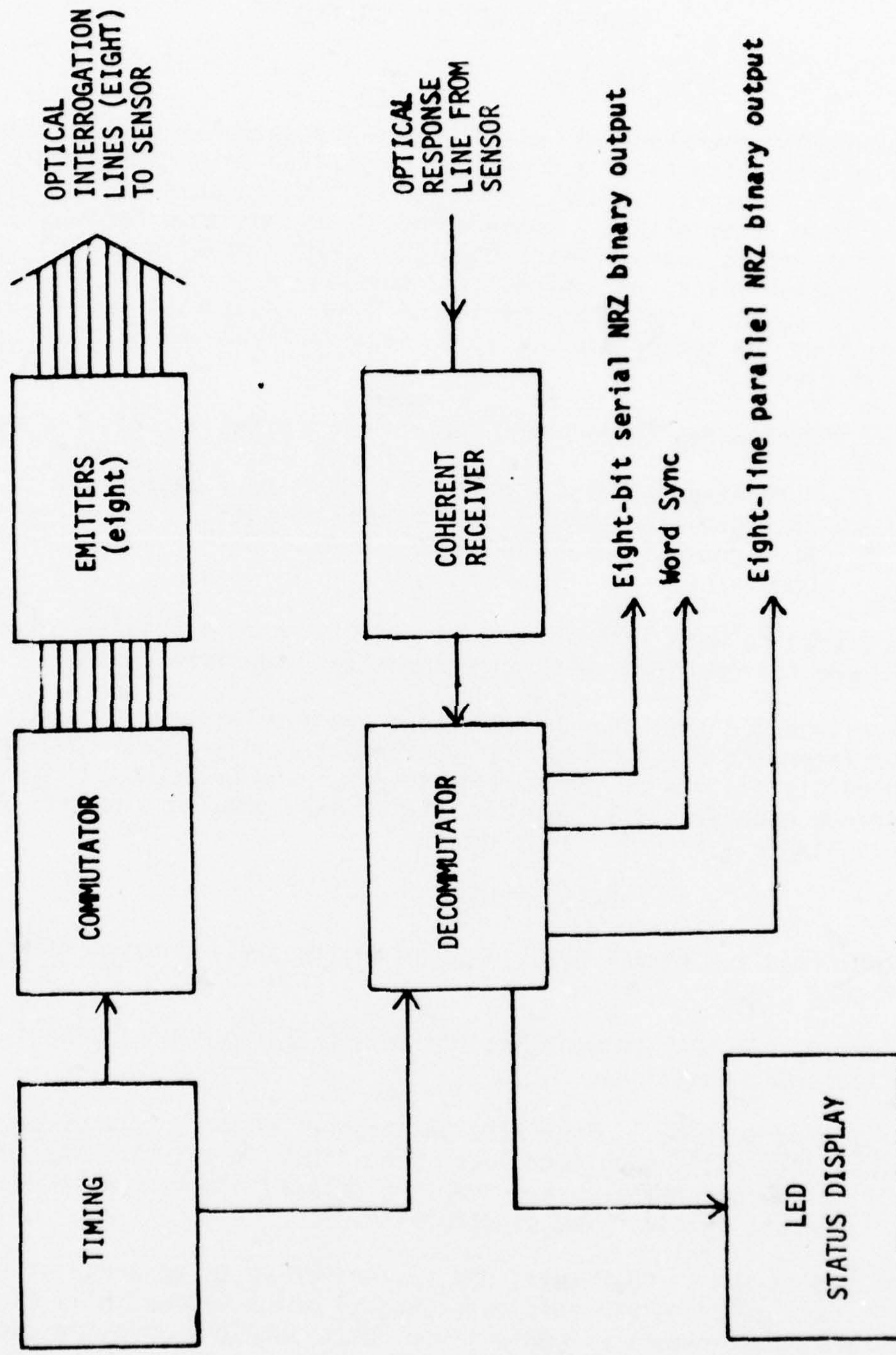

FIGURE 2.2.1
SR-1100 SCANNER/RECEIVER
SIMPLIFIED FUNCTIONAL BLOCK DIAGRAM

Decommutator - Synchronously demultiplexes the responses from the sensor so that each response can be correlated with a specific interrogation.

Status Display - Provides a visual display of those interrogations which result in a correlated response. The display in turn provides a direct digital readout of the parameter being measured by the sensor.

The feasibility model Scanner/Receiver is housed in a package 4.5 x 1.7 x 9 inches. The total power consuption is less than 2 watts. Figures 2.2.2 and 2.2.3 show construction details of the feasibility model.

As an aid to explaining the theory of operation, the following figures are provided:

Figure 2.3.1 Simplified Block Diagram
Figure 2.3.2 Scanner Timing Waveforms
Figure 2.3.3 Receiver Timing Waveforms
Figure 2.3.4 Scanner Electronics, Schematic
Figure 2.3.5 Scanner Electronics, Schematic
Figure 2.3.6 Receiver Electronics, Schematic

2.2.1 SCANNER ELECTRONICS

Timing for both the scanner and the receiver is provided by an internal clock operating at a 10-KHz rate or by an externally-supplied clock. The internal clock (E1) is a CMOS astable multivibrator tuned by an external resistor/capacitor network. The clock waveform is shown in Figure 2.3.2A and 2.3.3E. The clock is isolated by buffer E5-5 and drives an eight-stage counter E4, the eight parallel outputs of which feed current drivers E6, E7, E8, and E9. The current drivers sequentially drive eight Type LED55C emitters at a peak current level of approximately 100 ma. The driver voltage input waveforms are shown in Figure 2.3.2, B_0 through B7. A 25-microsecond pulse, Figure 2.3.2C, derived from one-shot multivibrator E2, inhibits the flow of emitter current for the first 25 microseconds of the commutation period of each emitter. The resultant emitter current waveforms are shown in Figure 2.3.2 D_0 through D_7. The eight emitters provide optical outputs with pulse shape and duration similar to their respective current drive pulses. The LED55C emitters provide optical outputs at a wavelength of approximately 900 nanometers. At a peak drive current of 100 ma, the peak radiant power output is approximately 5 milliwatts. The LED55C is a gallium-arsenide, edge-emitting, spontaneous emitter which has conical reflector to direct the radiant output forward and a lens to collimate the beam.

2.2.2 RECEIVER ELECTRONICS

The receiver incorporates a United Detector Technology Type PIN-6D-PIN photodiode as a detector. This is a silicon device which has a peak spectral response near 900 nanometers, which agrees closely with the peak spectral output of the emitters. The PIN-6D is of planar construction with an active region approximately 0.2 inch in diameter. This detector is operated with a

2.2.2 Continued

reverse bias of 10 volts in the photoconductive mode. The receiver input amplifier E26 is a National Semiconductor Type LH0062 low-noise, high-gain, FET-input operational amplifier configured as a transimpedance amplifier (or current-to-voltage converter.) The transimpedance of the input amplifier is 106 V/A. The second receiver amplifier stage E25 is also a type LH0062 operational amplifier, AC-coupled and configured to provide a voltage gain of ten. These first two amplifier stages are housed separately with the detector to provide system flexibility and to avoid electromagetic pickup from the scanner. This assembly has the following overall characteristics:

Sensitivity	4.2 volts/microwatt
Bandwidth (-3dB)	23.3 KHz
Equivalent optical noise power input	0.5 nanowatt
Average equivalent noise spectral density	3.3 (10^{-12}) W/Hz

The third receiver amplifier state E24 uses a National Semiconductor Type LH0042 FET-input operational amplifier. This stage has a voltage gain adjustable from zero to +34dB. The gain control adjusts the overall receiver gain to accommodate the various transducer types. Keyed clamping is applied to E24 by means of CMOS switch E21-1 as shown by the waveforms of Figure 2.3.3H and I. Clamping occurs during the 25-microsecond emitter "off" periods between interrogation pulses.

E24 of the receiver functions, as shown by Figure 2.3.3J, as an integrate-and-dump synchronous bit detector. E22 is a differential voltage comparator which establishes, for each interrogation, the presence or absence of a response by comparing an adjustable voltage against the integrated response waveform from integrator E23. The action is shown in Figure 2.3.3.

Decommutation of the received response (Figure 2.3.3K) is accomplished by a group of eight type "D" CMOS flip-flops E11 through E15 which are clocked synchronously at a time near the end of the integration period of the response from the corresponding interrogation. The waveforms of Figure 2.3.3 L1 through N3 show the derivation of the parallel NRZ binary outputs for responses 0, 1 and 2. The eight LED indicators which form the visual status display are driven from the parallel binary outputs by saturated switches E27 through E28. The serial NRZ binary output and word sync are buffered by E29 and E30 respectively.

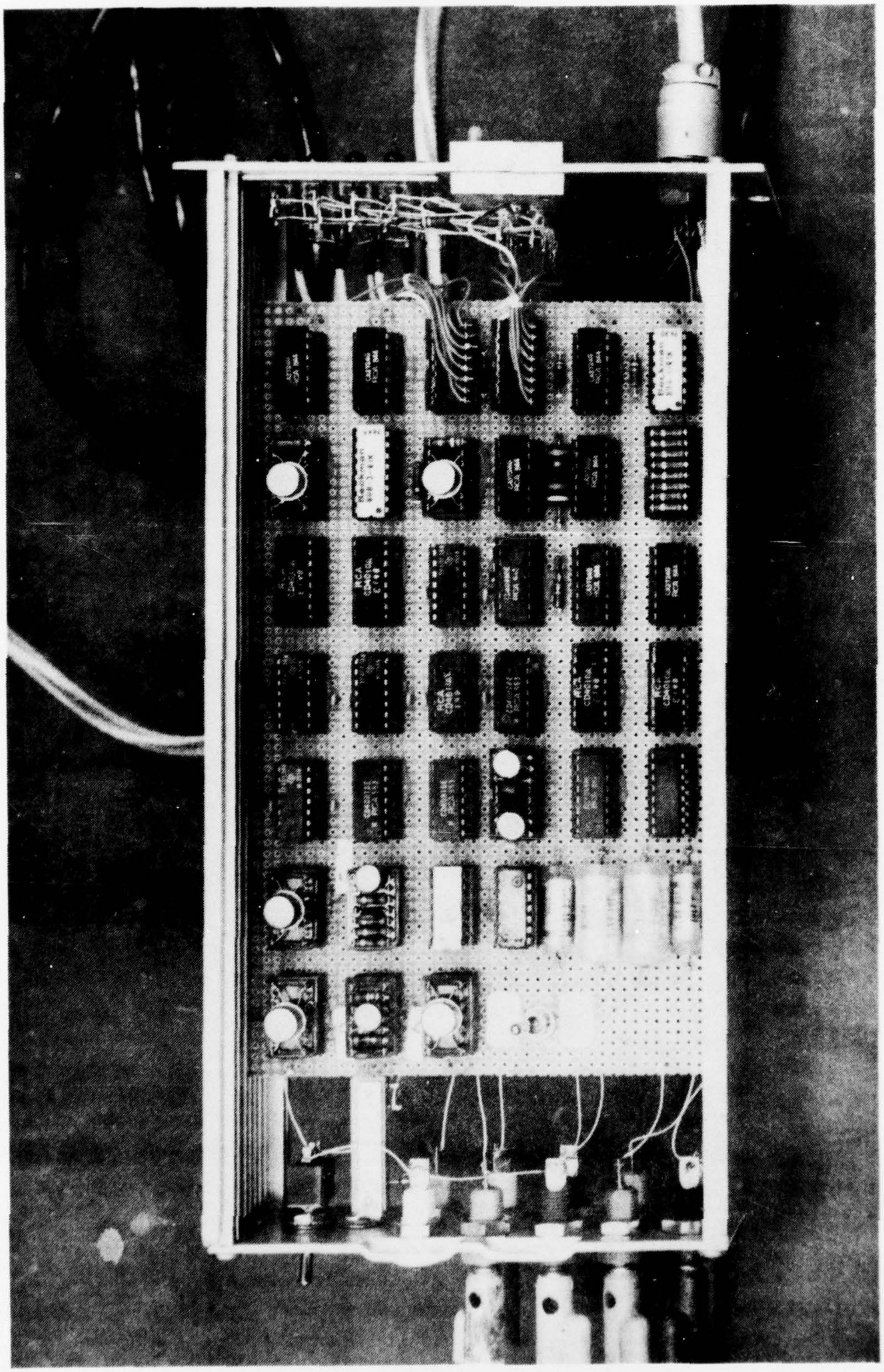

FIGURE 2.2.2
SR-1100 SCANNER/RECEIVER, CIRCUIT BOARD FRONT PLANE

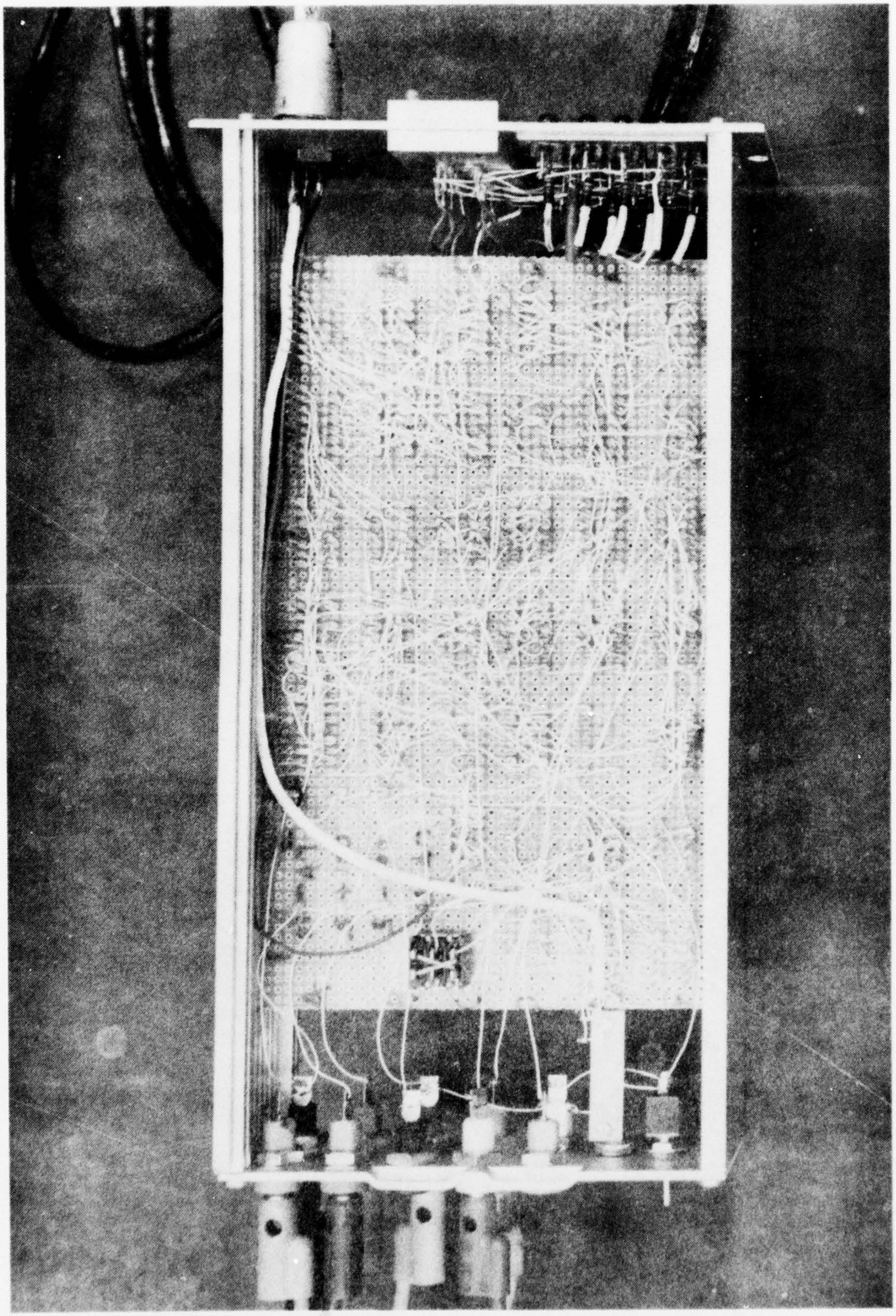

FIGURE 2.2.3
SR-1100 SCANNER/RECEIVER, CIRCUIT BOARD BACK PLANE

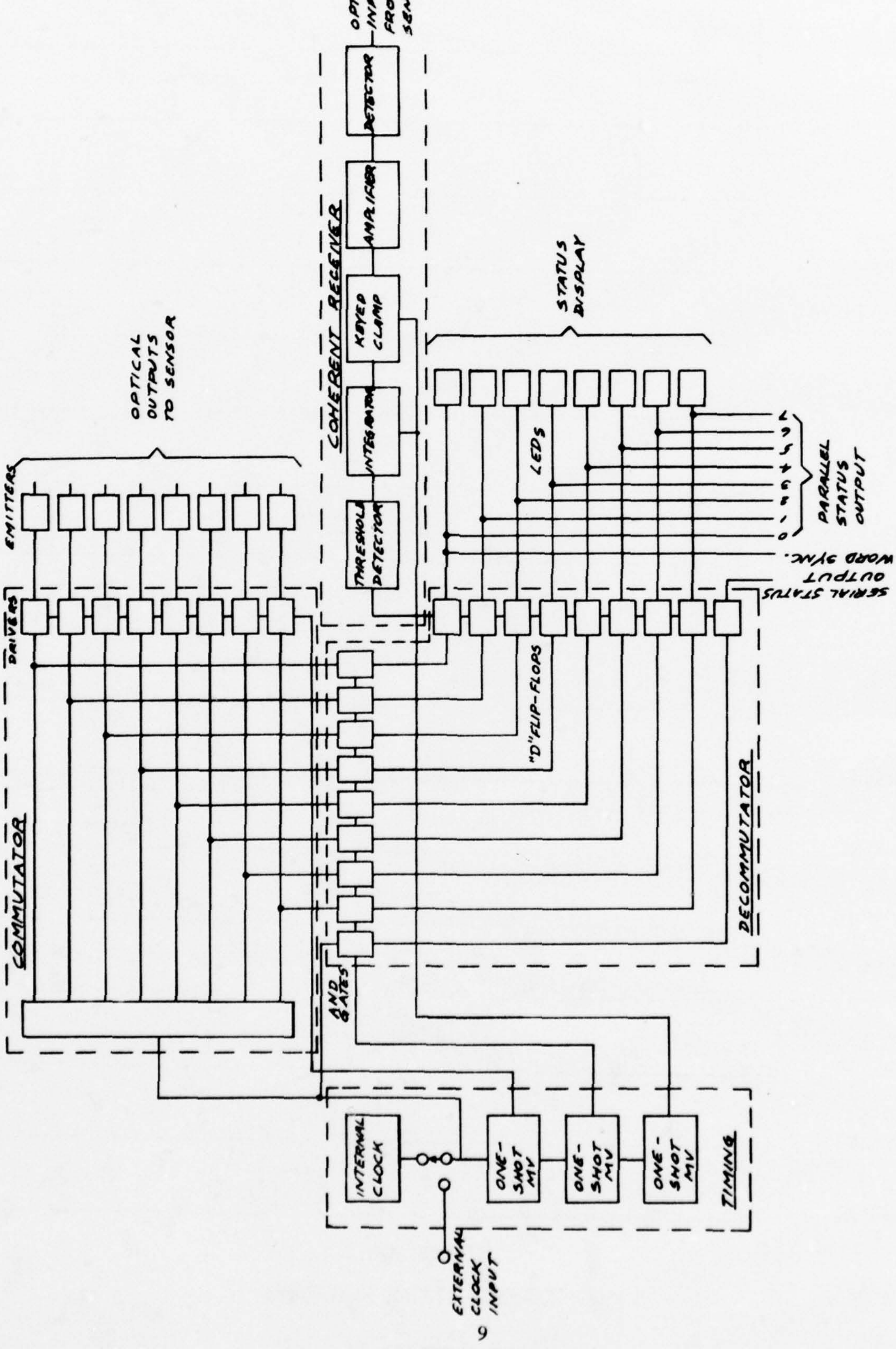

FIGURE 2.3.1
SIMPLIFIED BLOCK DIAGRAM

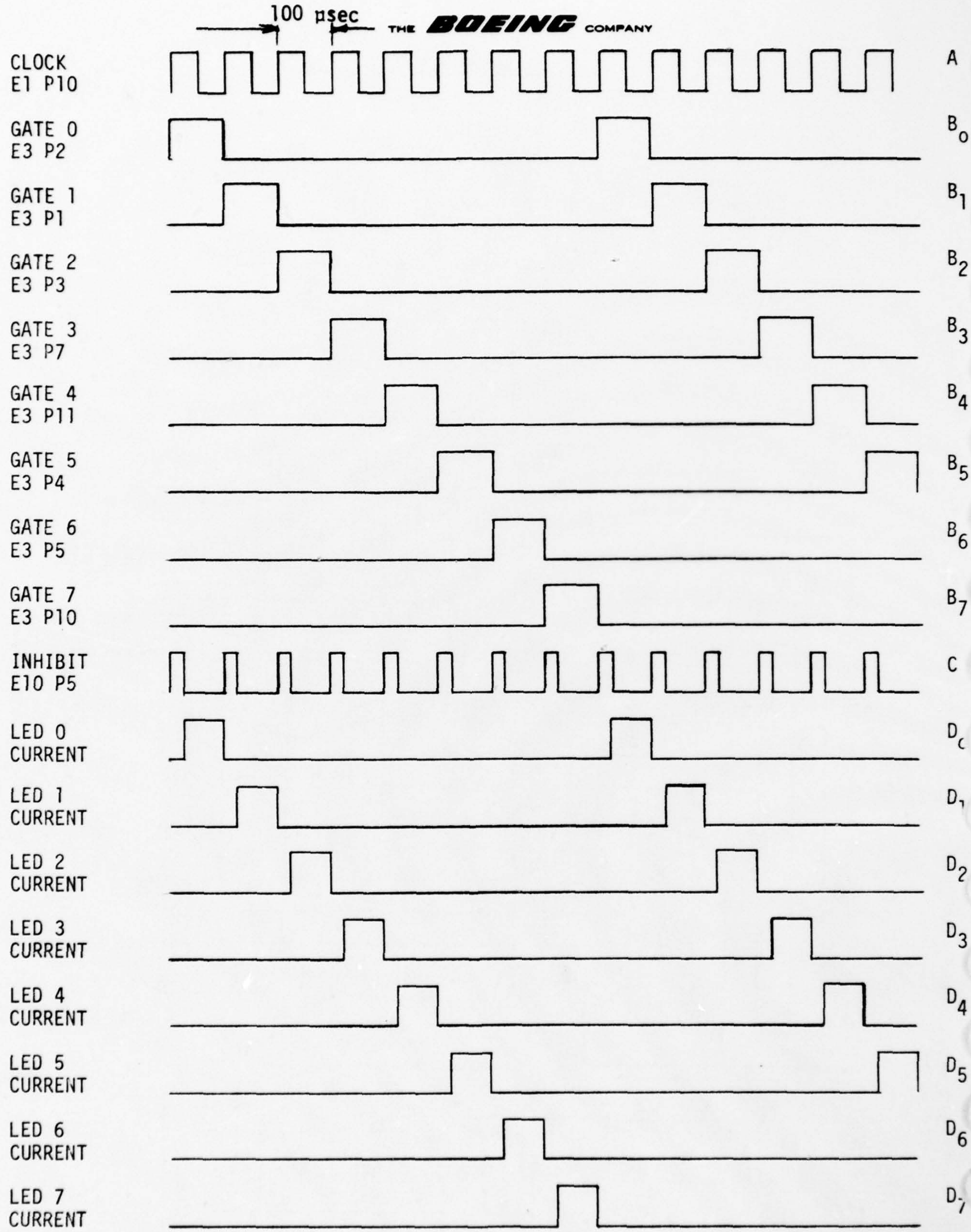

FIGURE 2.3.2

SCANNER TIMING WAVEFORMS

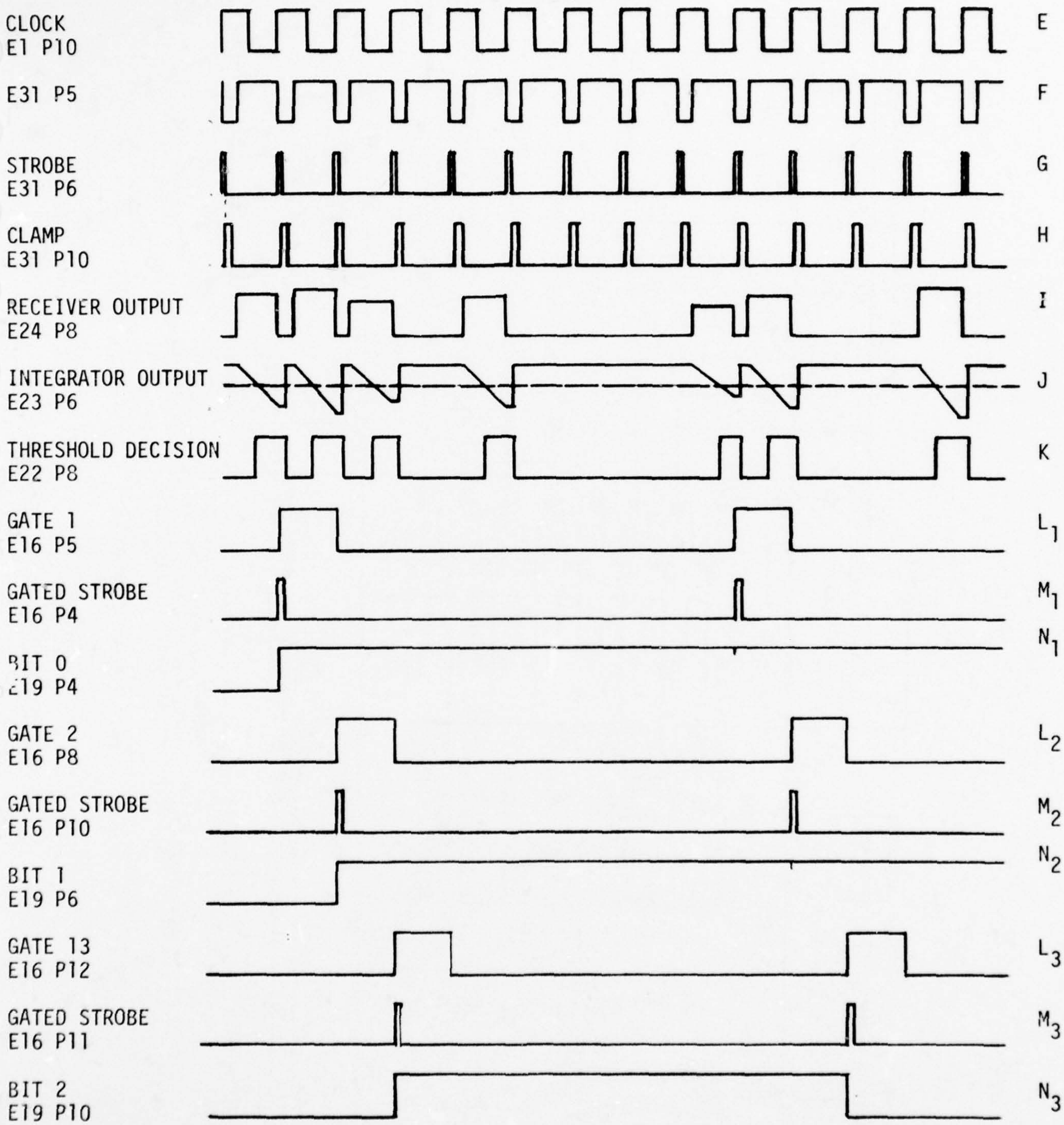

FIGURE 2.3.3

RECEIVER TIMING WAVEFORMS

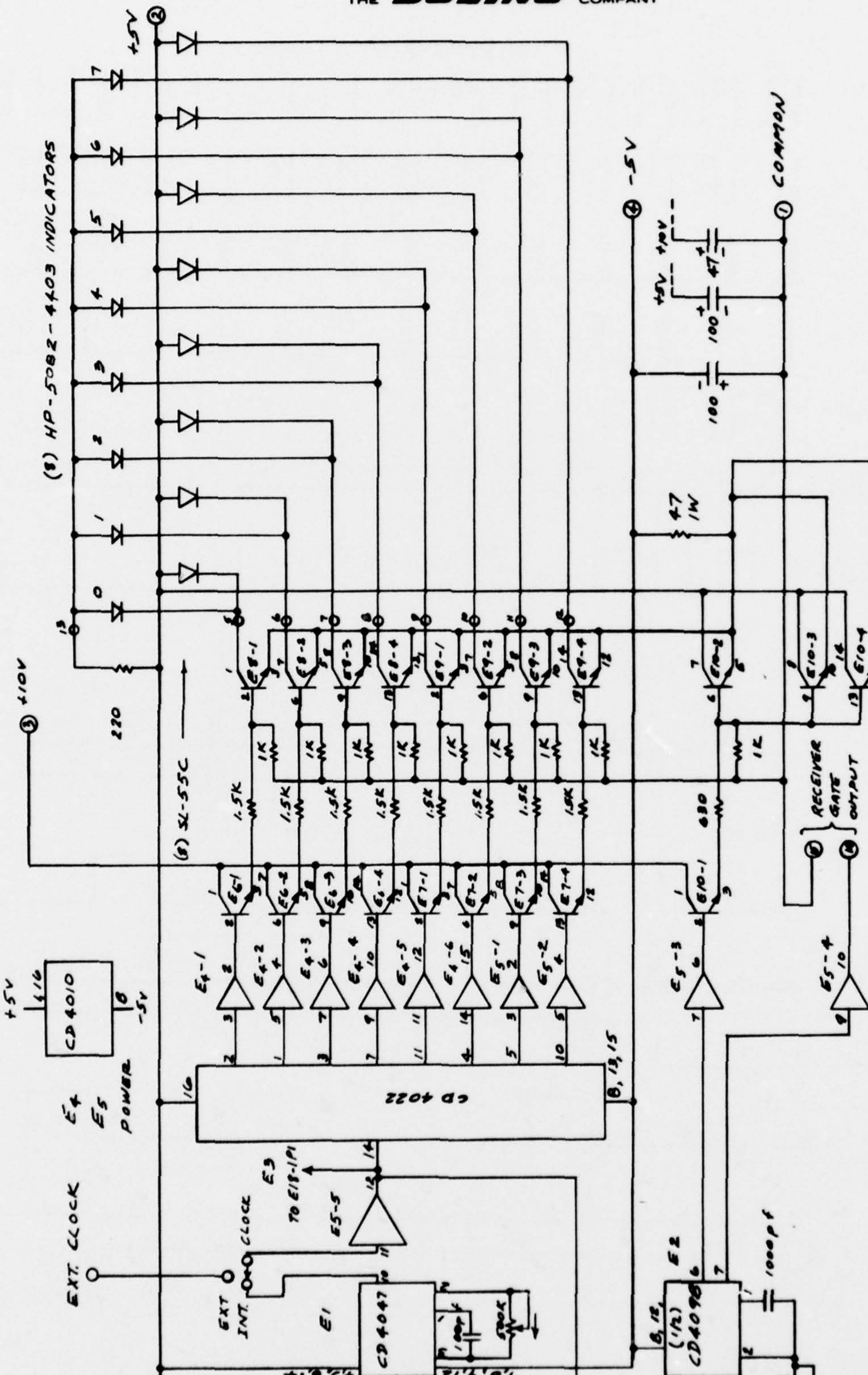

FIGURE 2.3.4
SCANNER ELECTRONICS, SCHEMATIC

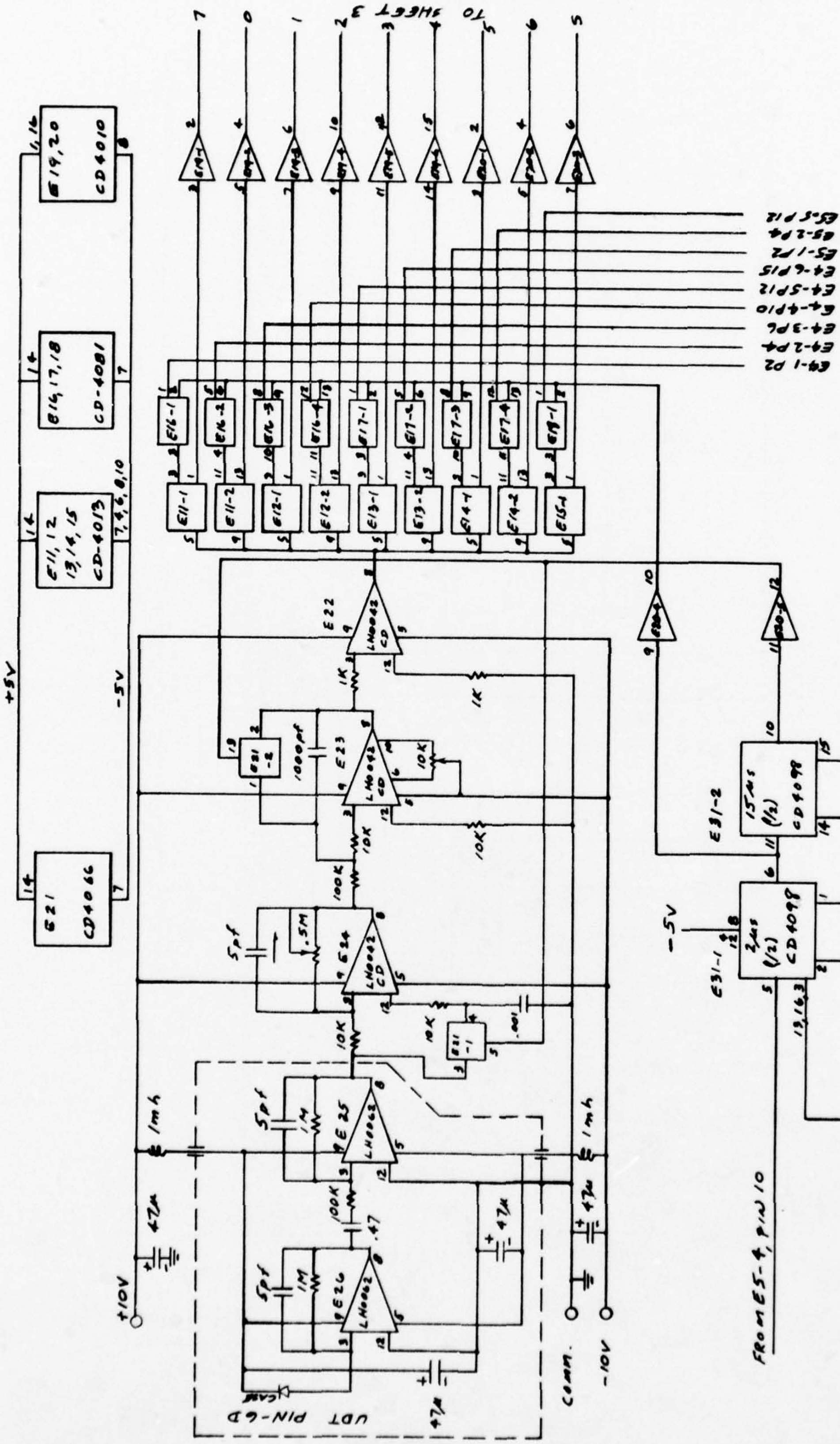

FIGURE 2.3.5

SCANNER ELECTRONICS, SCHEMATIC

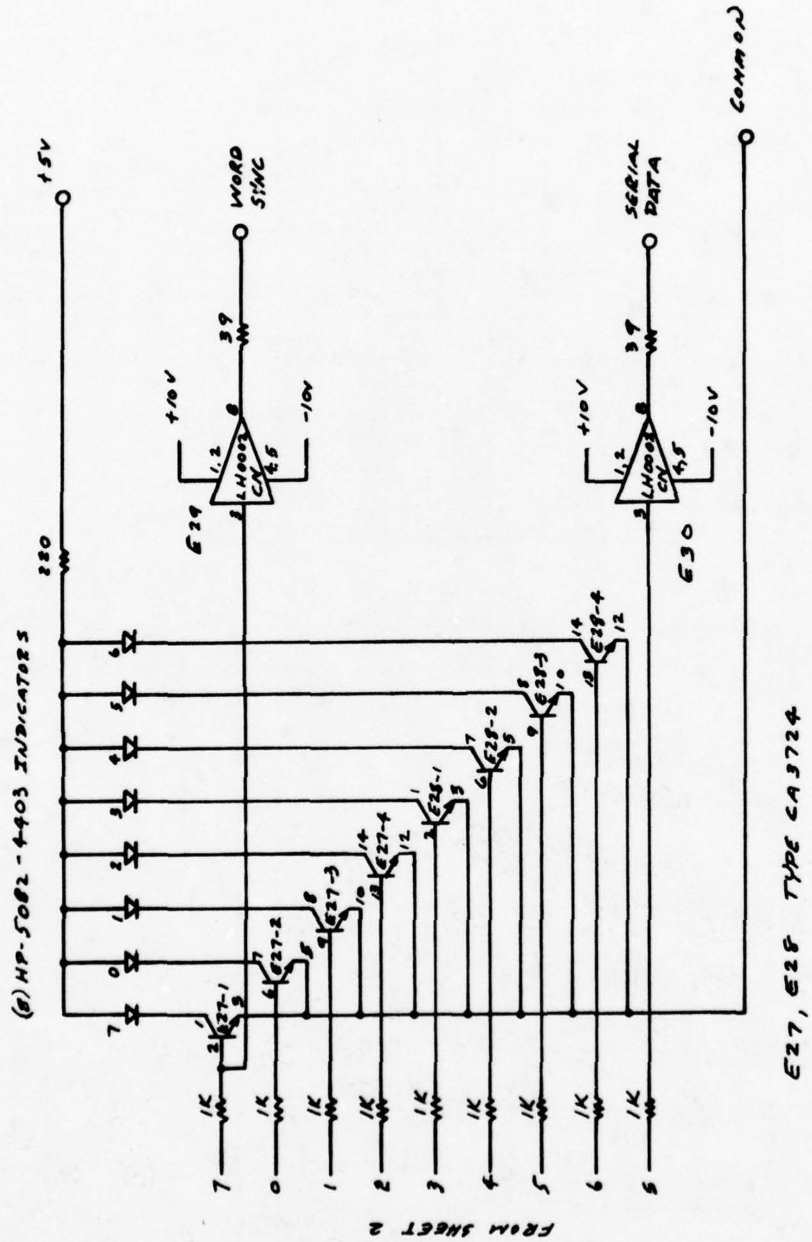

FIGURE 2.3.6

RECEIVER ELECTRONICS, SCHEMATIC

DO 6000 2145 ORIG. 4/71

2.3 DESIGN CONSIDERATIONS

The statement of work for this contract specifies performance goals only for overall status monitors. Since the contract is intended only to demonstrate concept feasibility, the bit rate, fiber optic cable length and bit error rate are also unspecified. The Boeing-established design goals for the Scanner/Receiver were to provide:

1. Large optical apertures at the scanner output and receiver input to eliminate critical fiber alignment problems during the initial development effort.

   In the plane of the fiber optic terminations, the scanner output optical aperture has a diameter of approximately 0.1 inch. The detector aperture has a diameter of approximately 0.2 inch.

2. At least 100 ma peak drive current to the scanner emitters so that the scanner may adapt to a wide variety of emitter types for specific applications.

3. Receiver sensitivity as high as consistent with good stability, high reliability and the use of uncooled components.

4. Sampling rates consistent with the types of sensors specified. The initial design uses a basic sampling rate of 10 Kb/s.

Because suitable commercial fiber optic connectors were not available at the time of this effort, connectors were fabricated for the purpose. The connector for the interrogation cable provides eight ports which are spaced appropriately to permit direct interfacing with a 4 x 2 array of eight emitters in a variety of standard packages. The connector for the response cable is a straight 0.25-inch diameter plug which fits into a collect chuck on the detector assembly. This simple connector adapts readily to bundle diameters from zero to 0.20 inch.

The circuit design uses CMOS logic wherever possible because of the inherent low power consumption, high reliaibility and ease with which larger-scale integration might eventually be considered.

Obviously, the electronics could be made to function as well with eight continuously-excited interrogation sources and eight continuous receivers, or with one continuously-excited interrogation source and eight scanned receivers. The option of eight scanned interrogation sources and one receiver was selected because of minimum overall circuit complexity, greater possible interrogation power output, minimum input power requirement and extended emitter life.

2.4 PERFORMANCE

At a peak drive current of 100 ma, the peak radiant power output of each of the emitters is approximately 5 milliwatts. The emitters were selected to provide power outputs equal within + 5%. Within the 0.1 inch diameter aperture the emitters are capable of coupling approximately 0.6 microwatt of power into a single fiber which has a numerical aperture of 0.5 and a core diameter of 0.003 inch. Power coupled into groups of fibers is greater in essentially direct proportion to the number of fibers within the group. The number of fibers used per group in the various sensors varies from twelve (Strain Sensor) to 212 (Liquid Level Sensor.)

Because the receiver noise originates largely in the amplifier stages, it is reasonable to assume that it has approximately a Gaussian distribution. Because the receiver employs coherent demodulation, it is also reasonable to assume that the bit detection process closely approaches the ideal. To achieve a bit error probability of 10^{-8} with a random bit sequence with an ideal bit detector in the presence of Gaussian-distributed noise requires an electrical peak signal to rms noise ratio of 12.6 dB at the bit detector input. Because of the square-law characteristic of the silicon detector, this translates into a (signal power) to (noise power) ratio of 4.27 or 6.3 dB at the detector input. For the measured equivalent optical noise power input of 0.5 nanowatt, the minimum receiver signal optical power input required for a bit error probability of 10^{-8} should be:

$$\begin{aligned} Pmn &= 4.27\ (0.5) \\ &= 2.14 \text{ nanowatt} \end{aligned}$$

Although the latter figure was not confirmed by actual bit error rate measurement, it was roughly confirmed by visual observation of oscilloscope presentations.

For a scanner peak radiant power output of 5 milliwatts, the maximum total optical path loss for a bit error rate probability of 10^{-8} is:

$$\begin{aligned} Lmax &= \frac{5(10^{-3})}{2.14\ (10^{-9})} \\ &= 2.33\ (10^{6}) \\ &= 63.7 \text{ dB} \end{aligned}$$

It was believed that all feasibility model sensors could be built with losses considerably less than the above maximum loss figure and this belief was confirmed in testing of the models.

At such time that a definite cable configuration is solidified, large improvements in system margin can be readily realized by selection of emitters which provide more efficient coupling. Receiver sensitivity can also be improved measurably by selection of a detector which provides a more nearly optimum match.

2.5 CONCLUSIONS

The concept of the Scanner/Receiver appears to be sound. The use of CMOS logic results in a total power consumption slightly less than 2 watts, which is reasonable considering the many functions being performed. It would appear that all logic functions could easily be combined in a single CMOS MSI package and that the remaining functions could be combined in one or two hybrid packages. The use of LED arrays and, particularly, self-scanning LED arrays should be considered in an eventual design. The incorporation of an automatic threshold detector adjustment and an automatic receiver gain control would probably represent significant improvements if the feasibility model were to be refined for field use.

The present effort addresses only single sensors coupled to single scanner/receivers. A logical extension to the effort might address the optimum architecture of various total digital data systems involving multiple fiber optic sensors. The optimum architecture of such a system might use a separate scanner/receiver for each sensor, for example, or it might take the form of a single scanner/receiver coupled to multiple sensors through star couplers or their equivalent. The optimum architecture might also hinge on whether the eventual scanner/receivers were fabricated from discrete components or were hybridized.

3.0 DISCRETE LIQUID-LEVEL SENSOR TD-1101

3.1 FUNCTION

The TD-1101 Liquid-Level Sensor was designed to demonstrate the feasibility of remote sensing of discrete liquid levels and transmission of this data a considerable distance over fiber optic cable. It was designed to operate with the SR-1100 Scanner/Receiver as the source of optical excitation and as the optical/electrical interface for conversion of the optical responses into an eight-bit binary word representing liquid level.

Because the TD-1101 is electrically-passive, and because only low-level optical excitation is used, it is particularly useful for measurement of levels of inflammable and explosive liquids such as fuels. Although designed for use with fuels such as JP4, it functions satisfactorily with nearly all common liquids provided that they have a refractive index significantly greater than unity. (See Section 3.3)

3.2 DESCRIPTION

The TD-1101 senses eight discrete levels within a range of 16 cm. It interfaces with the SR-1100 Scanner/Receiver through two fiber optic cables which terminate in fiber optic connectors; one cable transmits optical excitation from the SR-1100 to the transducer, the other cable transmits the responses back to the SR-1100.

The photograph of Figure 3.2.1 shows the TD-1101 (with slosh baffle in place), the SR-1100 and the associated fiber optic cables.

Figure 3.2.2 shows the TD-1101 (with slosh baffle removed), the excitation (or interrogation) fiber optic connector and three specimen sensing elements of slightly different configurations.

Figure 3.2.3 shows the TD-1101 with four of the eight sensing elements immersed in liquid. Note that four of the eight status monitor lamps are lit.

Figure 3.2.4 shows the TD-1101 with seven of the eight sensing elements immersed. Note that seven of the eight status monitor lamps are now lit.

The eight sensing elements are formed from borosilicate glass and are mounted in a channel that is separable from the body of the transducer - thereby permitting simple replacement or substitution of the sensing elements. All body parts are formed from anodized aluminum alloy. The entire cavity containing the optical fibers is filled with a silicone elastomer.

Because multi-terminal fiber optic connectors are not yet readily available, the eight-terminal connector shown in Figure 3.2.2 was fabricated in the Boeing Developmental Fiber Optic Lab. Note that the optical interface plane of this

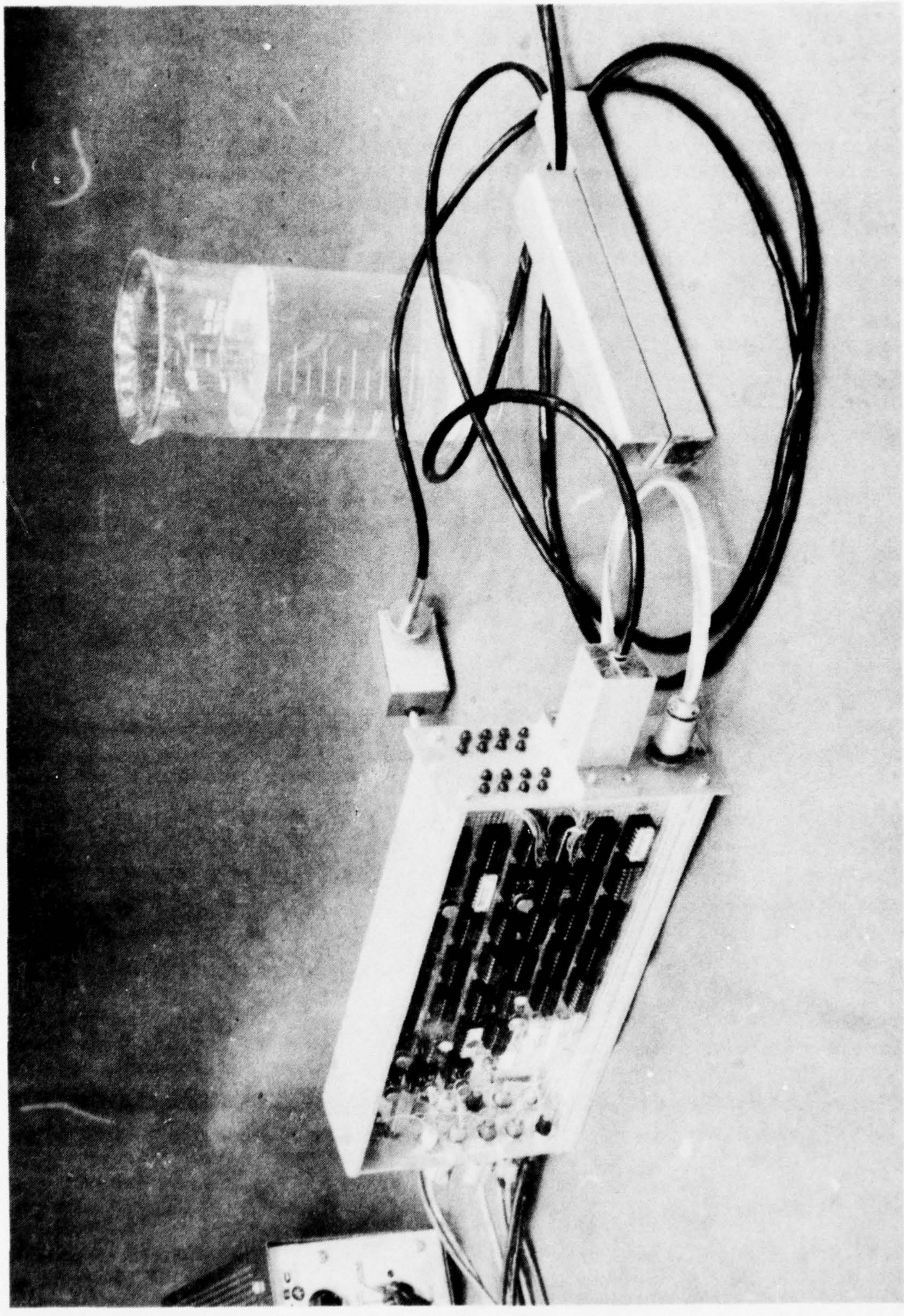

FIGURE 3.2.1
ASSEMBLY OF TD-1101 LIQUID LEVEL SENSOR WITH SR-1100 SCANNER/RECEIVER

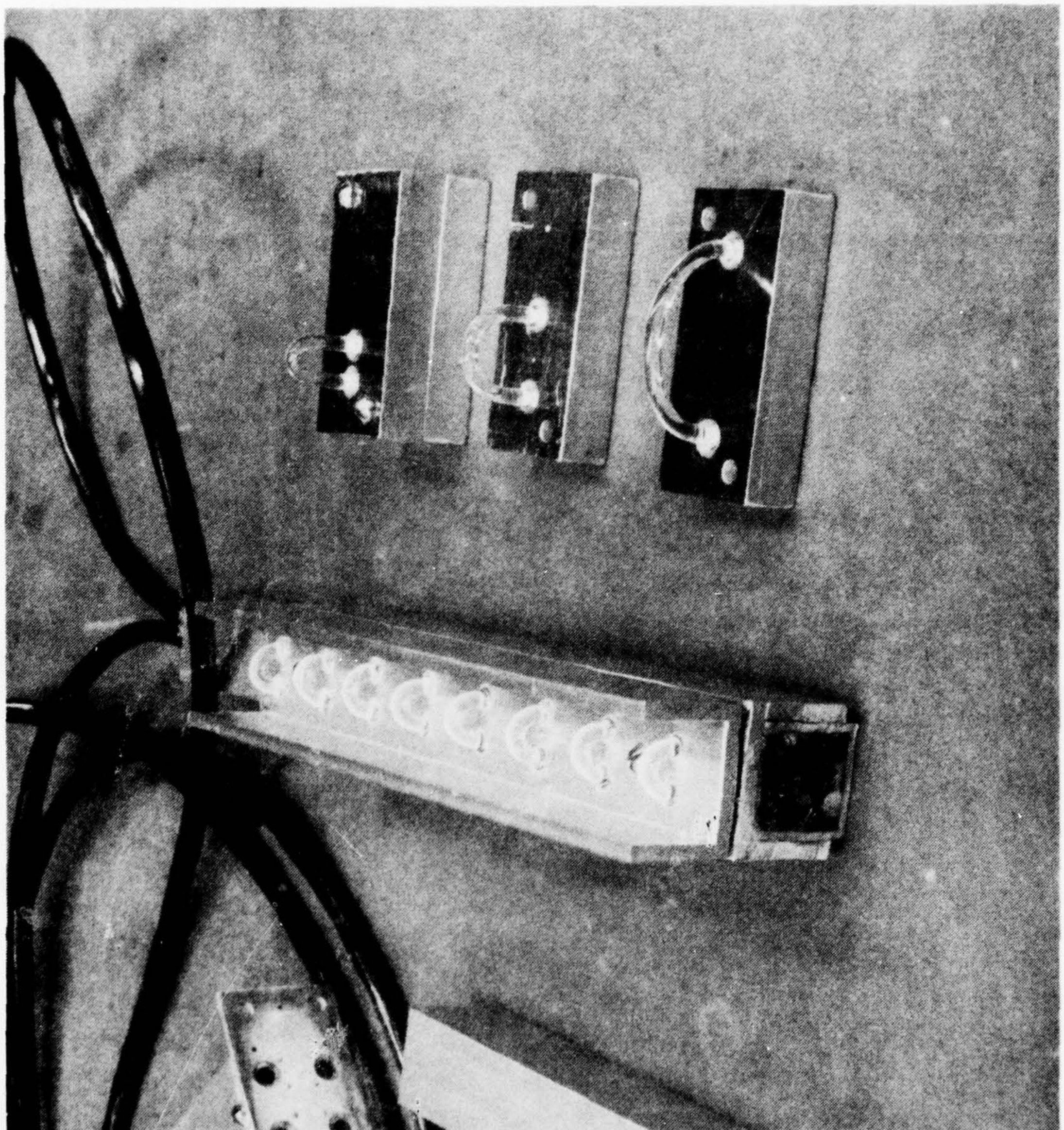

FIGURE 3.2.2
TD-1101 LIQUID LEVEL SENSOR (SLOSH BAFFLE REMOVED)

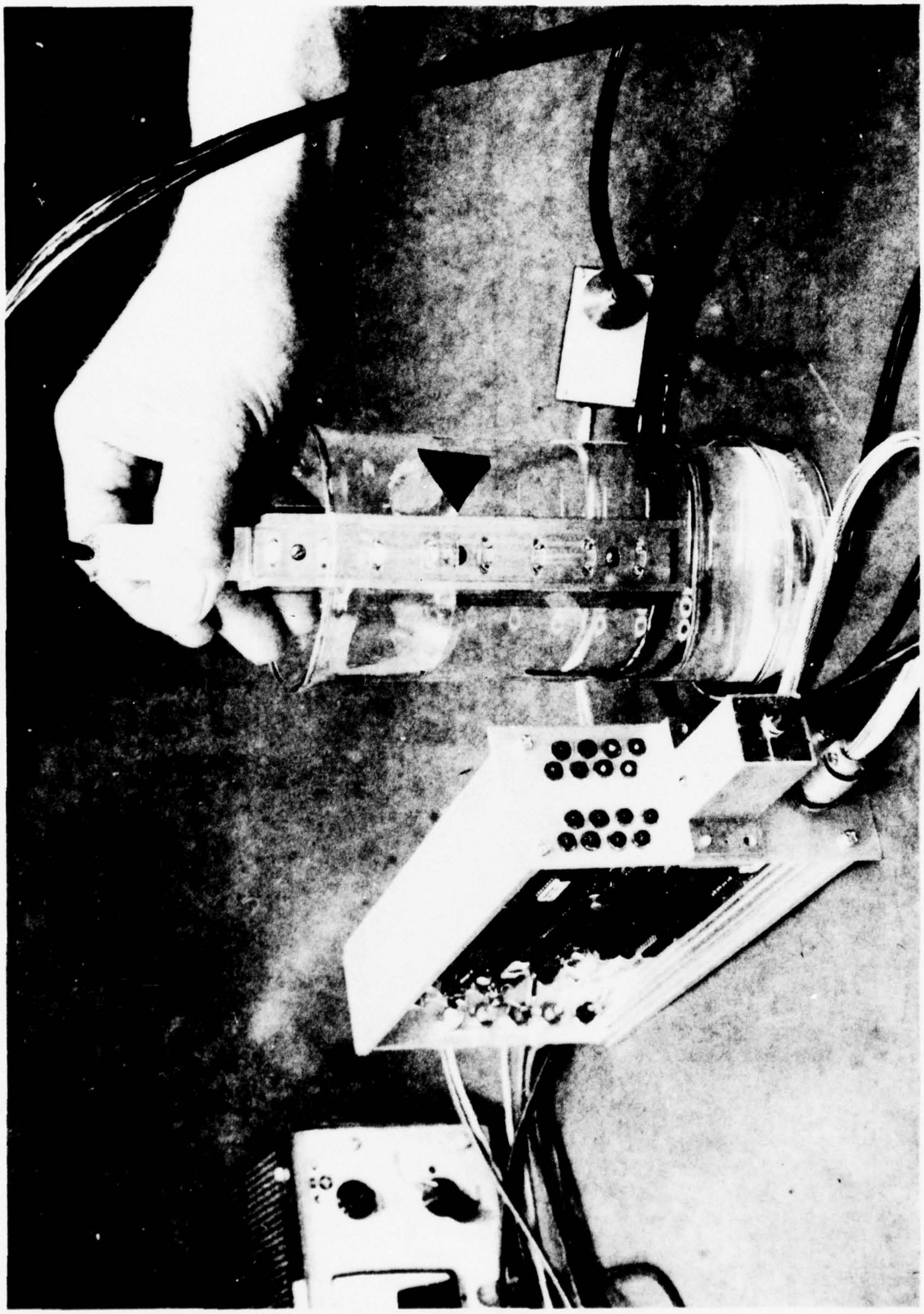

FIGURE 3.2.3
TD-1101 LIQUID LEVEL SENSOR DEMONSTRATION (4 ELEMENTS SUBMERGED)

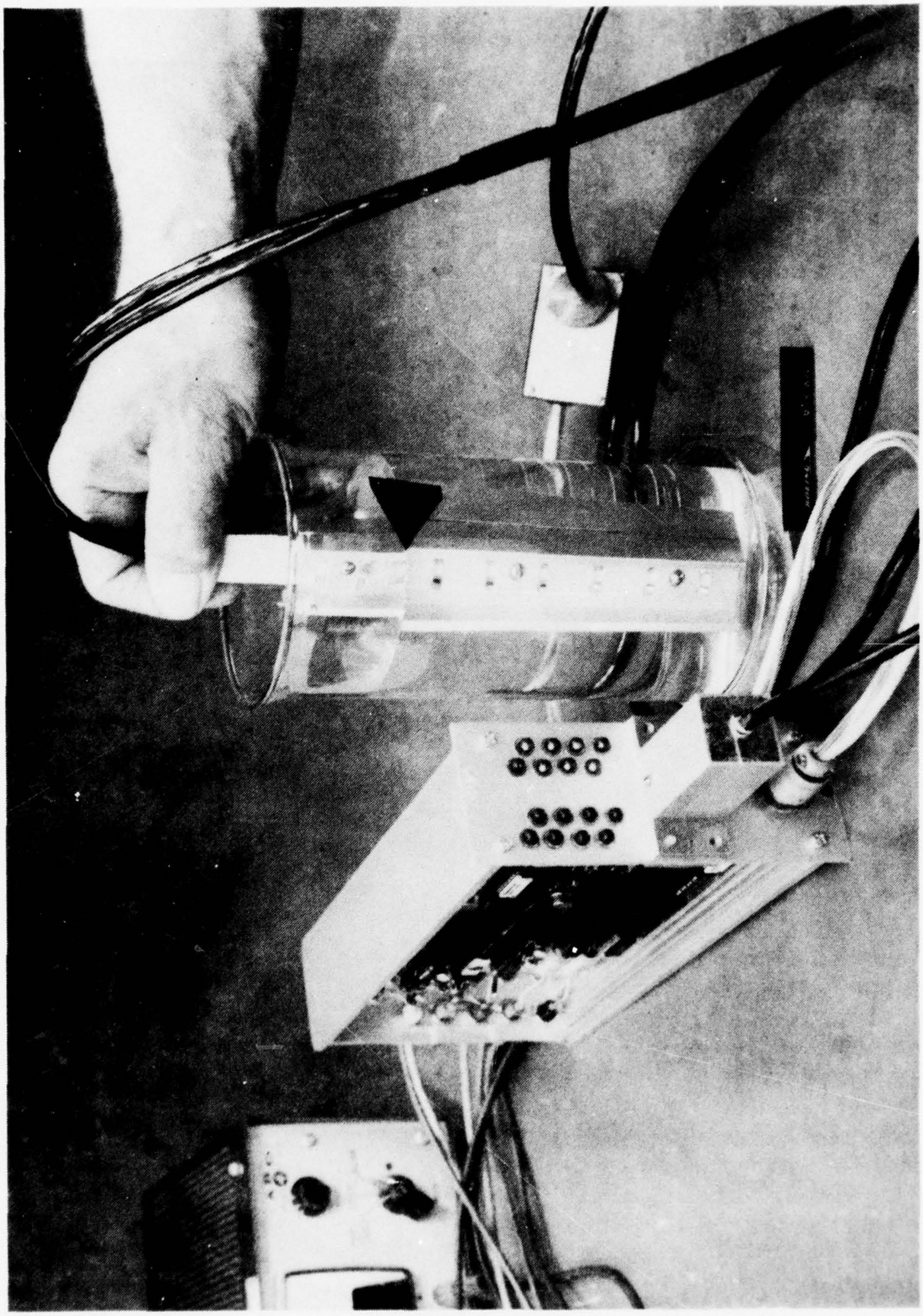

FIGURE 3.2.4
TD-1101 LIQUID LEVEL SENSOR DEMONSTRATION (7 ELEMENTS SUBMERGED)

3.2 Continued

connector is a flat surface. This permits grinding and polishing of all eight ports to be accomplished in one operation.

3.3 DESIGN CONSIDERATIONS

Each of the eight sensing elements of the TD-1101 sensor consists of a semicircular loop of borosilicate glass, the open ends of which are ground and polished to an optical finish and which interface with two fiber optic bundles. One bundle conducts an optical interrogation signal from the scanner into the loop. The other bundle conducts the response signal from the loop back to the receiver. When light enters the entry port of a loop surrounded by air (see Figure 3.3.1), those rays which strike the glass/air interface at an angle (from the normal) greater than the critical angle defined by the refractive index (1.47) of the glass and (1.00) of the air propagate around the bend by total internal reflection and emerge at the exit port of the loop where they enter the fiber optic bundle to the receiver. Light arriving at the receiver is detected and converted into a voltage of a value which defines the absence of a liquid at the loop.

When the loop is surrounded by a medium which has a refractive index greater than air (see Figure 3.3.2), the critical angle is correspondingly greater, proportionally more rays strike the interface at an angle less than the critical angle and pass into the surrounding medium rather than propagate to the exit port. At the receiver, the resultant attenuation of light is interpreted as the presence of a medium other than air surrounding the loop.

Although Figures 3.3.1 and 3.3.2 serve to illustrate the principle of the sensor elements, they also clearly represent a gross oversimplification of the total problem since only an axial ray is considered. In reality, rays enter the sensor element at all angles that can be supported by the interrogation fiber optic bundle. Because the sensor element (in air) has a much higher numerical aperture than most optical fibers, the higher-order modes are propagated until they reach the bend, at which time some, as shown in Figure 3.3.3, escape into the surrounding medium if their angle of incidence with the wall is less than the critical angle of sensor element. Certain other rays corresponding to low-order modes also escape, as shown in Figure 3.3.4, as they reach the bend.

It is believed that the best discrimination can be achieved when the sensor element is illuminated by an interrogation bundle with very low numerical aperture such that nearly all rays are propagated when the element is surrounded by air and nearly all rays escape when the element is surrounded by a medium of higher refractive index. Clearly also, for a fiber bundle of given numerical aperture, there exists an optimum ratio of bend radius to element diameter. A rigorous analyses of the optimumization process is probably worthwhile but has not yet been undertaken.

In the feasibility model, all fiber bundles were fabricated from Galite 1000 fiber with a bundle diameter of 0.045 inch and a numerical aperture $(n^2_{core} - n^2_{clad})^{1/2} = 0.66$. Using this fiber, a series of tests were performed to experimentally determine the optimum bend radius. In these tests, all elements had a diameter of 0.125 inch. Three different bend radii were tested and, with specimens of each of the three bend radii, measurements were

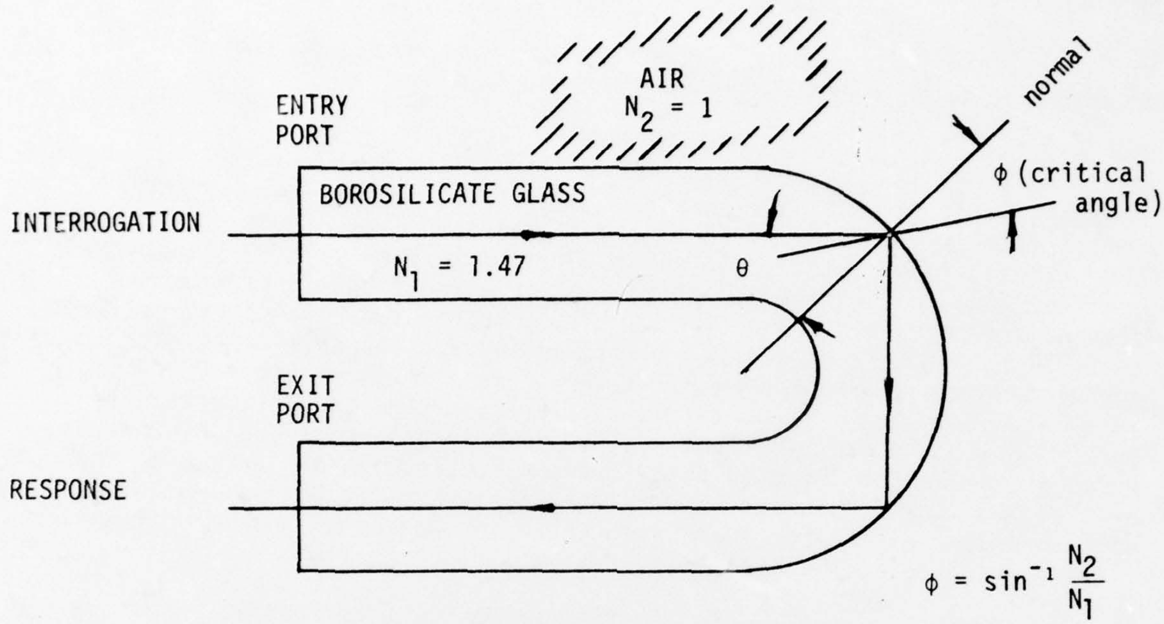

FIGURE 3.3.1

SENSING ELEMENT SURROUNDED BY AIR SUCH THAT $\theta > \sin^{-1} \frac{N_2}{N_1}$

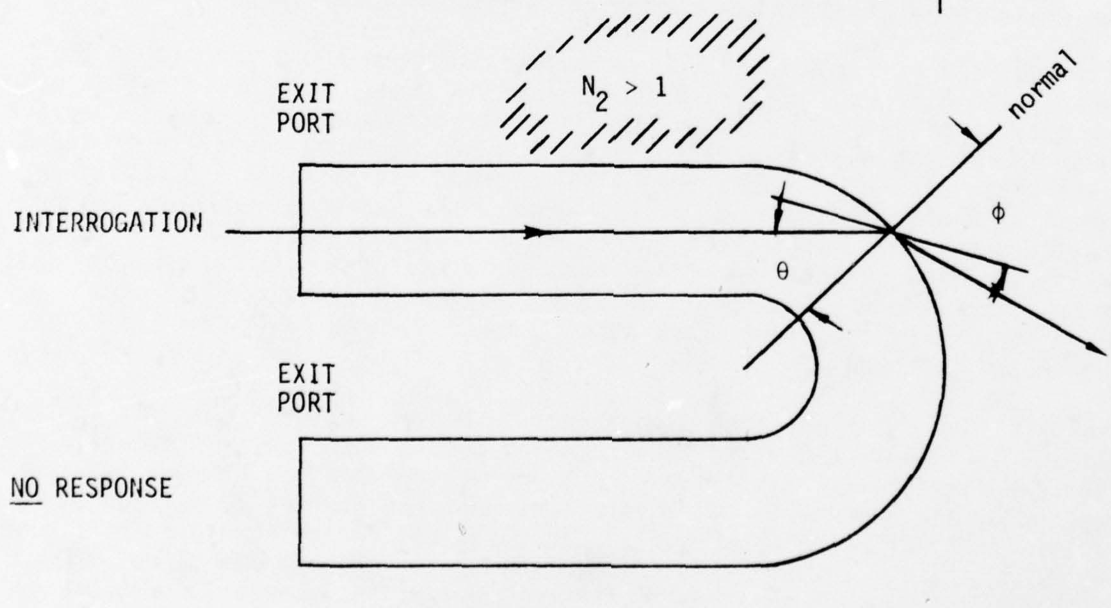

FIGURE 3.3.2

SENSING ELEMENT SURROUNDED BY MEDIUM SUCH THAT $\theta < \sin^{-1} \frac{N_2}{N_1}$

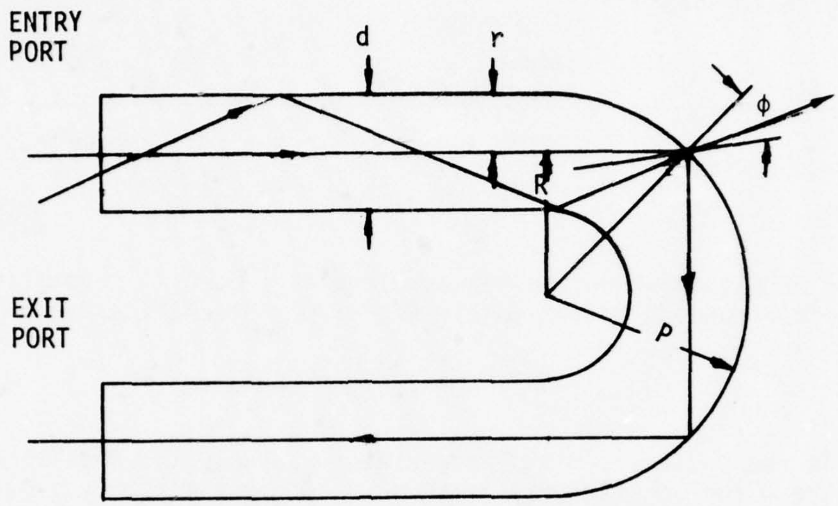

FIGURE 3.3.3

DERIVATION OF OPTIMUM BEND RADIUS (R) AND ESCAPE OF CERTAIN HIGH-ORDER MODES

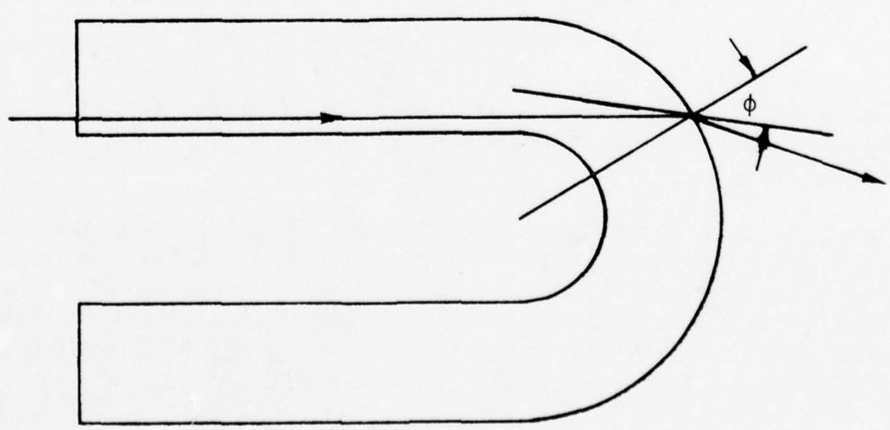

FIGURE 3.3.4

ESCAPE OF CERTAIN LOW-ORDER MODES

made using three liquids, each with a different refractive index. In the following tabulation of test results, the number shown represents the difference (expressed in dB) in output power observed at the far end of a sixteen-foot fiber optic bundle when the element under test was immersed in the indicated liquid.

Bend Radius (in)	Water (N_2 = 1.33)	JP4 (N_2 = 1.4)	Carbon Bisulfide (N_2 = 1.62)
0.15	7.21 dB	16.73 dB	23.47 dB
0.30	3.57	11.05	22.71
0.60	3.55	20.69	23.55

For the condition where the sensor element is borosilicate glass (N_1 = 1.47) and the surrounding medium is air (N_2 = 1.0) the critical angle is:

$$\phi = \sin^{-1} \frac{1}{1.47} = 42.86^0$$

For this reason, the minimum bend radius was selected such that the angle of incidence θ for an axial ray was 45^0 --- or just slightly greater than the critical angle. The geometry for this condition is shown in Figure 3.3.3. For this geometry:

$$P = \frac{R}{\cos 45^0}$$

$$r = P - R$$

$$= \frac{R}{\cos 45^0} - R$$

$$= \sqrt{2}\, R - R$$

$$= R(\sqrt{2} - 1)$$

$$R = \frac{d}{2(\sqrt{2} - 1)} = 1.207\, d$$

For d = 0.125 inch, the bend radius R = 0.15 inch---which was the minimum bend radius selected for evaluation and also the bend radius used in the feasibility model.

The test data shows that, when immersed in JP4, a bend radius of 0.15 inch is 5.7dB better than a bend radius of 0.30 inch but 4dB poorer than a bend radius of 0.60 inch. A bend radius of 0.15 inch was finally selected for the feasibility model because of greater mechanical strength and because it would also function satisfactorily in water---which, for routine demonstration purposes, is far less messy than JP4 fuel.

3.4 PERFORMANCE

As was noted in Section 2.4, the feasibility model Scanner/Receiver will tolerate a total loss as great as 63.7dB and still maintain a bit error rate as low as 10^{-8}.

In the feasibility model, known losses include:

Emitter-fiber loss	14.3 dB
Fiber loss (10 ft @ 0.2 dB/ft)	2.0
Sensor area mismatch	10.7
Sensor fresnel reflection loss	2.0
Total	29.0 dB

The total measured loss from emitter output to receiver input was 34.9 dB. The average loss of individual sensor elements was therefore 34.9 - 29.0 or 5.9 dB.

The operating system margin (for a bit error rate of 10^{-8}) was:

$$\text{System Margin} = \frac{\text{Measured peak receiver input power}}{\text{Minimum required peak receiver input power}}$$

$$= \frac{1600 \text{ nanowatt}}{2.14 \text{ nanowatt}} = 747.7$$

$$= 28.7 \text{ dB}$$

With all other conditions fixed, this margin would permit the addition of 143.5 ft of fiber optic cable (at 0.2 dB/ft) and still maintain a bit error probability of 10^{-8}. It follows that the feasibility model transducer would be operable at a distance of at least 75 feet from the Scanner/Receiver using the same type of fiber optic cable.

Distances greater than 75 feet can best be accommodated either by reducing the data rate (and the receiver bandwidth) or by reducing the system losses. The largest single loss (14.3 dB) occurs at the emitter/fiber interface. This loss can be reduced significantly by careful selection of emitters and fibers which yield maximum coupled power. It was felt that feasibility could be demonstrated without resorting to such costly components.

The second largest loss (10.7 dB) occurs at the interface between the sensing element and the response fiber optic bundle. This loss is the result of using a sensor element much greater in diameter (to provide ruggedness) than the fiber optic bundle. This loss can be reduced by using a sensor element of smaller diameter (and proportional ruggedness), by using a larger fiber optic bundle or, to some extent, by using imaging optics at the interface.

During the testing of the feasibility model, it was found that the Liquid Level sensor repeatedly indicated the true liquid level. It was possible to adjust the detection threshold such that indication occurred as the element barely touched the fluid surface, as the element became fully immersed or at any point in between. The model was tested in a wide variety of fluids including water, water with detergent suds, water emulsions, JP4, methyl alcohol and

carbon bisulfide. The fluid level could be detected in all of these fluids without readjustment of the electronics. Naturally, the depth of immersion of a sensor element at the detection point varied slightly as a function of the refractive index of the fluid. On only one occasion out of perhaps 100 did the sensor falsely indicate the presence of a fluid, in this case water. Examination showed that a large drop had formed at a critical point on the sensor element. It is doubtful that this could happen in a vibration environment such as aboard an aircraft. When immersed in fluid with foam on the surface, the sensor correctly indicated the fluid level--probably because the refractive index was still very close to that of air.

Performance of the sensor in low-temperature fluids was not investigated. One would suspect that, at some low-temperature limit, the fluid would become sufficiently viscous that it might form a film on the sensor element sufficiently thick to cause a false indication.

In one test, freon was sprayed on an otherwise dry sensor to create frozen atmospheric moisture on the sensor elements. As might be expected, this did result in a false indication. This condition requires that the transducer be colder than the surrounding air. The extent to which this might be a problem in aircraft fuel tanks is, at this time, unknown.

It has been suggested that microbial and fungus growth, which occasionally appear in aircraft JP fuel tanks, might impair the performance of the Fiber Optic Fuel Level Sensor. The subject was discussed with the Boeing Commercial Airplane Company Propulsion Staff and the findings are summarized as follows:

1. There have been some problems encountered by airlines, particularly those in the far east subject to high humidity and less-than-optimum maintenance practices. Microbial growth has occurred at the water/fuel interface and is evidenced by deterioration of the fuel cells.

2. Most of the airlines inhibit organic growth in fuel tanks by periodically treating the fuel with an additive called "Biofor JF".

3. Although no assurance could be offered that organic growth would not be a problem, it seems improbable because such growth appears primarily in the presence of water.

4. It appears that the only way to find a conclusive answer to the question would be to run a series of tests using contaminated fuel specimens in which such organic growth was encouraged. Such tests would require considerable time and effort beyond the scope of this contract.

3.5 CONCLUSIONS

The feasibility of this type of sensor has been demonstrated in JP4 fuel and in a variety of other common liquids with widely differing refractive index. These tests were all performed at room temperature and the effects of extreme temperature are not yet known. It is expected that extreme low temperature might increase fuel viscosity to the point where the sensing elements would accumulate a film of sufficient thickness to cause a false indication. It is also possible that a highly viscous fluid might tend to form a large drop which could remain suspended between the two parallel legs of an element and possibly produce a false indication. Viscosity will also determine the minimum possible spacing between sensor elements.

Tests involving several different fuel types should be conducted at temperature extremes to determine whether or not these are problems.

With highly viscous fuels it might be necessary to increase the physical size (while maintaining the optimum proportions) of the sensor elements. If this were necessary, and the same size fiber optic bundles were retained, the area mismatch loss at the sensor element/fiber interface would increase accordingly unless some form of imaging optics were employed at this interface. The use of spherical surfaces on the element ends, tapered matching sections and independent (lens) optics should be investigated as means for reducing the area mismatch loss.

The feasibility model used glass sensor elements. Glass has good optical properties but also wets readily with most fluids and can fracture. The use of certain plastics with poor wetting properties, such as silicones, fluorocarbons and vinyls should be investigated.

In the feasibility model, the glass sensor elements were cemented into the supporting structure with polyester resin. The use of silicone, teflon and vinyl "O" rings should be considered, as should glass-to-metal fritted bonds.

A few of the different sensor configurations considered are shown in Figure 3.5.1. The reflective type shown in 3.5.1a was rejected because of the small change in reflected power that could be realized. The types shown in Figure 3.5.1b and 3.5.1c were rejected because they depend upon the optical clarity of the fuel. The prismatic type shown in Figure 3.5.1d has been used for many years for visual observation of liquid levels in ambient light but was rejected from this investigation because of the large attenuation that results from the constant divergence of a beam over the long unguided path length through a prism of any reasonable size.

The type shown in Figure 3.5.1e was selected for detailed evaluation because of the inherent simplicity, because the absence of sharp edges results in a structure which resists fracture, because the guided path results in low loss and because a large change in transmission can be realized if the geometry is optimized. As noted in the test results of Section 3.3, a change in optical power transmission as great as 20 dB was noted between dry and immersed conditions in JP4. These results were obtained with fiber optic cables having a numerical aperture of 0.66. The optimum geometry, and realizable signal

3.5 Continued

level change, with fibers of low numerical aperture should be investigated. Fibers with low numerical aperture support fewer high-order propagation modes and should greatly increase the realizable signal level change between wet and dry conditions of the sensor element.

For use in environments demanding extreme ruggedness, the hemispherical and hemiellipsoidal sensor forms of Figure 3.5.2 should be investigated also with high and low numerical aperture fibers.

The hemispherical sensor element of Figure 3.5.2a has entry and exit fibers located on a diameter of the base circle and equidistant from the periphery. Mechanically, this sensor element offers great ruggedness and is relatively simple to fabricate. Since a sphere has only one focal point, there is little focussing of entrance rays to the exit port. The insertion loss can be expected to be high and proportional to the radius of the sphere.

The hemiellipsoidal sensor element of Figure 3.5.2b would appear to be nearly ideal. It offers great mechanical ruggedness and, in addition, has ideal optical properties. The elipsoid has two foci (F_1 and F_2). Theoretically, a ray entering at F_1 at any angle in any plane will exit at F_2 at the same angle. This property should provide the hemiellipsoidal sensor element with low insertion loss and the ability to function well with either single fibers or with fiber bundles. Another valuable property of the ellipsoid is that, over a wide range of entry angle Ψ, the angle of incidence θ with the surface changes only slighty. The latter property should give the hemiellipsoidal sensor element an extremely high wet/dry power output ratio. Although more difficult to fabricate, the overwhelming advantages of the hemiellipsoidal sensor element would appear to justify further investigation.

The Fiber Optic Fuel Level Sensor investigated during this study effort senses eight discrete levels within a total span of 16 cm. The resolution is therefore rather coarse, but probably adequate for the intended application. It should, however, be noted that the same basic principles can be applied to liquid level sensors requiring extremely fine resolution. For example, it would be completely feasible to produce a liquid level sensor in which actual optical fibers formed the sensing elements --- in which case the resolution would be equal to the fiber diameter, which is typically 0.002 inch to 0.010 inch.

Fiber optic liquid level sensors adapt well to a variety of special applications. For example, Boeing has produced a prismatic-type sensor 0.1 inch in diameter with single-fiber interrogation and response lines in which the entire structure, including fibers, is composed of fused silica. This particular sensor was intended for use at cryogenic temperatures, but should be equally useful at high temperatures up to the softening point of fused silica (about 3000^{o} F.)

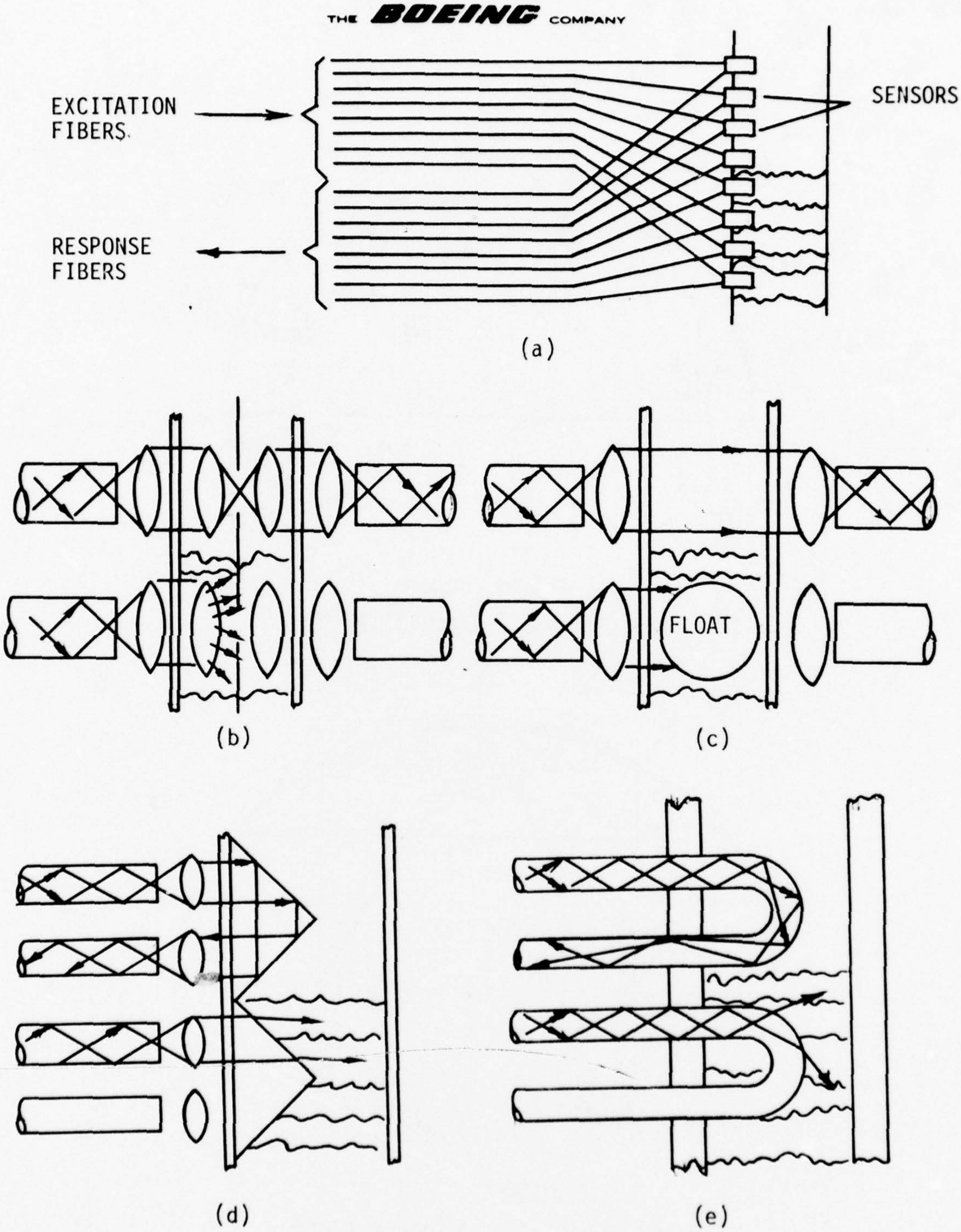

FIGURE 3.5.1

BASIC DISCRETE LIQUID LEVEL SENSORS

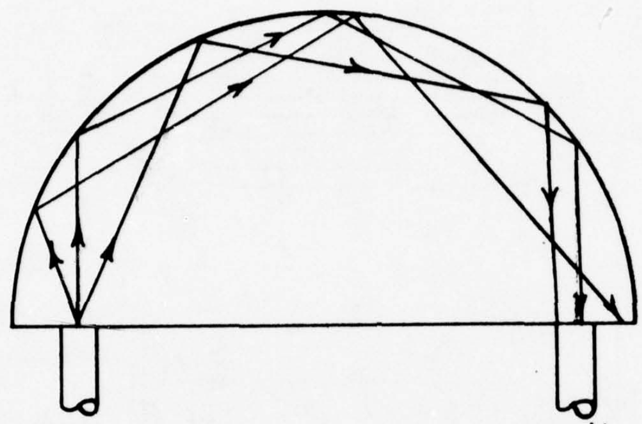

FIGURE 3.5.2a
HEMISPHERICAL SENSOR ELEMENT

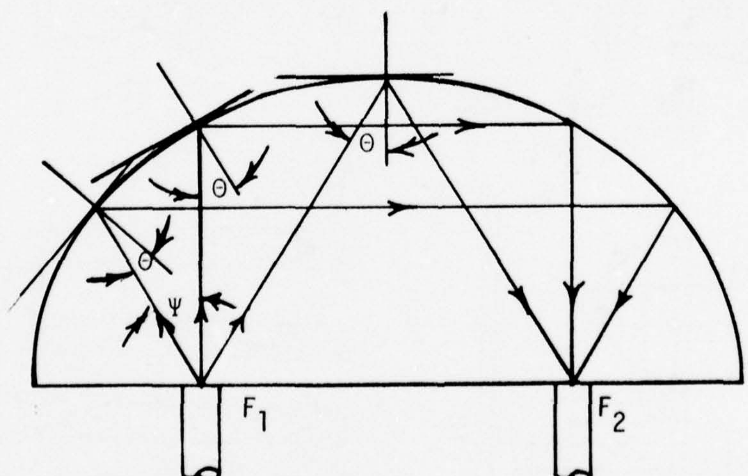

FIGURE 3.5.2b
HEMIELLIPSOIDAL SENSOR ELEMENT

4.0 LINEAR DISPLACEMENT TRANSDUCER (TD-1102)

4.1 FUNCTION

The TD-1102 Linear Displacement Sensor was designed to demonstrate the feasibility of digitally sensing linear mechanical displacement with an electrically passive optical transducer, the input (interrogation) and outputs (response) of which are coupled by means of fiber optic cables. It was designed to operate with the SR-1100 Scanner/Receiver as the source of optical excitation and as the optical/electrical interface for conversion of the optical responses into an eight-bit binary word representing linear mechanical displacement.

4.2 DESCRIPTION

The TD-1102 sensor consists of two basic elements (1) an encoding plate and (2) a sensor head with fiber optic cables and connectors. The encoding plate is the moving element of the transducer and is designed to provide eight-bit digital encoding of a three-inch mechanical displacement. The encoding plate has eight parallel tracks printed with an eight-bit Gray code. The sensor head contains eight corresponding groups of fibers which provide optical interrogation and sensing of reflected light. Fiber optic cables connect the sensor head to the SR-1100 Scanner/Receiver.

The block diagram of Figure 4.2.1 illustrates the principle of the sensor and shows the interconnections with the Scanner/Receiver.

The sensor associated with each of the eight tracks consists of two collinear arrays of fifteen 5-mil glass fibers each. The two arrays of fibers are mounted in the sensor head such that, at the open ends, they form adjacent parallel rows of optical apertures. One array carries the optical interrogation signal to the reflective encoding plate. The second array carries the reflected response signal back to the receiver detector. Construction details of the sensor head are shown in Figures 4.2.2 through 4.2.4. Figure 4.2.2 shows one of two identical halves of the sensor head, Figure 4.2.3 shows the two halves assembled together and Figure 4.2.4 shows a photograph of one half during the fabrication process prior to cutting and polishing the fibers.

The sensor was assembled using fibers with an outside diameter of 132 microns, a core diameter of 85 microns and a measured numerical aperture of 0.11 (acceptance half-angle of 6.3^{o}). Fibers of relatively large diameter were used to simplify handling and sorting problems. A low numerical aperture was selected to provide a narrow field of view of the encoding plate. Four 61-fiber bundles connect the sensor head with the SR-1100 Scanner/Receiver. Each bundle is divided during the assembly process into four groups of fifteen fibers each. Two optical connectors are used. One connector with eight ports carries the interrogation signals to the sensor head. A single-port carries all response signals back to the receiver.

The completed Linear Displacement Sensor is shown in the photograph of Figure 4.2.5. Details of the encoding plate are shown in Figure 4.2.6.

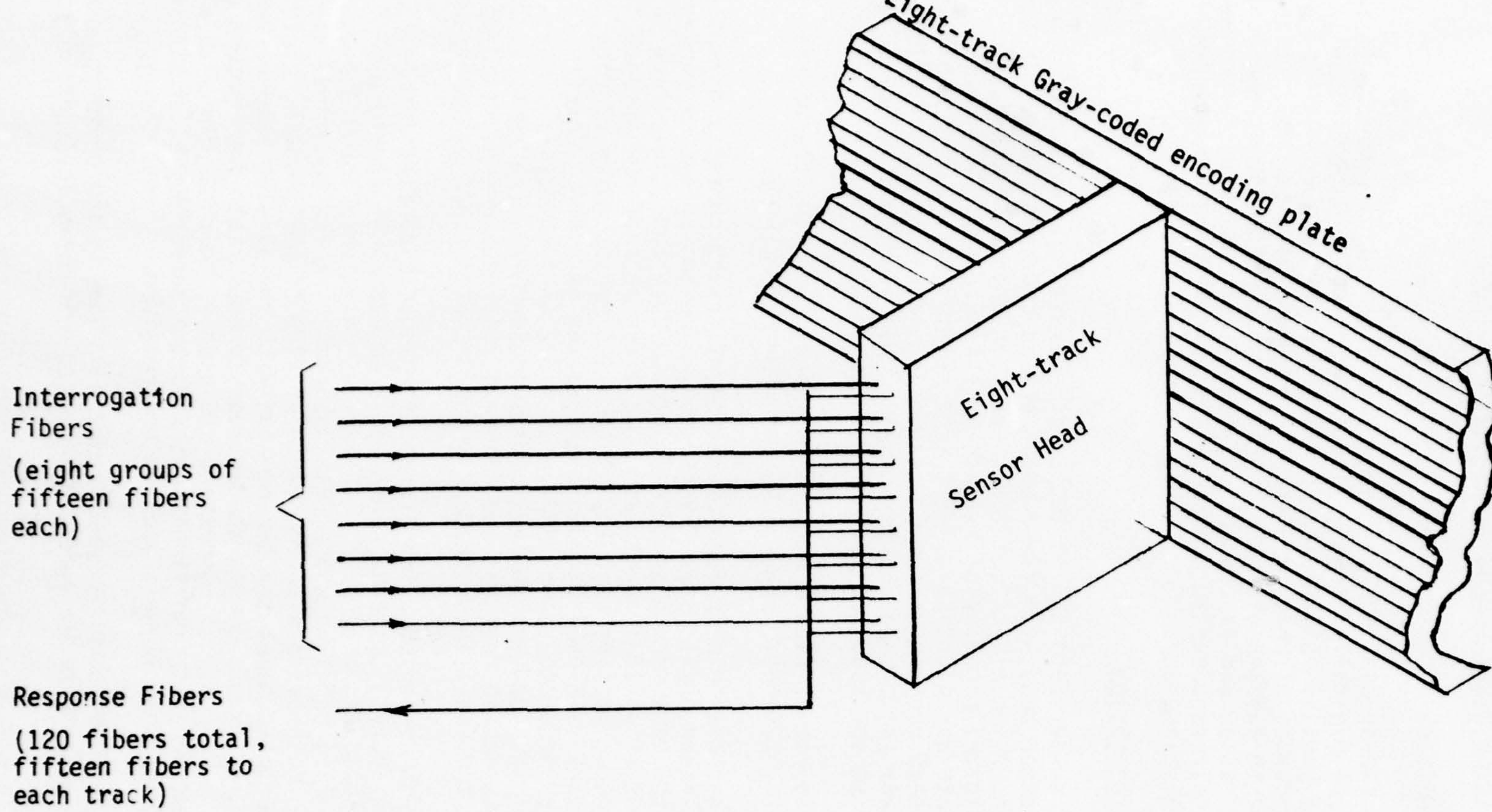

FIGURE 4.2.1

CONCEPTUAL BLOCK DIAGRAM OF LINEAR DISPLACEMENT SENSOR

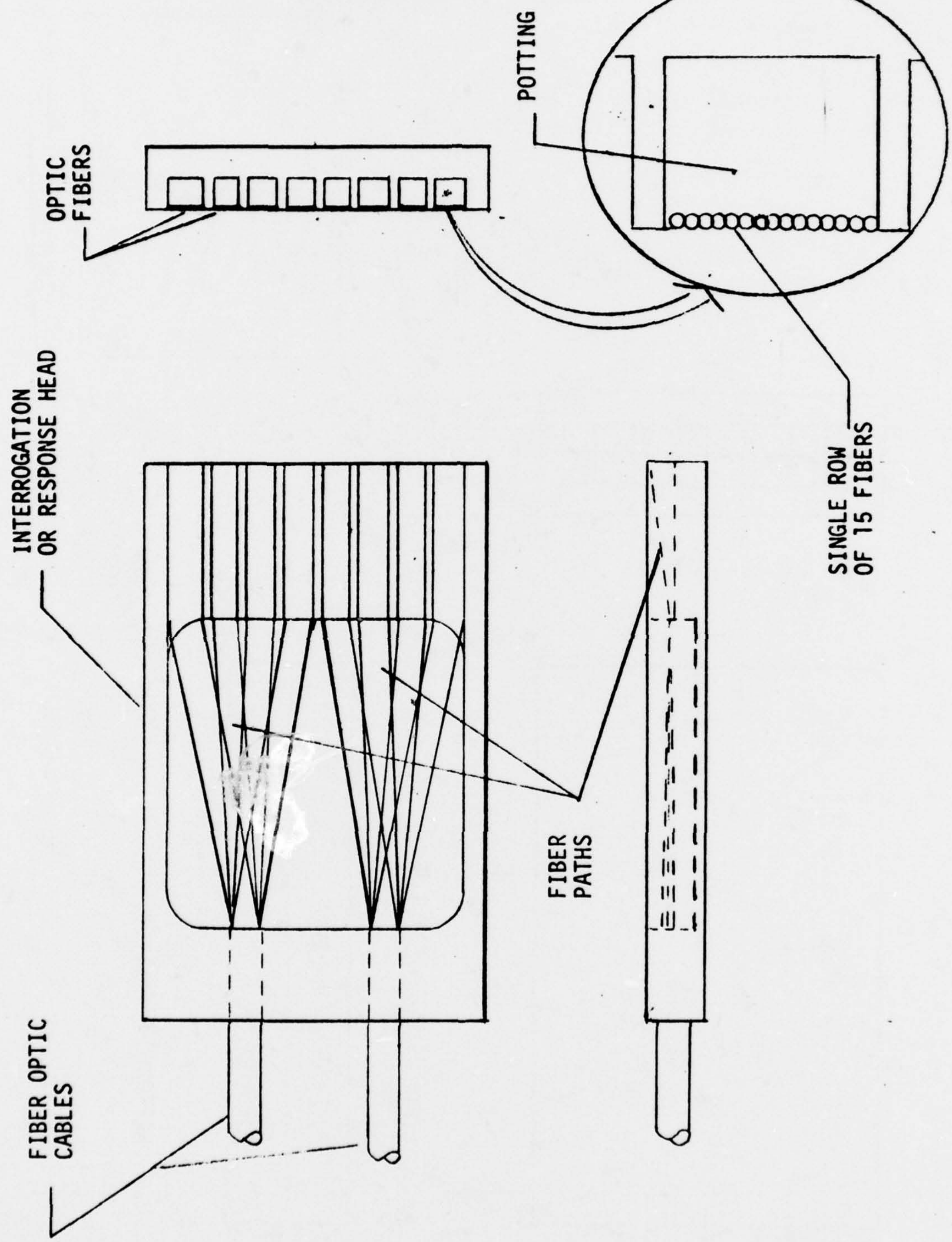

FIGURE 4.2.2

SENSOR HEAD CONSTRUCTION DETAILS

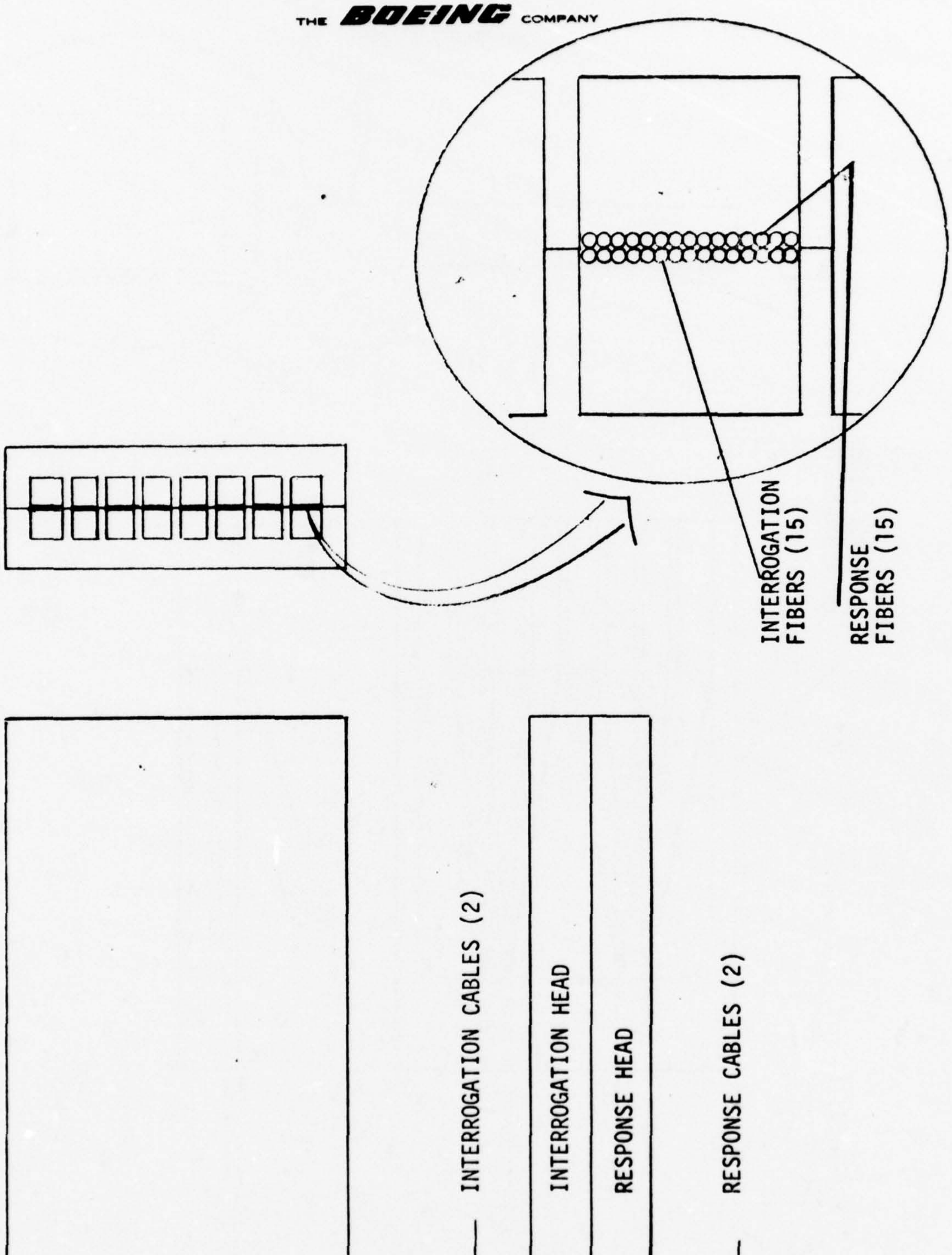

FIGURE 4.2.3
SENSOR HEAD ASSEMBLY

FIGURE 4.2.4
INTERNAL VIEW OF ONE-HALF SENSOR HEAD

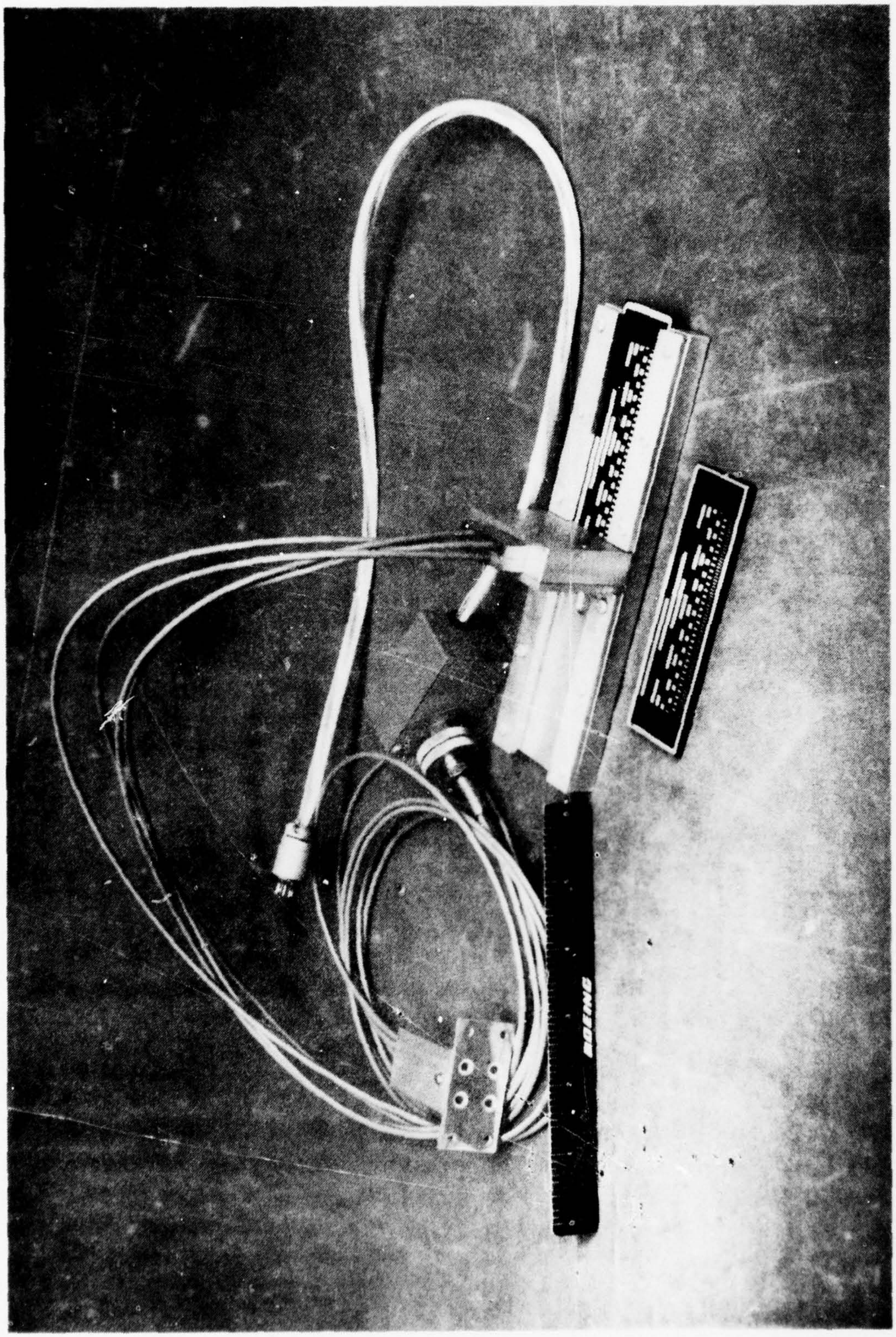

FIGURE 4.2.5
TD-1102 LINEAR DISPLACEMENT SENSOR ASSEMBLY

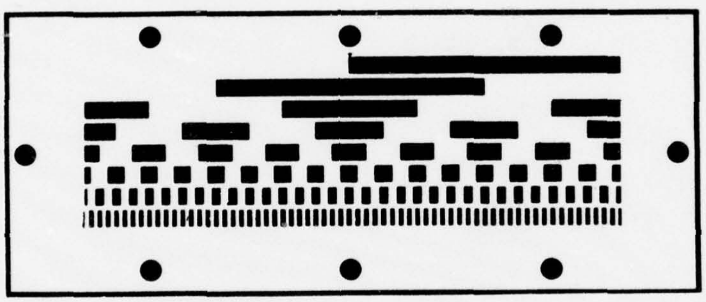

FIGURE 4.2.6

ENCODING PLATE (8-BIT GRAY CODE)

4.3 DESIGN CONSIDERATIONS

The optical geometry of the sensor head is shown in Figure 4.3.1. At the intersection of the interrogation and response fibers, the fiber claddings are ground away so that the fiber cores are tangent to each other in the sensor plane. This was done to minimize the thickness of the sensor in the plane of motion and to thereby improve the ability of the sensor to resolve transitions from absorbtive to reflective with minimum uncertainty. The interrogation and response fibers both intersect the detection plane at a slight angle (approximately 5^0) such that, for a given spacing s between the aperture plane and the encoding plate, an axial ray leaving an interrogation fiber and reflecting from the encoding plate enters a response fiber again . as an axial ray. This was done to maximize coupling between fibers and to reduce uncertainties in the detection of transitions.

The relationship between the angle α and the spacing s may be derived as follows:

$$n_1 \sin\alpha = n_2 \sin\beta$$

$$\beta = \sin^{-1}\left(\frac{n_1}{n_2}\sin\alpha\right)$$

$$= \frac{\frac{d/2}{\cos\alpha}}{\tan\beta}$$

$$= \frac{d}{2\cos\alpha\ \tan\left(\sin^{-1}\left(n_1/n_2\sin\alpha\right)\right)}$$

For $d = 3$ mils, $n_1 = 1.46$, $n_2 = 1$ and $\alpha = 5^0$,

$$s = 11.7 \text{ mils}$$

Figure 4.3.2(a) shows the relative sensor response as a function of spacing s as measured on the feasibility model. The measured peak response occurred for a spacing of 9 mils, which is in fair agreement with the above calculated value.

Figure 4.3.2 (b) shows the relative sensor response (at optimum spacing) as a function of encoding plate displacement past an absorptive/reflective transition.

4.4 PERFORMANCE

The edge resolution and spacing sensitivity of the completed sensor head was measured on an optical bench with precision X-Y-Z micropositioners. The edge used for the measurement was a highly polished steel block with razor-sharp edges. The interrogation ports were individually illuminated with radiation at 900 nm and the reflected power was measured with a United Detector Technology Model 11A Photometer. Figures 4.3.2(a) and 4.3.2(b) show the normalized results of this test. Figure 4.3.2 (a) shows the relative coupled power as a function of the spacing s between the sensor

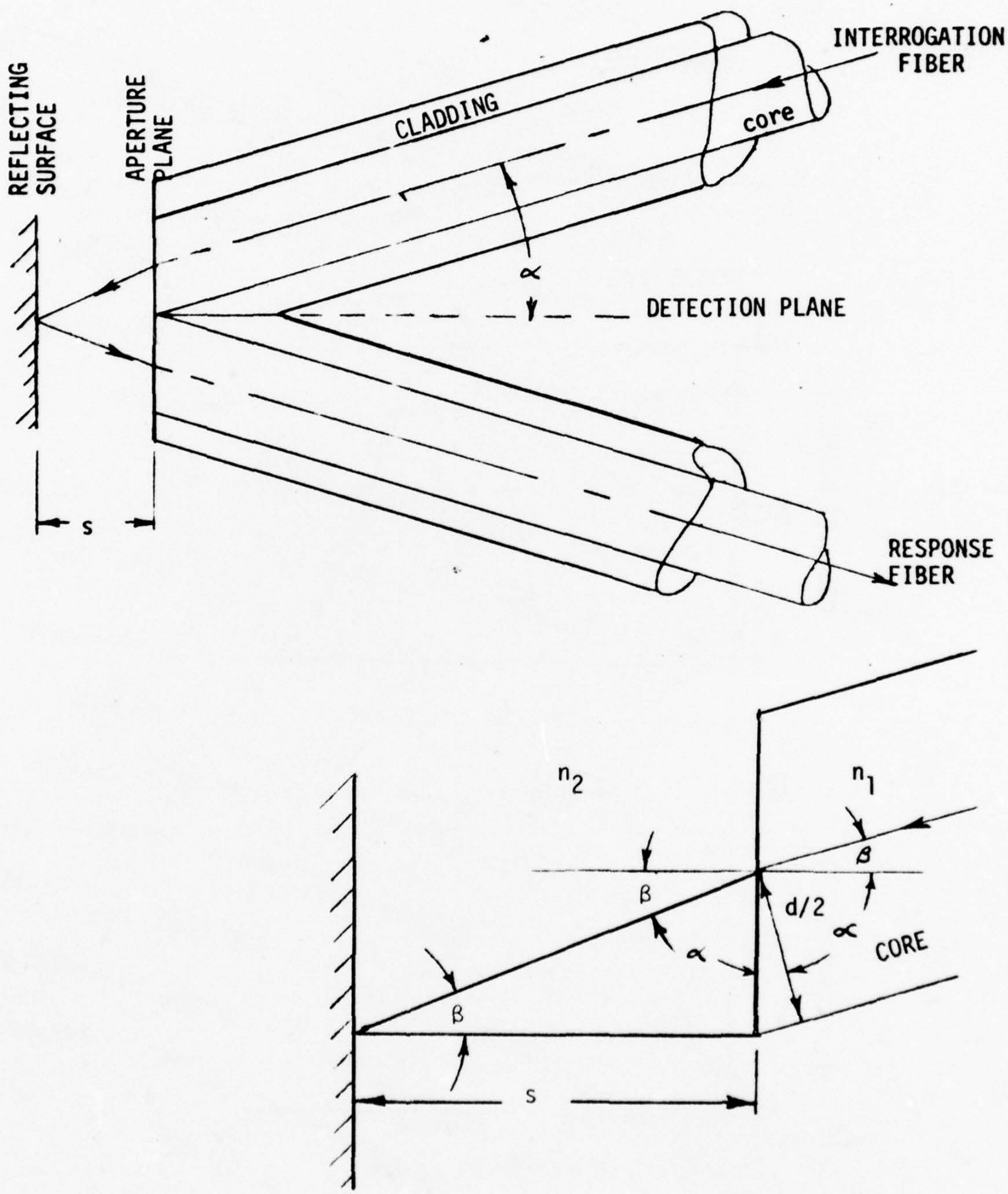

FIGURE 4.3.1

OPTICAL GEOMETRY OF SENSOR HEAD

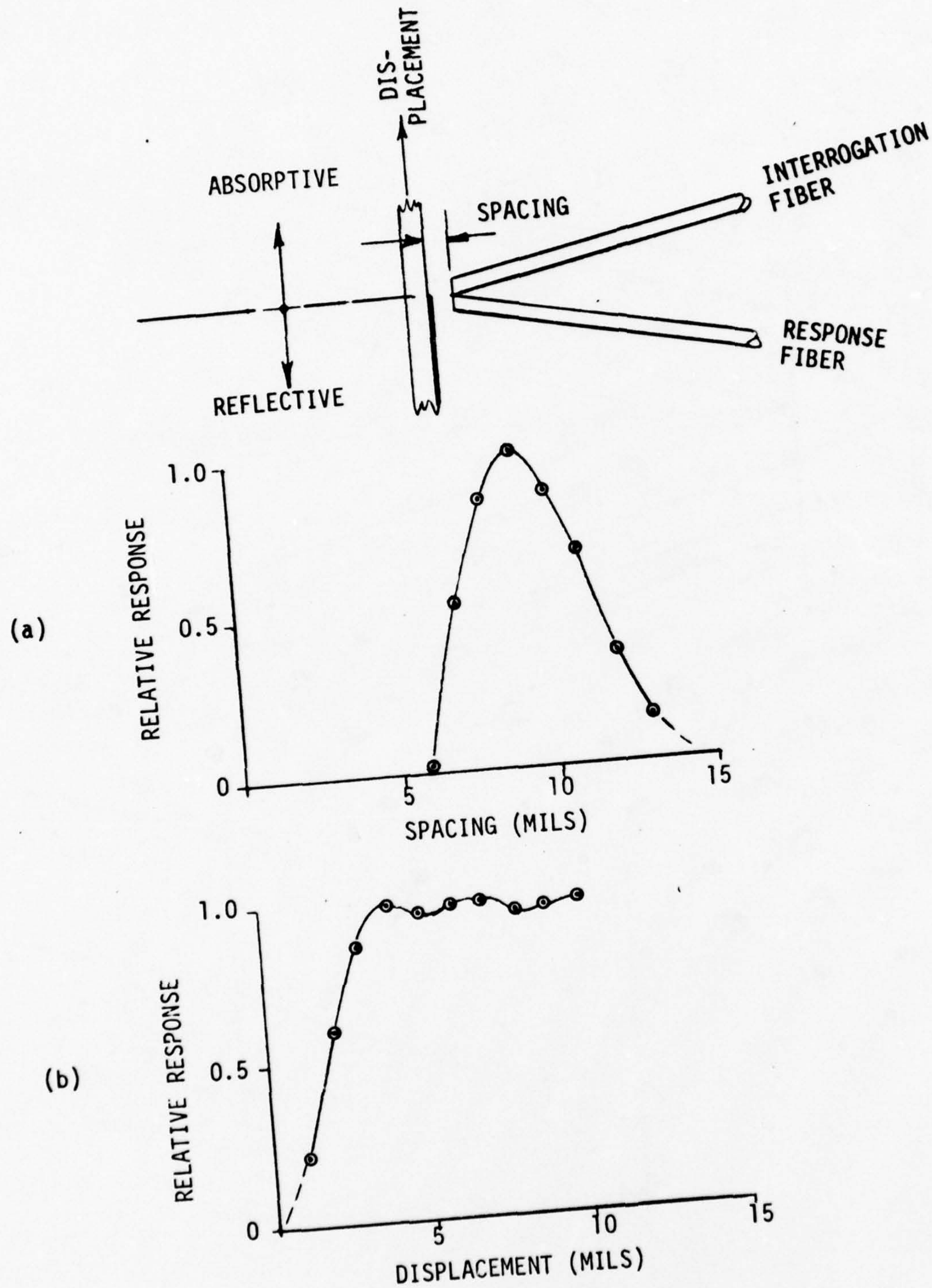

FIGURE 4.3.2

RELATIVE POSITIONAL RESPONSE OF SENSOR HEAD

4.4 PERFORMANCE (Continued)

head and the reflecting surface. This data shows that the optimum spacing is approximately 0.009 inch, or about three fiber core diameters.

Figure 4.3.2 (b) shows the relative coupled power, with a spacing of 0.009 inch, as a function of lateral displacement of the detection plane past the sharp edge. This data shows that the sensor head is capable of resolving, at the half-power point, a sharp transition within approximately 0.003 inch, or about one fiber core diameter.

The edge resolution of 0.003 inch permits the sensor head to resolve 1000 transitions within the three-inch travel of the encoding plate. This resolution is more than adequate for the eight-bit encoding which provides 256 discrete levels.

The original artwork for the encoding plate of Figure 4.2.6 was done on mylar sheet with a X10 scale factor. It was subsequently photo reduced to true scale on Kodalith Ortho. The original encoding plate was photo etched in pure nickel sheet with a thickness of 0.007 inch and was then stretched in a framework to form the moving element of the transducer. The reduced artwork was tested for accuracy on a precision optical comparator.

The three-inch pattern length was found to be 3.0004 inches---an error of one part in 7500, which is far better than necessary for eight-bit encoding.

As derived in Section 4.3, the edge resolution and sensor to encoding plate spacing are mathematically inter-related such that high edge resolution results in high sensitivity to spacing. The curve of Figure 4.3.2 (a) shows that, for the feasibility model sensor head, a spacing error of 0.0025 inch results in a 50% reduction of signal power. With the original encoding plate it was found that it was impossible to maintain the spacing accurately enough to ensure reliable encoding of position.

To provide the required spacing accuracy, a second encoding plate was fabricated from 0.125-inch aluminum. The pattern was deep-etched such that the reflective pattern remained high. The background was then filled with absorptive material, after which the entire surface was lapped to precise flatness and a high polish. The encoding plate and sensor head were then mounted in a support structure as shown in Figure 4.2.5. Head spacing was adjusted to the optimum value of 0.009 inch.

The transducer model was tested using a precision micrometer to provide known displacement. Figure 4.4.1 shows a plot of absolute reading error as a function of displacement over the three-inch travel. This data shows a periodic error which has peak values of approximately 0.5%. In an effort to find the source of this error, the original mylar artwork was investigated and found to be the major source of error.

Figure 4.4.1 also shows the measured artwork error which had a peak error of 0.29%. The remaining error is believed due to minor variations in the photo etch process used to produce the encoding plate and had a peak value of 0.17%. Most of the artwork error was attributable to registration problems

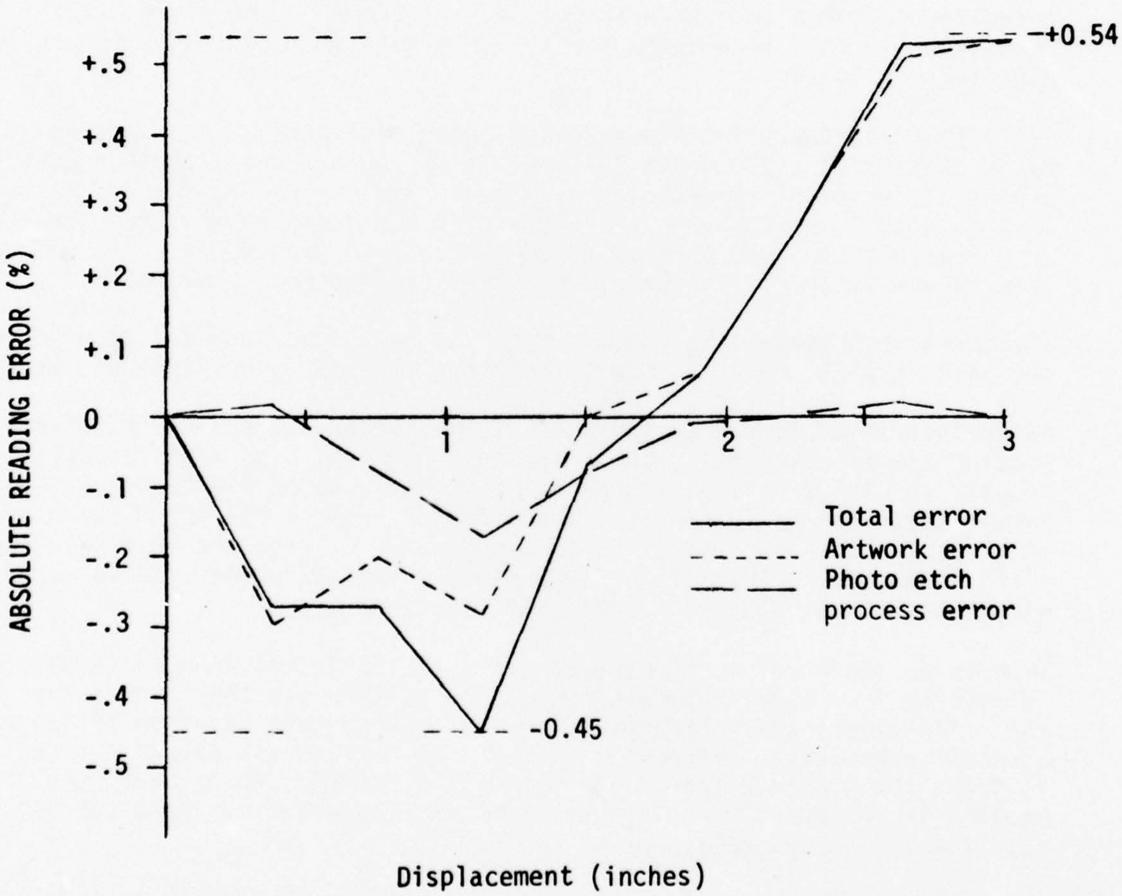

FIGURE 4.4.1

ABSOLUTE READING ERROR VS DISPLACEMENT

4.4 PERFORMANCE (CONTINUED)

encountered in manually laying out an offset Gray code pattern using standard-width lithographic tape. In this case, an odd artwork scale was selected to accommodate the tape width and an odd photo-reduction ratio was used to produce the pattern with the required length. While this approach is satisfactory for a one-of-a-kind feasibility model, a computer-plotted pattern would be preferable for production devices.

4.5 CONCLUSIONS

Although manual layout of encoding patterns may be satisfactory for non-demanding one-of-a-kind feasibility models, computer-plotted patterns are preferred for precision production devices. For example, the Boeing Computer-Aided Design Organization has the capability of converting tabulated data such as the Gray code into a large-scale machine-cut Rubylith pattern accurate to within 0.001 inch in several feet. Using this technique, combined with photo reduction, the art work error can be reduced to an insignificant value. Thin film deposition techniques largely eliminate the photo etch process errors. These technqiues were used to generate the encoding and slit patterns used in the Digital Fiber Optic Strain Sensor. For construction and performance details, refer to Section 7.0 of this report.

The model transducer shown in Figure 4.4.2 was fabricated only to demonstrate feasibility, not to demonstrate a packaging concept. In a production version it is recommended that the fibers be bent 90^{o} into the plane of the encoding plate to improve the shape factor and reduce the package volume. This approach was used in the design of the Digital Fiber Strain Sensor described in Section 7.0.

5.0 EVENT - COUNTING SENSOR (TD-1103)

5.1 FUNCTION

The TD-1103 Event-Counting Sensor was designed to detect mechanical motion and count mechanical events. This is accomplished by purely optical means and without physical contact with the mechanical part.

As an event counter, the sensor can be used to:

1. Sense the angular velocity of rotating parts (tachometer).
2. Sense the passing of moving objects.
3. Sense the rate of vibrating structures.
4. Sense the proximity of a fluid surface, as in a tank.

As an analog detector of motion, the same sensor can be used to:

1. Measure amplitude of mechanical vibration.
2. Measure amplitude and angular position of deflection of rotating shafts, as in rotor dynamics.
3. Measure dimensions of moving parts in production quality control.
4. Gage finish and surface texture of materials.

5.2 DESCRIPTION

The Event-Counting Sensor consists of three elements: (1) an optical source, (2) a fiber optic probe assembly and (3) an optical detector.

The optical source was a Type LED-55C light-emitting diode packaged with a series resitor to limit the forward current to 100 milliamperes. Peak spectral emission was at a wavelength of 940 nanometers with a total power output of approximately five milliwatts. The radiation pattern had a beamwidth of approximately 30^{0}.

The fiber optic probe as shown in Figure 5.2.1 was fabricated from two fiber optic cables, each with approximately 200 glass fibers with a cladding diameter of 0.0027 inch. The calculated numerical aperture of the fibers was 0.66 and the diameter of each bundle was 0.045 inch. The two bundles were joined in the optical probe to form a single randomized bundle with a diameter of 0.062 inch. The optical surface of this termination was ground and polished and fitted with a hemispherical lens with a diameter of 0.125 inch. A head-on view of the probe is shown in the photograph of Figure 5.2.2. The other end of each of the fiber optic bundles was terminated in a connector suitable for mating with the source and the detector.

The detector consisted of a United Detector Corporation Type PIN6D silicon PIN photodiode. This was followed by two stages of low-noise FET-input amplification. The detector/preamplifier had a measured sensitivity 0.42 millivolts/microwatt with a bandwidth of approximately 30 KHz. The equivalent noise power input was 0.5 nanowatt.

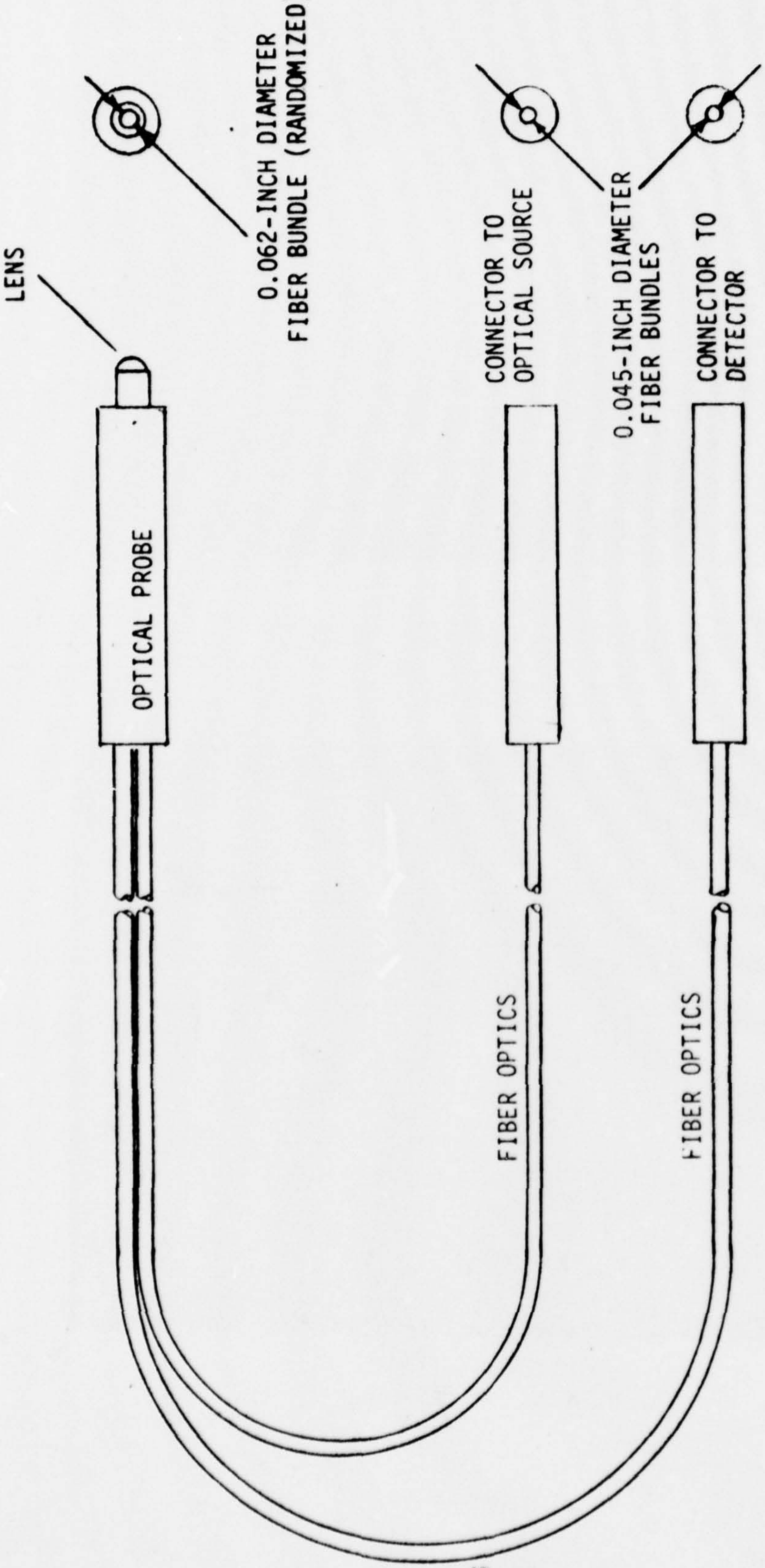

FIGURE 5.2.1
OPTICAL PROBE ASSEMBLY

FIGURE 5.2.2(a)
OBLIQUE VIEW OF OPTICAL PROBE TIP

FIGURE 5.2.2(b)
END VIEW OF OPTICAL PROBE TIP

5.3 DESIGN CONSIDERATIONS

Many different designs are possible for an optical probe for sensing of physical events. In general, all designs must provide optical paths for illuminating the subject and for returning the reflected signal corresponding to the happening of the physical event. The two paths may share the same optics, as with a single fiber or group of fibers. Using this approach, it is necessary to incorporate a directional coupler at the input end of the optics. Boeing has designed and built such directional couplers for use in an optical time-domain reflectometer. The two paths may also have separate optics as, for example, two separate fibers or groups of fibers. Using this approach, the sensing end of the fibers are combined to produce overlapping fields of view. Excitation fibers may form a core which is surrounded by response fibers, or vice versa. The fibers may also be randomly mixed or "scrambled" to produce similar results. The combined fibers may also be shaped into various forms such as a strip, a circle, a square or any geometry which provides maximum response from the object being sensed.

Unless the shape of the object being sensed is specified, a circular randomly mixed bundle is probably as satisfactory as any and, for that reason, was fabricated for this application.

5.4 PERFORMANCE

The spatial resolution and the spacing sensitivity of the probe assembly was measured on an optical bench with precision micropositioners. As with the tests of the linear displacement transducer head, a polished steel block with razor-sharp edges was used as a highly reflecting surface, the interrogation fibers were illuminated by the described light-emitting diode package, and the reflected power was measured with a United Detector Technology Model 11A Photometer.

The probe assembly was first tested with the tip polished flat. The lens of polyester resin was later added and the tests were run a second time. The normalized results of the tests are shown in Figures 5.4.1(a) and 5.4.1(b) for both cases. Figure 5.4.1(a) shows the normalized signal coupled to the photometer as a function of spacing S. For both cases, with or without a lens, the optimum coupling occurs at approximately 30 mils.

Figure 5.4.1(b) shows the relative power as the probe was moved laterally past the sharp edge of the steel block. Without the lens, it is seen that approximately 50 mils of lateral displacement was needed to effect essentially total contrast. With the lens, the required displacement was reduced slightly, thereby showing some focusing properties for the lens. With an ideal lens and parallel rays emerging from the fibers, focusing would be sharp and spatial resolution could be considerably narrowed. With the fibers used (N.A. = 0.66), only partial focusing effects could be hoped for. It is of interest to note that a slight increase in overall coupling efficiency was observed when the lens was added.

The TD-1103 Event-Counting Transducer was tested with the setup shown in Figures 5.4.2 and 5.4.3. Figure 5.4.2 shows a stroboscopic disc on the end of a rotatable magnetic drum assembly. The optical probe shown with the detector and source, is positioned at the optimum spacing of 30 mils from the disc and is looking at the inner strobe pattern with 77 marks per revolution. A close-up of the probe looking at the outer track with 133 marks per revolution is shown in the photograph of Figure 5.4.3.

Testing of the event-counter was performed by recording a magnetic "spike" signal onto a single track of the magnetic drum assembly, and comparing the ratio of the optical and magnetic counts (totaled as the drum rotated) with the known number of marks on the stroboscopic disc. To determine if the system met the desired specification of an error rate of 10^{-5} or less, tests were run until the magnetic count exceeded 10^5 counts. The rotational speed of the drum was adjusted until the specified count rate of 30,000 counts per second was achieved.

To achieve a range of count rates, various motor speeds and both 77-line and 133-line strobe disc tracks were used in the tests. The tests yielded the following results:

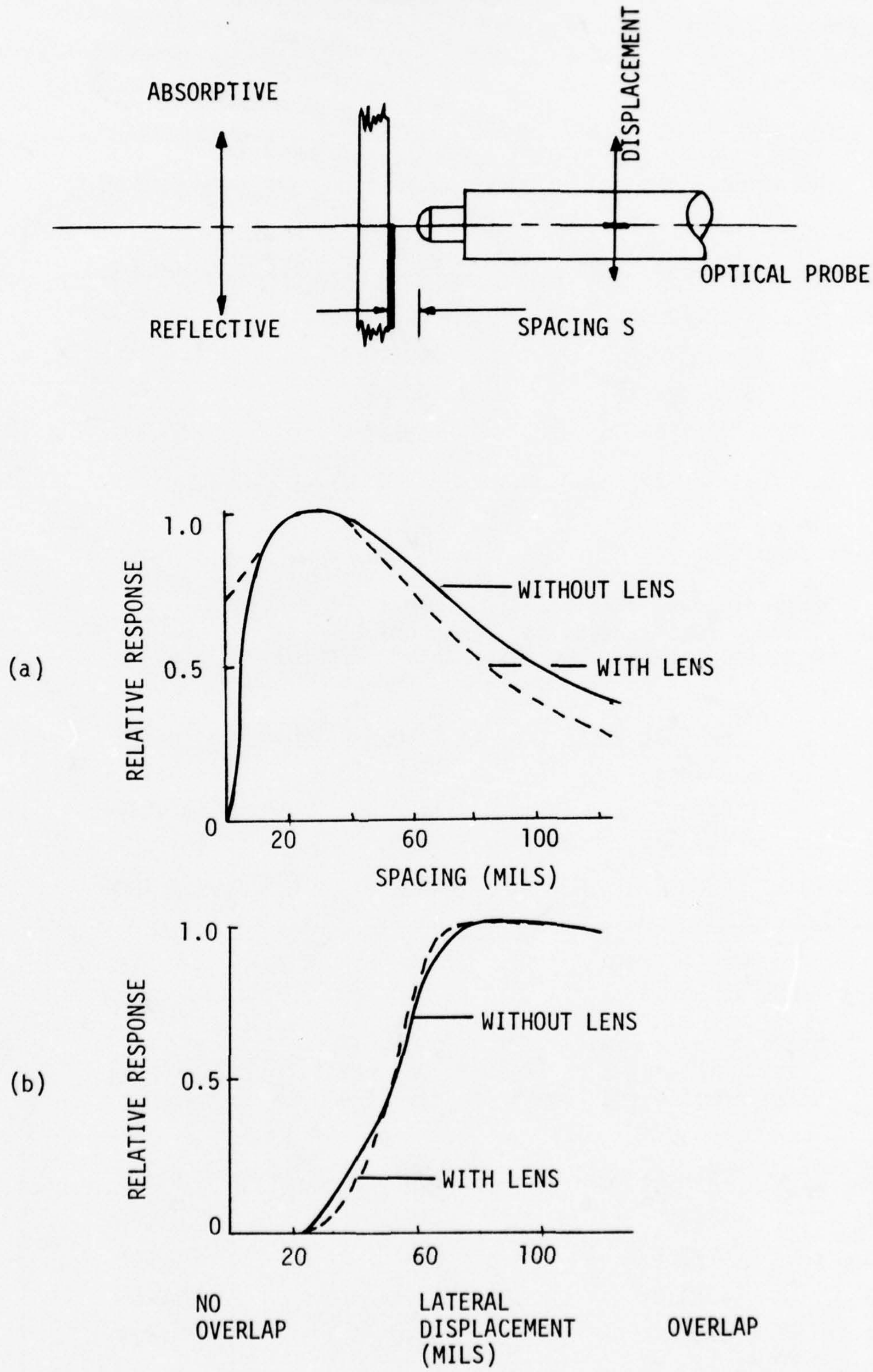

FIGURE 5.4.1

RELATIVE POSITIONAL RESPONSE

5.4 PERFORMANCE (Continued)

Test Group #1.

Optical count rate: 30,300 counts per second
Track: Outer track, 133 marks per revolution
Rotational speed: Approximately 14,000 rpm (strobe light)

Test	Optical Count	Magnetic Count	Ratio	Allowable Tolerance
1	13310653	100093	132.9829	± .0013
2	13313224	100100	132.9992	± .0013
3	13313917	100105	132.9995	± .0013
4	13315606	100117	133.0004	± .0013

Test Group #2.

Optical count rate: 20,800 counts per second
Track: Outer track, 133 marks per revolution
Rotational speed: Approximately 9,400 rpm (strobe)

Test	Optical Count	Magnetic Count	Ratio	Allowable Tolerance
1	636843	4789	132.9804	± .0276
2	624841	4700	132.9449	± .0281
3	933559	7027	132.8531	± .0188
4	732289	5506	132.9984	± .0240

Test Group #3.

Optical count rate: 15,700 counts per second
Track: Inner track, 77 marks per revolution
Rotational speed: Approximately 12,000 rpm (strobe)

Test	Optical Count	Magnetic Count	Ratio	Allowable Tolerance
1	476455	6187	77.0090	±.0123
2	477191	6197	77.0035	±.0123
3	481330	6251	77.0005	±.0122
4	476648	6190	77.0029	±.0123

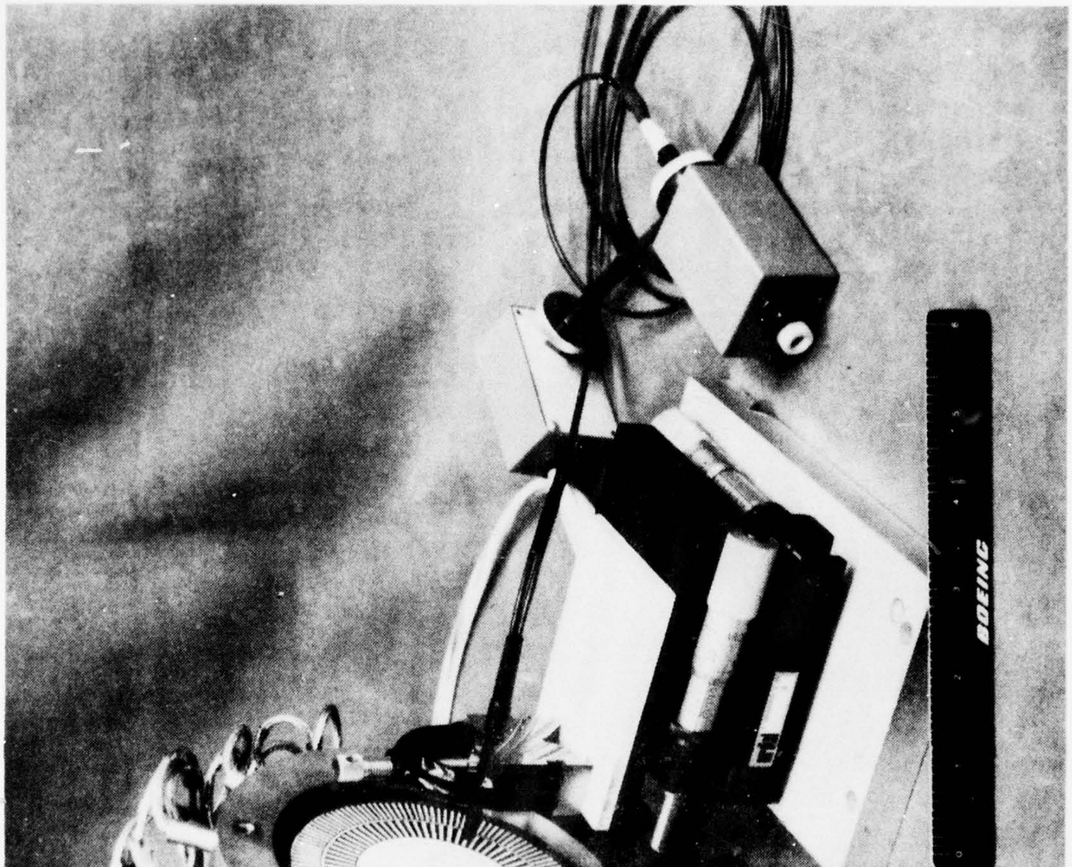

FIGURE 5.4.2
TD-1103 EVENT COUNTER AND TEST ASSEMBLY

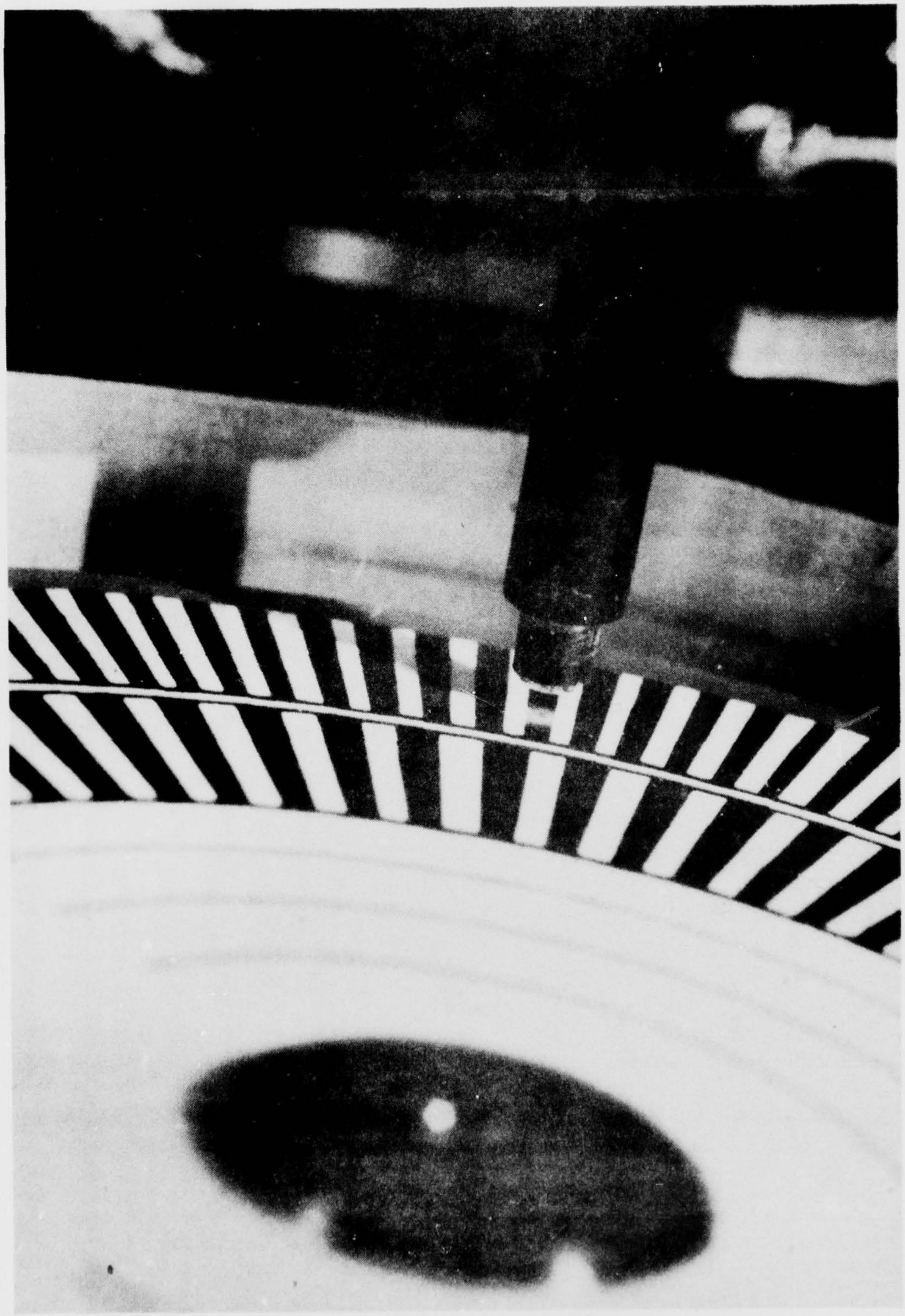

FIGURE 5.4.3
CLOSE-UP OF PROBE AND STROBE DISC

5.4 PERFORMANCE (Continued)

Test Group #4.

Optical count rate: 10,400 counts per second
Track: Inner track, 77 marks per revolution
Rotational speed: Approximately 8100 rpm (strobe)

Test	Optical Count	Magnetic Count	Ratio	Allowable Tolerance
1	312492	4058	77.0064	± 0.187
2	314526	4084	77.0142	± 0.186
3	316268	4107	77.0071	± 0.185

Test Groups #2 through #4 are included to show performance at lesser count rates. Test Group #1 (30.3 KHz) was run to check specifications. Waveforms for group #1 for the optical and magnetic pickoffs are shown in Figure 5.4.4. Part (a) shows the waveform for a complete revolution of the disc, and Part (b) displays the shape of the individual pulses. The magnetic waveforms are not clear in the photographs.

Since the event counters count integers only, a type of quantizing error is possible. The limits of the ratio error due to such effects is given by:

$$\text{Max error} = \pm \frac{R-1}{n}$$

where R = theoretical ratio

n = number of magnetic counts

These error limits are expressed as "Allowable Tolerance" in the tables.

The results of Test Groups #3 and #4 all fall within the allowable tolerance. Therefore, no error can be determined. In Groups #1 and #2, some errors are seen and are believed to be caused by nonuniformities of the stroboscopic disc along the outer track, which has bar and space widths approximately equal to the resolution of the probe. These widths were measured and were found to vary from 33 mils to 53 mils. The narrow lines in particular are troublesome as when they were viewed by the probe, considerable overlap occurred, which reduced apparent contrast. The inner track had, with only 77 marks per revolution, sufficiently wide marks and spaces to not cause a problem.

A similar type of effect would be caused by variations in the intensity of the marks. In some cases, the bars were of low density, and the spaces were occasionally dirty. Such variations would also reduce contrast at their respective points. The effects of intensity variations and width variations are obvious in Figure 5.4.4. Errors would easily occur due to difficulties in setting a proper threshold level for the optical counter. The solution to these problems lies simply in obtaining or producing a more uniform stroboscopic disc.

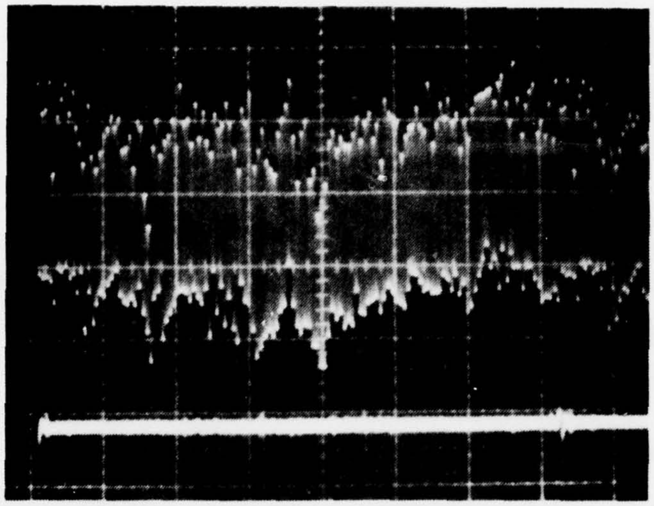

FIGURE 5.4.4(a)
EVENT COUNTER WAVEFORMS

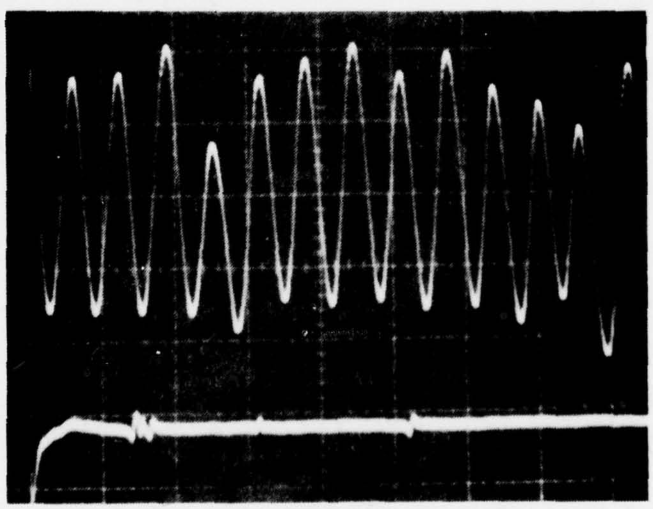

FIGURE 5.4.4(b)
EVENT COUNTER WAVEFORMS

5.4 PERFORMANCE (Continued)

Electrical noise in the system can also cause errors. If noise is assumed to be additive and gaussian the probability of error due to its effects (per bit) is given as:

$$P_e = \frac{1}{2}\left(1-\mathrm{erf}\ \frac{A}{2\sqrt{2N}}\right)$$

where: A = peak signal voltage at comparator input

N = mean square noise voltage at comparator input

A ratio of $A/\sqrt{N}$ of 19 db ensures a probability of error of less than 10^{-5}. In our case, the signal to noise ratio was measured to be almost 60 db, greatly exceeding the requirements for a bit error probability of 10^{-5}.

5.5 CONCLUSIONS

The results of the test indicate the feasibility of a fiber optic event counting transducer. The measured ratios never substantially deviated from ideal values, and what deviations did occur could be adequately explained by stroboscopic disc nonuniformities or by the inevitable quantizing effects of the counters used.

In future work, it is recommended that further research be carried out regarding a focusing lens on the tip of the fiber optic probe. Perhaps low numerical aperture fibers should be investigated as well as various lens shapes. Resolution can also be improved through the use of smaller fibers and fewer fibers, with less coupled power as a penalty unless a small-area high-radiance source is used.

The purpose of this study has been to investigate this form of fiber optic probe strictly as a two-state event counter and has not dealt with a host of possible analog applications. Figures 5.4.1(a) and (b) show the analog response of this probe in two planes. Because the probe contains a large number of parallel fibers of large numerical aperture, the analog response is quite broad in both planes. Similar characteristics are shown in Figures 4.3.2(a) and (b) for a probe with fewer nonparallel fibers of low numerical aperture. The general shapes of the two sets of curves are generally similar but the sensitivities to motion differ greatly. With proper tailoring, probes can be designed with sensitivities adequate to measure vibration, shaft runout, bearing "noise", acceleration, etc. It is felt that the principle can be applied profitably to many difficult analog instrumentation problems and is worthy of further detailed investigation.

6.0 FLOW-RATE SENSOR (TD-1104)

6.1 FUNCTION

The TD-1104 Flow-Rate Sensor was designed to demonstrate the feasibility of digitally sensing the flow rate of liquids and gasses with an electrically passive optical transducer, the input (interrogation) and outputs (response) of which are coupled by means of fiber optic cables. The basic sensor operates on a mass-flow principle and the output is a series of optical pulses with a repetition rate proportional to flow rate. For this particular sensor, 10,800 ± 10% optical pulses are produced for each US gallon of flow. For a flow rate of one US gallon per minute, the output pulse rate is 180 Hz ± 10%. Conversion of flow rate to any desired engineering units may be accomplished by selecting an appropriate counting period. Volume of flow during a given time interval can be determined by totalizing the output pulses during that interval.

Because this transducer has no electrical connections, it should be particularly useful for the measurement of flow rate of flammable and/or explosive materials.

6.2 DESCRIPTION

The TD-1104 Sensor is shown in the photograph of Figure 6.2.1. It consists of four basic elements: (1) an optical source, (2) a fiber optic probe assembly, (3) a turbine-type converter which converts flow rate to angular velocity, and (4) a response detector assembly. Light from the optical source is conducted from the source by one fiber optic bundle to the turbine where it illuminates the tips of the turbine rotor blades. Light reflected from the rotor blade tips enters a second fiber optic bundle and is conducted to the detector where it is converted into a proportional electrical signal.

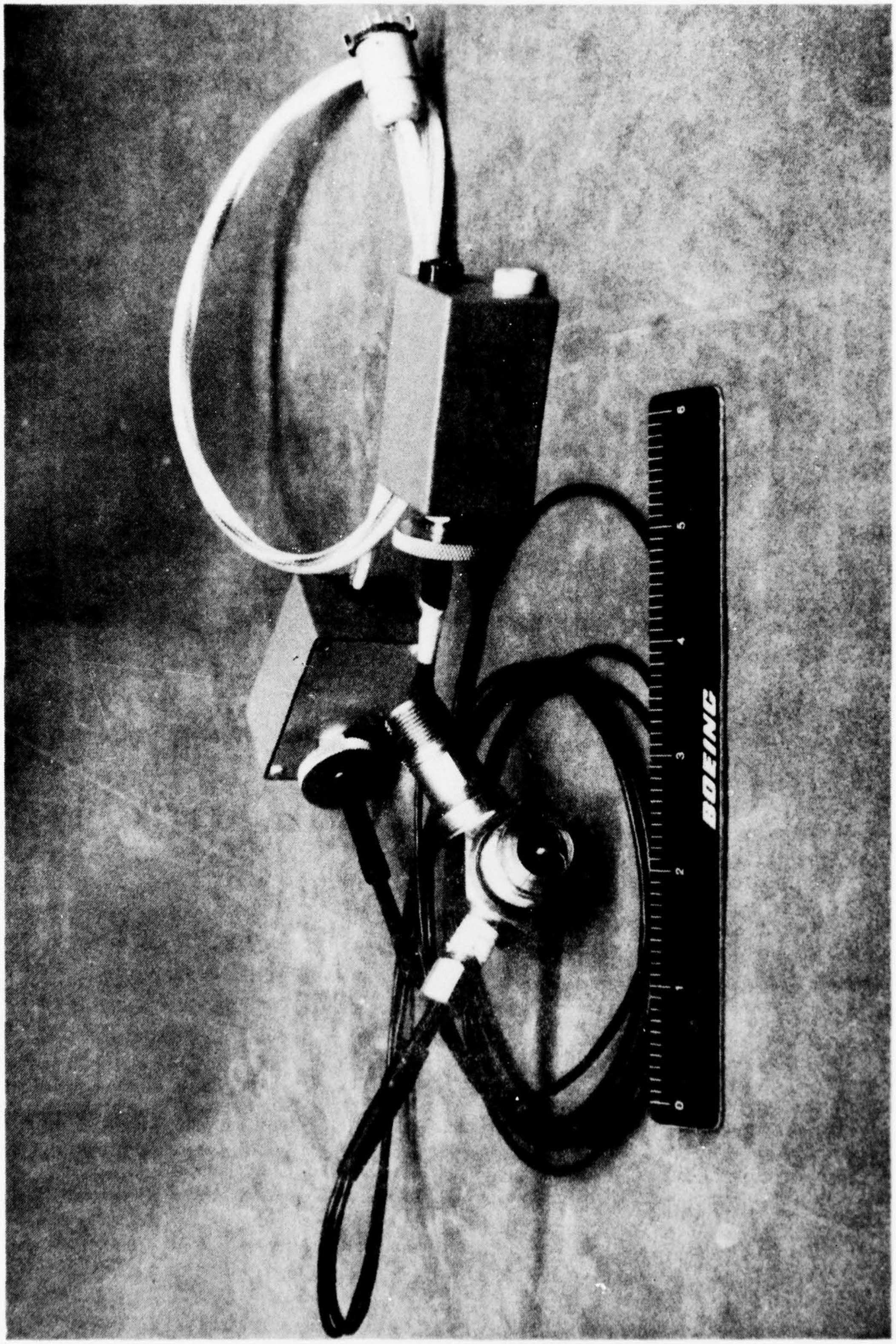

FIGURE 6.2.1
TD-1104 FLOW RATE SENSOR ASSEMBLY

6.3 DESIGN CONSIDERATIONS

The principle of the TD-1104 Flow-Rate Sensor is illustrated in Figure 6.3.1.

The turbine-type converter assembly is a modified Flow Sensor, Boeing Drawing Number SE 5/8-5005A. This sensor contains a rotor with a diameter of 0.625 inch with twelve blades which have a pitch of 30°. The rotor has four magnetic poles which are sensed as the turbine rotates by a magnetic pickup, which was left intact for comparison with the optical probe response. The gage factor of this sensor with the magnetic pickup is 1800 cycles/U.S. Gallon ± 10%. The converter assembly was modified to accept the optical probe such that the passage of the rotor blades would be sensed. The electrical outputs from the magnetic pickup and the optical probe were coupled into separate counters for comparison.

The optical source for the flow rate sensor was a type LED-55c light-emitting diode mounted in an enclosure with a series resistor which limited the forward current to 100 milliamperes. The enclosure has also a connector which mates with the fiber optic connector to the probe assembly.

The optical probe assembly shown in Figure 6.3.1 was made up of two 0.045-inch diameter fiber optic cables which merge within the probe to form a single randomized bundle with a diameter of 0.062 inch. The other ends of the fiber optic cables were terminated in connectors to mate with the optical source and the detector. The optical probe was fitted with a 0.125-inch diameter polyester lens which serve to positively seal the fiber termination against fluid leakage and also to concentrate the radiated light as well as distribute the reflected light. The optical probe is identical to the one described in Section 5.0 "Event-Counting Transducer".

Typical electrical waveforms for the magnetic pickup and the optical probe are shown in Figure 6.3.2. The waveforms show a 6:1 frequency ratio which results from the optical probe producing twelve cycles (from twelve blades) per rotor rotation and the magnetic pickup producing only two (from four magnetic poles). The optical probe waveform photograph of Figure 6.2.4 shows a periodic amplitude modulation which is synchronous with the magnetic pickup waveform and, hence, synchronous with rotor rotation. The modulation is believed to have been caused by a slight rotor eccentricity.

The detector consists of a UDT Type PIN6D large-area PIN photodiode coupled to a low-noise FET-input amplifier. The bandwidth of the detector/preamplifier is approximately 30 KHz.

6.4 PERFORMANCE

Rather than using a separate flowmeter as a comparison reference for determining the accuracy of the TD-1102, the original magnetic pickup was retained for this purpose. As discussed previously, there was a 6:1 ratio between the rate outputs of the optical and magnetic pickup outputs.

For performance verification, a series of tests were ran using compressed air and several different fluids. The optical and magnetic outputs were

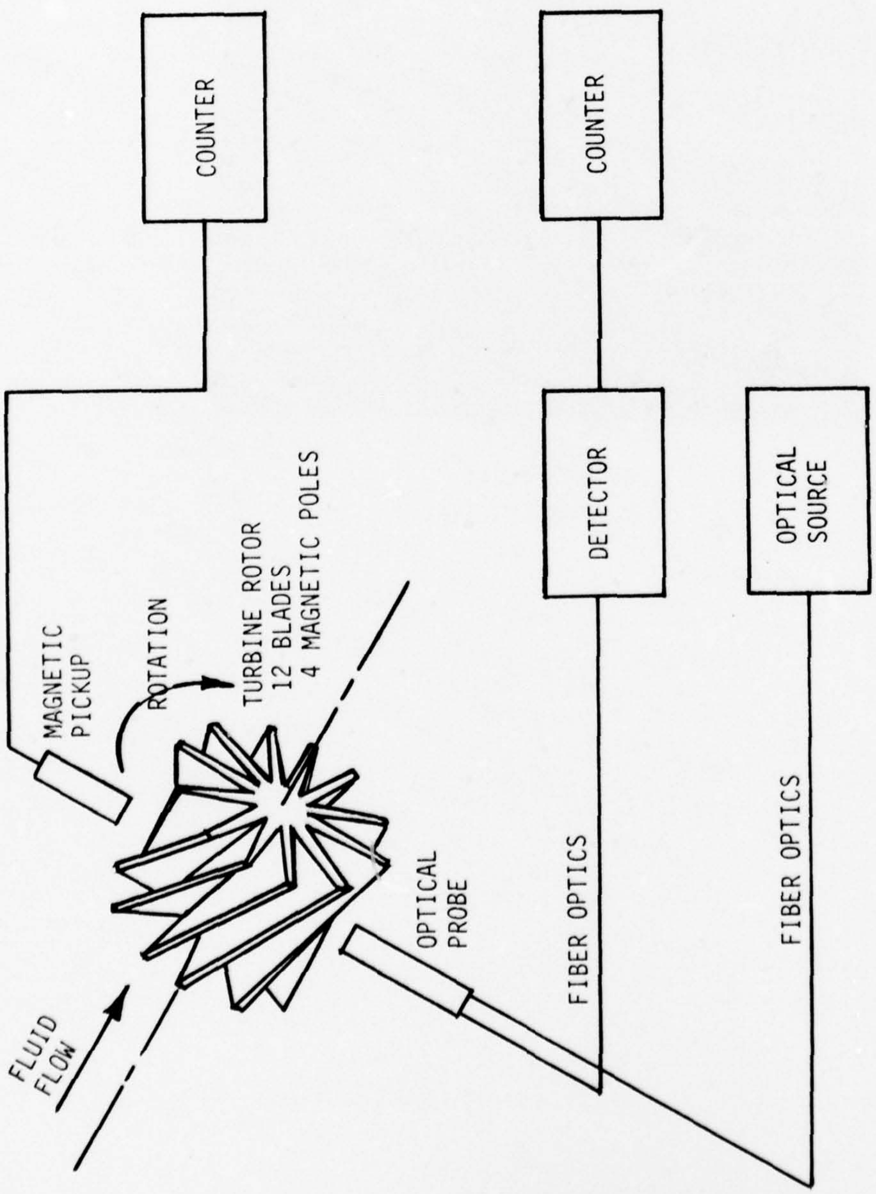

FIGURE 6.3.1
FIBER OPTIC FLOW RATE SENSOR
CONCEPTUAL BLOCK DIAGRAM

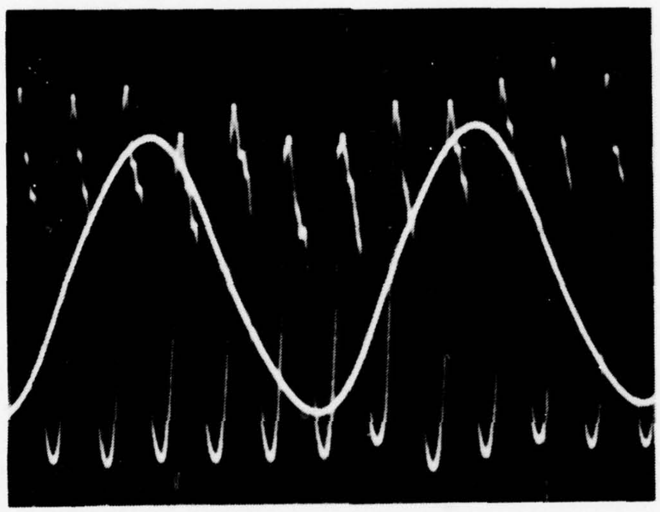

FIGURE 6.3.2
WAVEFORM PHOTO

6.4 PERFORMANCE (Continued)

counted by separate counters with a common gate for a period of 30 seconds. The ratio of the two counts was then compared to the ideal ratio of six to verify the performance. Following is a tabulation of the test results:

FLUID: Air; Time - 30 seconds

Approx. Optical Pulse rate (sec^{-1})	Total Optical Count	Total Magnetic Count	Ratio
3000	90480	15080	6.0000
2500	76574	12762	6.0002
2000	60829	10139	5.9995
1500	45562	7594	6.0013
1000	31337	5223	5.9998
500	15084	2514	6.0000

FLUID: Water; Time - 30 seconds

Approx, Optical Pulse rate (sec^{-1})	Total Optical Count	Total Magnetic Count	Ratio
1400	43157	7193	5.9999
1250	37750	6292	5.9997
1100	33474	5579	6.0000
1000	30183	5030	6.0006
850	25699	4284	5.9988
650	19588	3264	6.0012
500	14962	2493	6.0016
300	9242	1540	6.0013
100	2809	468	6.0021

6.4 PERFORMANCE (Continued)

FLUID: Hydraulic fluid; Time = 30 seconds

Approx. Optical Pulse rate (sec^{-1})	Total Optical Count	Total Magnetic Count	Ratio
800	23967	3995	5.9992
700	20917	3486	6.0003
500	15048	2508	6.0000
300	8826	1471	6.0000
100	3125	521	5.9981

FLUID: Stoddard solvent (properties similar to JP4 fuel); Time = 30 seconds

Approx. Optical Pulse rate (sec^{-1})	Total Optical Count	Total Magnetic Count	Ratio
1300	39736	6623	5.9997
1100	33393	5566	5.9995
900	27188	4531	6.0004
700	21509	3584	6.0014
500	14894	2482	6.0008
300	8826	1471	6.0000
100	2750	459	5.9913

FLUID: Water and hydraulic fluid emulsion; Time - 30 seconds

Approx. Optical Pulse rate (sec^{-1})	Total Optical Count	Total Magnetic Count	Ratio
1400	42672	7112	6.0000
1250	37862	6310	6.0003
1100	33083	5514	5.9998
1000	30653	5109	5.9998
850	25313	4218	6.0012
650	19434	3195	6.0826
500	14928	2488	6.0000
300	8979	1496	6.0020
100	2742	457	6.0000

6.5 CONCLUSIONS

The test results clearly demonstrate the feasibility of using an optical pickup in a turbine-type flowmeter. It was originally felt that turbulence around the rotor might prevent the optical detection of the turbine blade tips, particularly with certain types of fluid. This effect was not noted. Even though the oscilloscope waveform showed somewhat more noise at the higher flow rates, in no case did the count ratio depart significantly from the ideal ratio of six. The hydraulic fluid/water emulsion should have created the most unfavorable condition. At high flow rates this emulsion was whipped into a pink creamy froth which should have both absorbed and scattered the radiation. Even in this test, the magnetic and optical counts differed by only 1.4%.

The optical probe was examined after the test and the polyester lens showed considerable erosion. In any future design, it is recommended that the probe be made from a single large clad glass rod---possibly with a lens surface ground on the tip. The glass rod would be easily sealed into the housing and would resist erosion better than the polyester. The fiber optics would interface with the rod external to the transducer.

The use of a turbine-type converter for measurement of flow rate is not new. However, the conventional pickup for such a converter is magnetic rather than optical. The relative advantages and disadvantages of the magnetic and optical pickups are as follows:

MAGNETIC PICKUPS

Advantages	Disadvantages
Simplicity. Self-generating electrical output.	Finite drag on rotor because of self-generation.
	Output amplitude non-constant-proportional to flow rate.
	Limited flow rate range.
	Electrical connections unattractive in inflammable and explosive environments
Count unaffected by bubbles and turbulence.	Not suitable for fluids with magnetic properties.

OPTICAL PICKUPS

Advantages	Disadvantages
Zero drag on rotor.	Requires associated electronics.
Output amplitude constant with varying flow rate.	
Will function with fluids with magnetic properties.	Will not function with densely opaque fluids.
Completely safe in inflammable and explosive environments.	

7.0 STRAIN SENSOR (TD-1105)

7.1 FUNCTION

The function of the Strain Sensor is to demonstrate the feasibility of digitally sensing mechanical strain or very small mechanical motion with an electrically passive optical sensor, the input (interrogation) and outputs (response) of which are coupled by means of fiber optic cables.

A principal objective of this effort was to determine the practical resolution limit of such a sensor using gratings to form an optical encoding pattern. The model resulting from this effort successfully demonstrates a resolution of 0.25 mil over a range of 64 mils.

7.2 DESCRIPTION

The feasibility model Strain Sensor assembly is shown in the photograph of Figure 7.2.1. As illustrated in Figure 7.2.2, the sensor is composed of four basic elements:

1. A viewing slit array containing eight parallel transparent slits, each 0.25 mil wide. The array of slits is on a glass substrate 5 mils thick. The background is an opaque chromium thin film.
2. An encoding plate containing a pattern of seven 50% gratings, each progressively coarser by a factor of two. This pattern is likewise chromium, deposited by thin-film techniques on a 5-mil thick glass substrate.
3. An interrogation fiber head assembly containing eight slots which align with corresponding slits of the slit array. Each slot contains a linear array of twelve interrogation fibers.
4. A response fiber head assembly containing eight slits which also align with corresponding slits of the slit array. Each slot contains a linear array of twelve response fibers.

These four elements are shown enlarged in the photograph of Figure 7.2.3.

The slit pattern is aligned relative to the grating pattern in a manner such that, when viewed through the slit pattern, an eight-bit Gray-coded binary word is formed which indicates the position of the sliding encoding plate relative to the fixed slit array.

The interrogation and response fibers are bundled into cables which interface with the SR-1100 Scanner/Receiver.

The design dimensions of the slit array and encoding plate are detailed in Figures 7.2.4(a) and (b) respectively. The slits have a width of 0.25 mil, as do the lines in the finest of the seven gratings. Slits and grating lines both have a length of 31 mils. The wide parallel tracks along both edges of both patterns provide large bearing surfaces upon which the two elements may slide relative to each other without danger of abrading the gratings or the slits. Since the sensor provides eight-bit encoding of 0.25-mil quanta, each

7.2 DESCRIPTION (Continued)

grating pattern has a length of 256 x 0.25 = 64 mils. Isolation between tracks is provided by including a six-mil spacing between gratings.

Following is a brief discussion of the processes used in producing the slit array and encoding plate. The original artwork was cut onto Ruby Studnite (rubylith) with a Haag-Streit Coordinatograph. See Figure 7.2.5. The Gray-code pattern was begun by cutting single slits that were 16 inches long and as wide as needed to generate the final bars and spaces after x512 photo reduction. The full-size artwork slits were each run through a step and repeat exposure process on a Borrowsdale "Microminiaturization" Camera (Figure 7.2.6) to generate the needed bar and space patterns on low-shrinkage high contrast film. The tracks were simultaneously reduced x8.

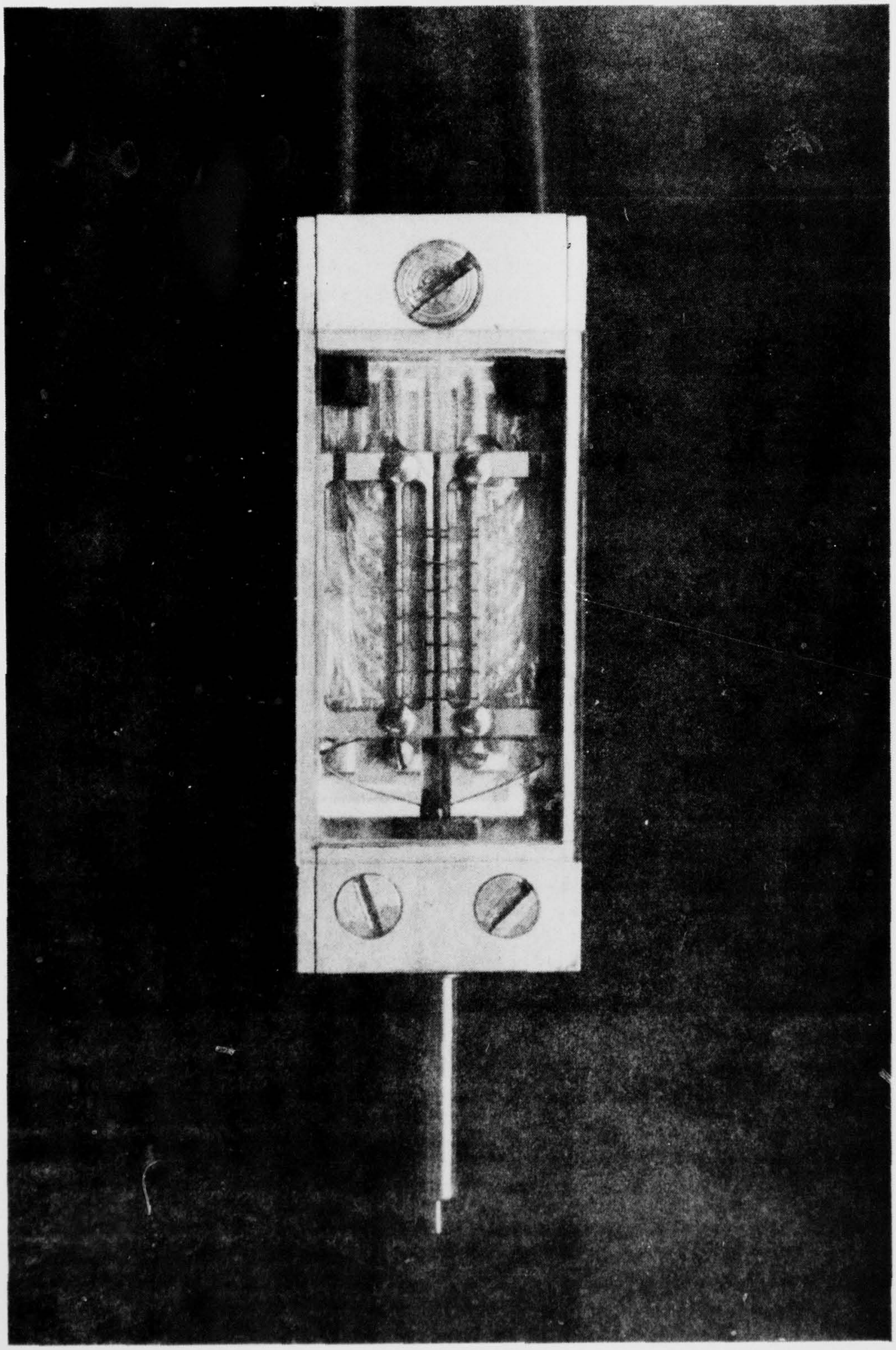

FIGURE 7.2.1
TD-1105 STRAIN SENSOR

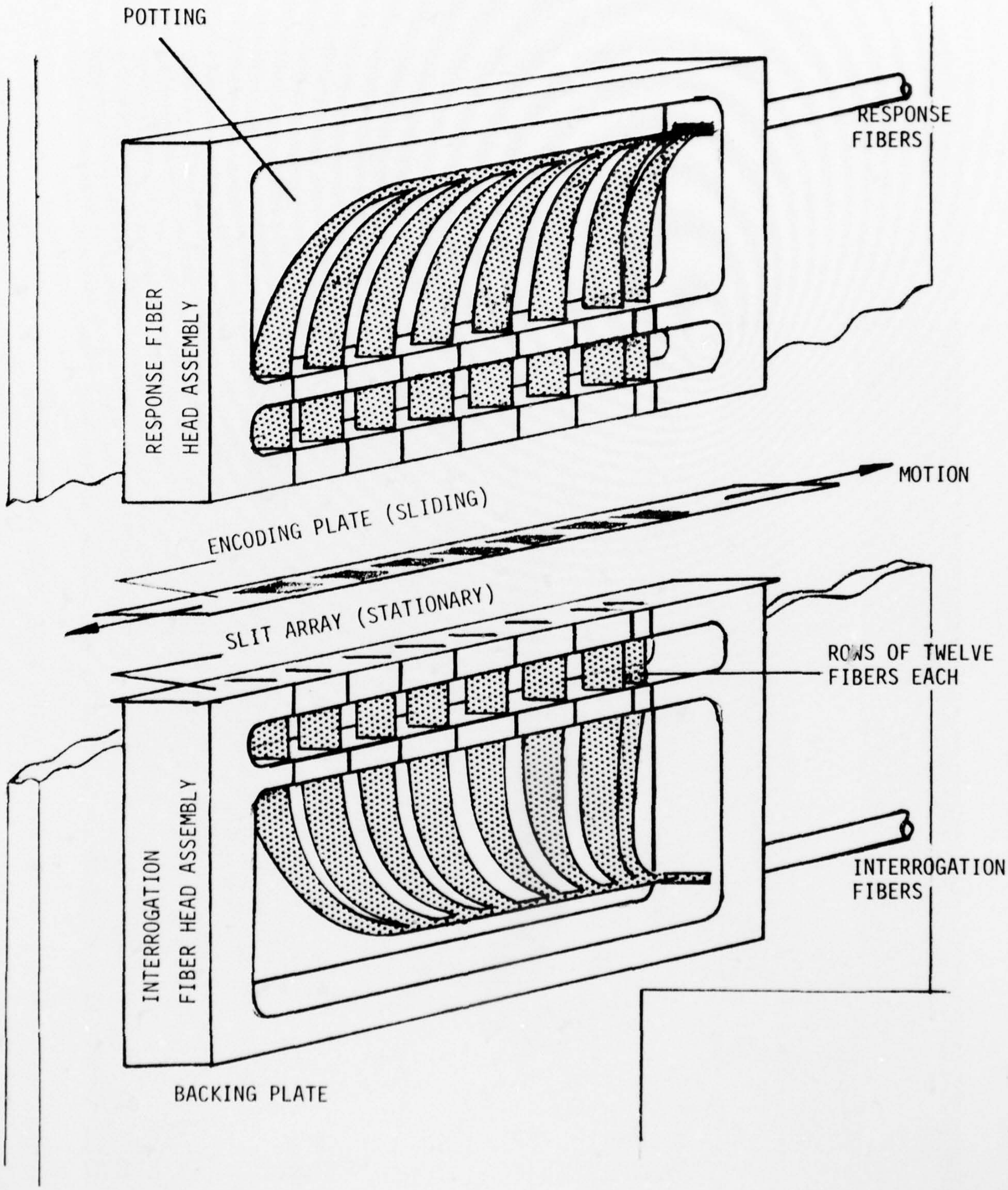

FIGURE 7.2.2
FIBER OPTICS STRAIN SENSOR
(SEMI-EXPLODED VIEW)

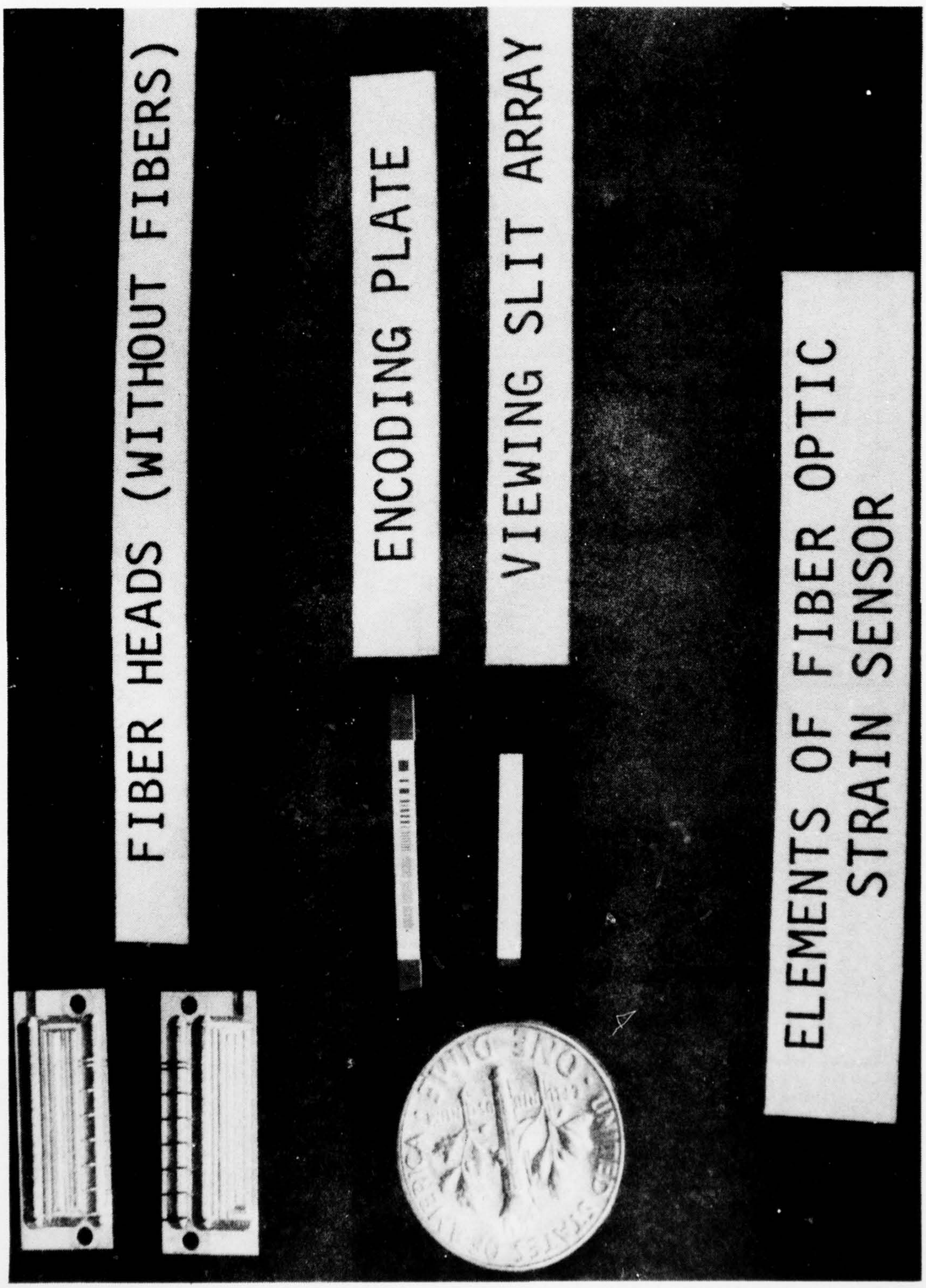

FIGURE 7.2.3
ELEMENTS OF FIBER OPTIC STRAIN SENSOR

A) 0.25 MIL VIEWING SLIT ARRAY

B) TRANSMISSIVE GRAY-CODED PLATE

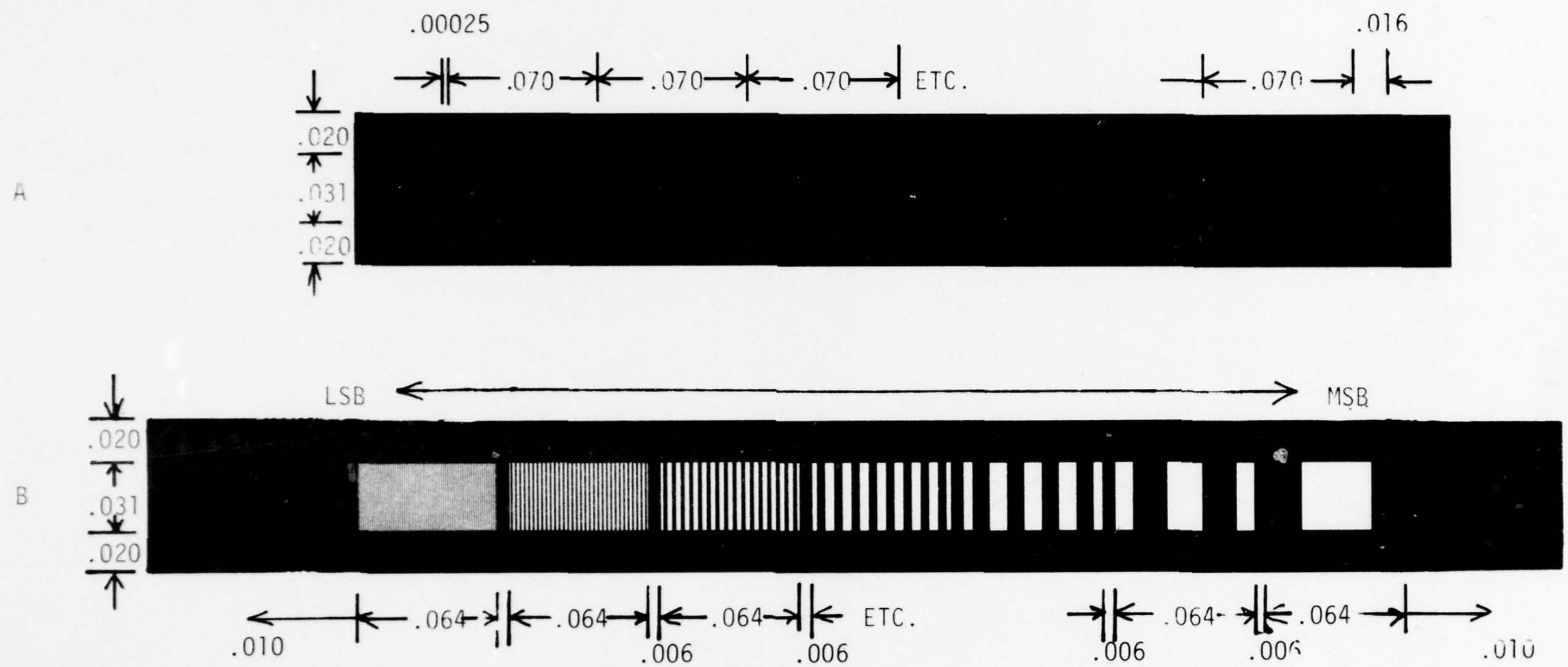

FIGURE 7.2.4

PATTERN DIMENSIONS

7.2 DESCRIPTION (Continued)

The seven sections of film (notice that the seventh and eight track of the Gray code have been combined into one track) were then assembled to an accuracy of 0.1 mils across the pattern on the Coordinatograph. This artwork was then photo reduced by x64 to yield the final pattern with 0.25 mil resolution. Kodak high-resolution glass plates were used.

The viewing slit array was cut x64 scale and was used as an alignment aid for the assembly of the grating pattern. It was then reduced x64 also.

The two patterns were then individually deposited onto 22mm x 22mm microscope slide cover glass plates that are 5 mils in thickness. The vacuum deposition chamber was a Temescal BJD-1800, with a CV-8 Electron gun and a Kronos Thin Film Deposition Controller ADS-100. The deposition assembly is shown in Figure 7.2.7.

The patterns were next scribed and broken to a size slightly greater than final design on a Tempress Diamond Scribing Tool, and were then lapped down to a final working width of 71 mils and with polished edges. The lengths are as shown previously.

Figures 7.2.8 and 7.2.9 show the configuration of the individual fibers inside the heads. The fibers chosen were from bundles of Galite 1000 of the Galileo Corp. for good strength and flexibility, and also for consistency in fiber sizes. The average diameter of an individual fiber (with cladding) is 2.7 mils.

It was calculated in the third quarterly report that with a 0.5 mil-slit and a single fiber, nearly 50 nanowatts of power could be coupled to the receiver. With a 0.25 mil slit, and twelve fibers as used in the shown configuration, power in the neighborhood of 250 nanowatts should be expected per channel. Several factors such as diffraction, scattering, reflection, etc. will be encountered, but their effects should not be damaging.

FIGURE 7.2.5
COORDINATOGRAPH

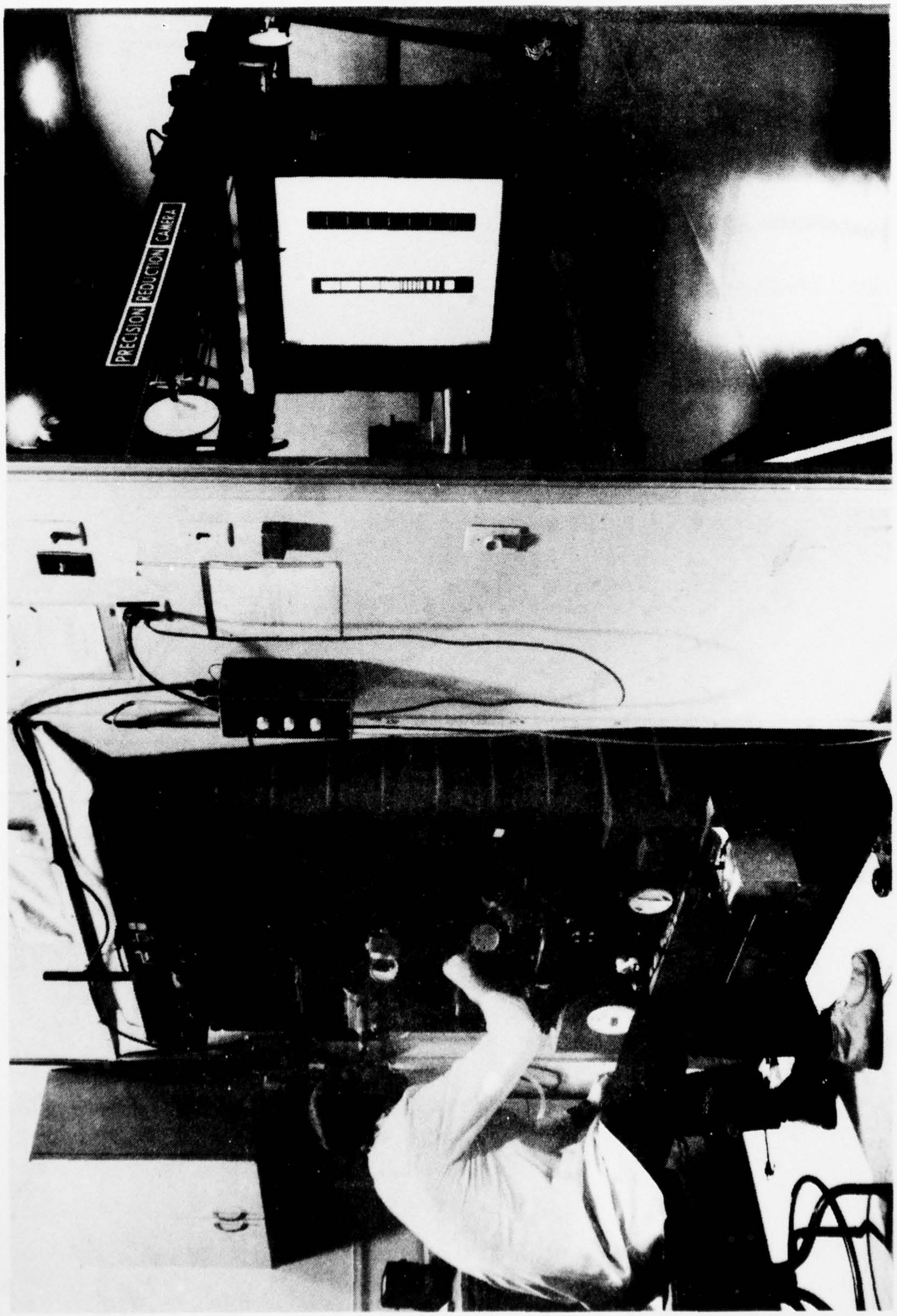

FIGURE 7.2.6
PHOTOREDUCTION CAMERA

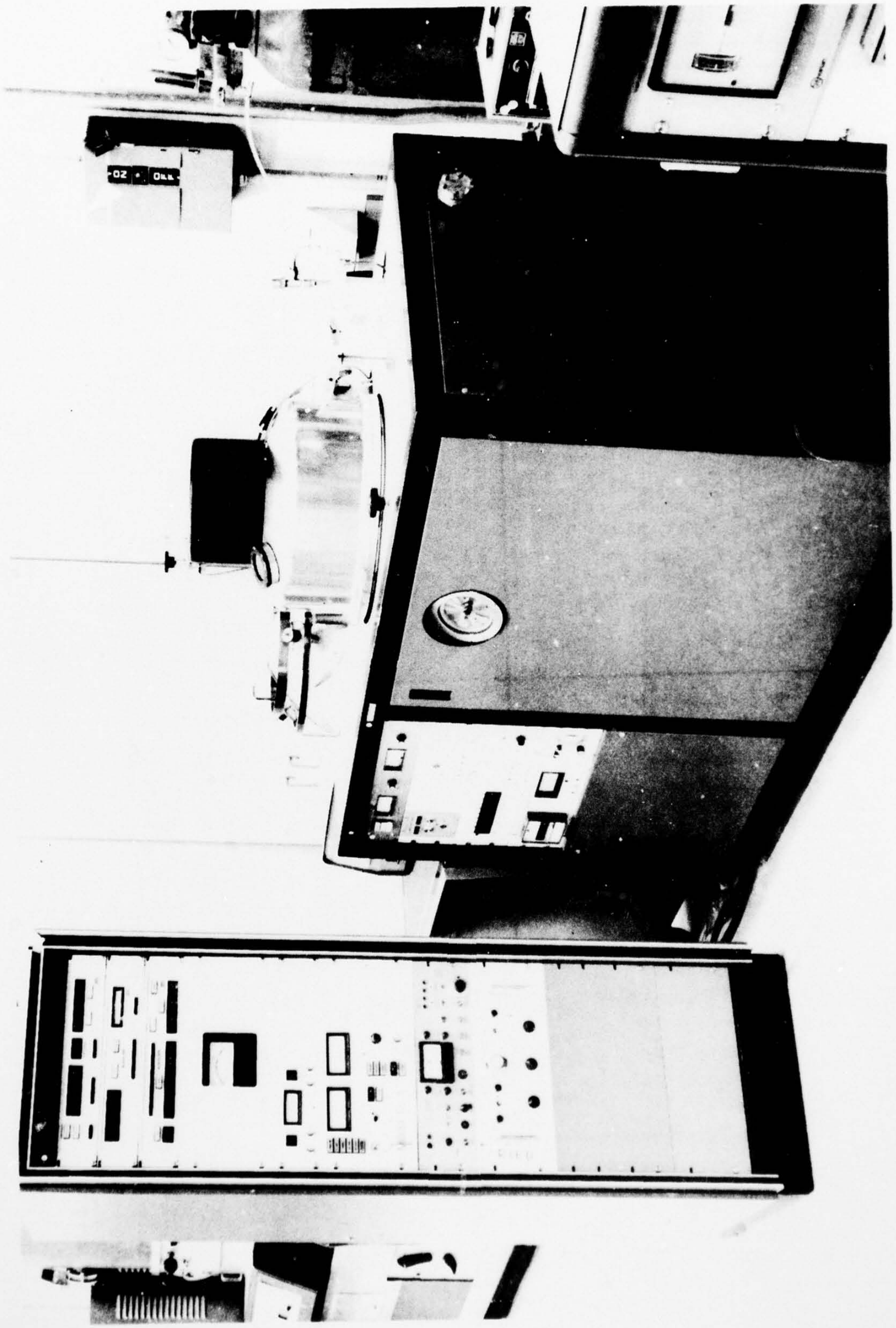

FIGURE 7.2.7
VACUUM DEPOSITION UNIT

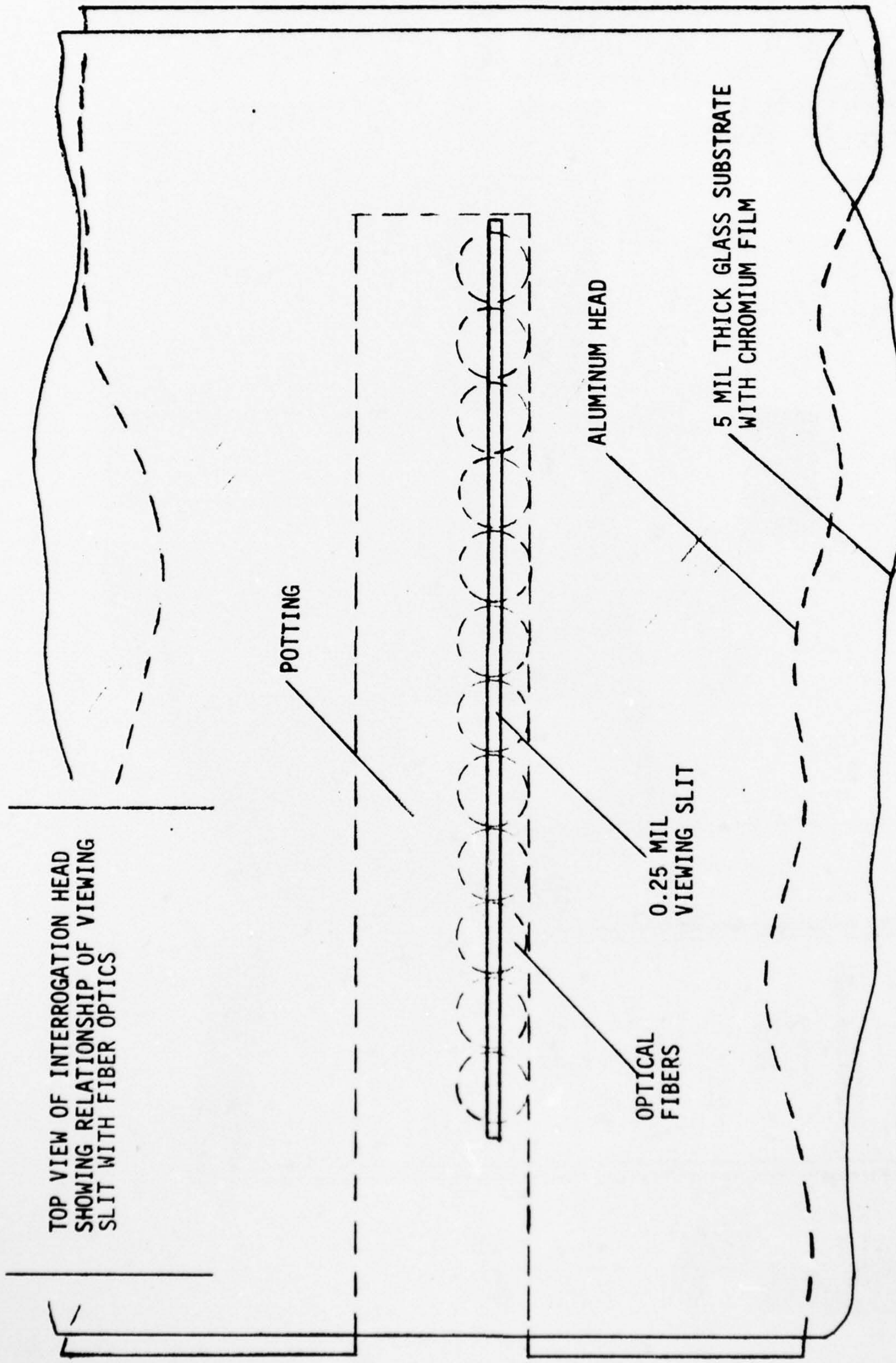

FIGURE 7.2.8
FIBER AND SLIT CONFIGURATION

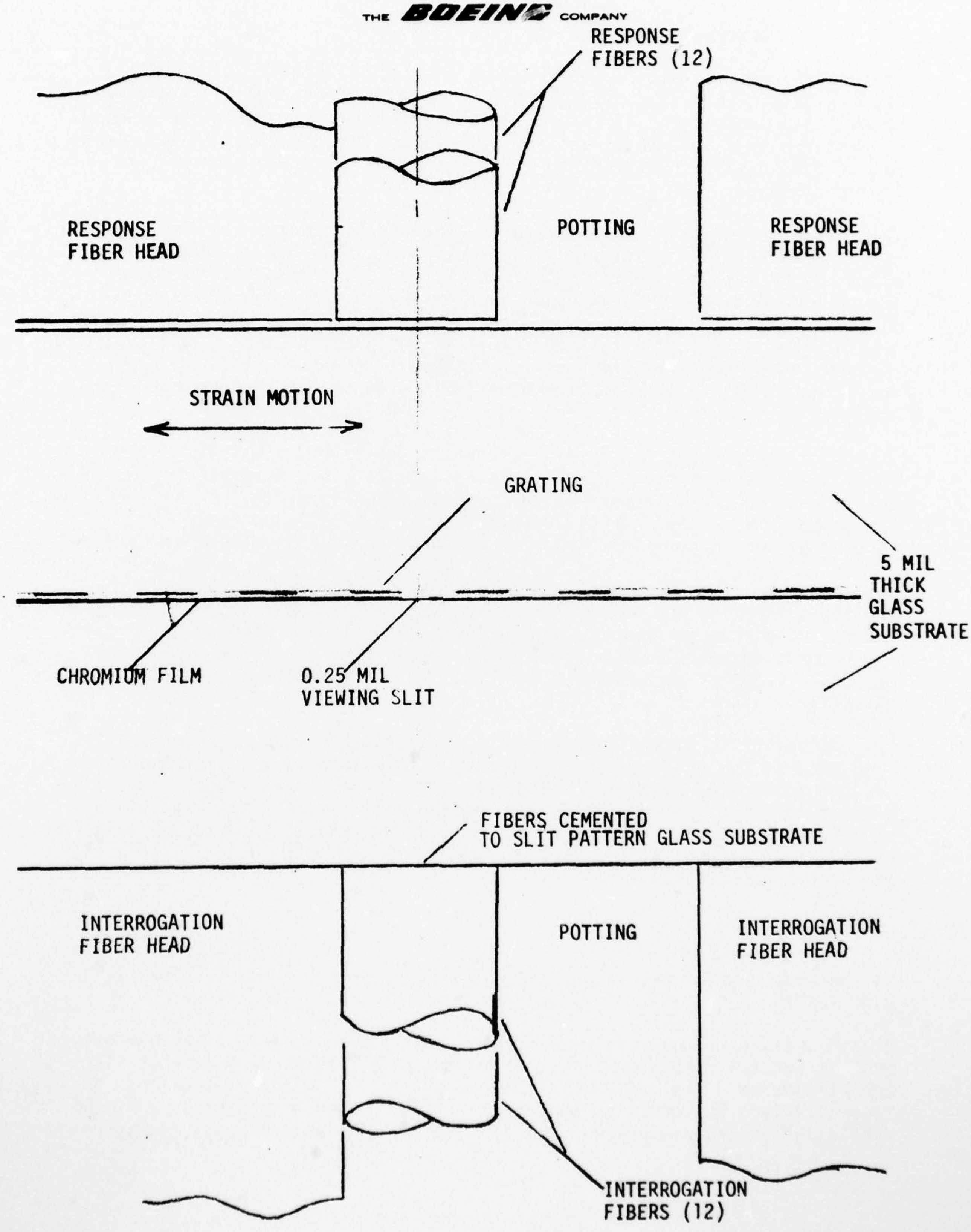

FIGURE 7.2.9

STRAIN SENSOR CONFIGURATION

7.3 DESIGN CONSIDERATIONS

The original design goal was to resolve one microstrain or better in the least-significant bit using eight-bit encoding. After initial investigation showed that achievement of this goal would be impossible using the original concept and available materials and techniques, the objective of the study was changed, by the customer, to explore the limitations of the original concept instead.

The original concept to be explored is shown in Figure 7.3.1. The strain or small motion sensor consists basically of two opposed 50% gratings, A and B. Alternate excitation and response fibers C and D are mounted in proximity to, or are cemented to, grating A which is 50% absorptive and 50% transmissive. Grating B is 50% absorptive and 50% reflective. As motion occurs in the plane of the grating, and normal to the grating lines, the reflective regions are alternately exposed and obscured to the optical fibers. A motion equal to one grating line-width will produce a change from maximum absorptive to maximum reflective, thereby quantizing the motion.

The concept of Figure 7.3.1 requires the use of both transmissive and reflective plane gratings with 1:1 mark/space ratios. By employing several gratings which are successively coarser by multiples of two, or by tailoring the geometry such that the differential motions differ successively by factors of two, a parallel binary encoding of the motion can be achieved.

The sensor as shown operates on a reflection principle. If both gratings are 50% absorptive and 50% transmissive, and if the excitation and response fibers are placed on opposite sides, then a sensor with similar properties can be made to operate on a transmission principle. A transmissive case may prove superior as transmission losses could most likely be made less than reflection losses.

In application to strain measurement, sensitivity greater than the spatial frequency of the grating can be had simply by extending the length of the grating substrates as shown in Figure 7.3.2. A substrate length 1,000 times greater than the half-period of the grating will increase the sensitivity by a factor of 1,000. Considering a strain gage with a length L between points of attachment to a structure, and a grating space d, the resolvable strain or unit deformation δ is:

$$\delta = \frac{d}{2L}$$

To meet the design goal of one microstrain, or $\delta = 10^{-6}$ requires that the gage length be $0.5(10^6)$ times greater than the grating spacing.

Blazed gratings are commonly available with as many as 1200 lines per millimeter. Special blazed gratings may be obtained with as many as 3600 lines per millimeter. The grating spacings are 0.833 and 0.278 micrometers respectively. The corresponding gage lengths required to achieve a resolution of one microstrain are 417 and 139 millimeters respectively.

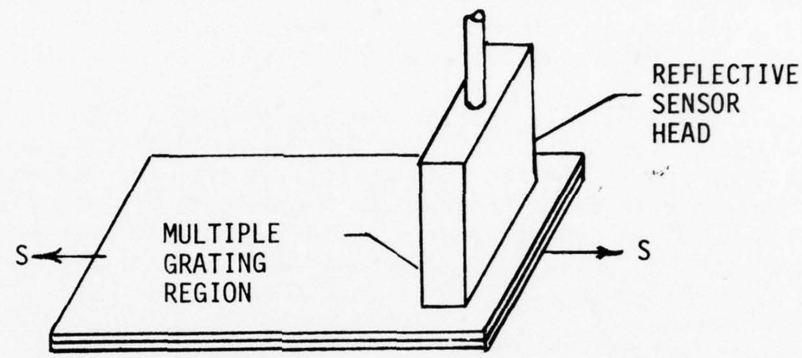

FIGURE 7.3.1(a)

BASIC CONCEPT---REFLECTIVE

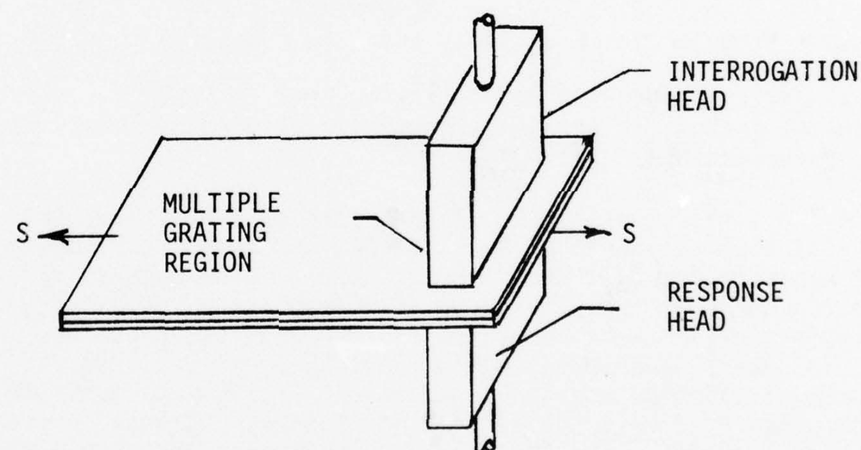

FIGURE 7.3.1(b)

BASIC CONCEPT---TRANSMISSIVE

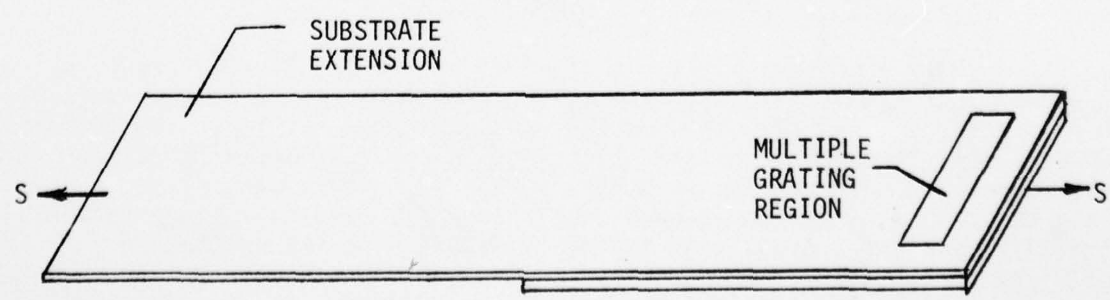

FIGURE 7.3.2

INCREASING SENSITIVITY BY EXTENSION

7.3 DESIGN CONSIDERATIONS (Continued)

Ideally, the grating coating materials would be sufficiently hard and abrasion-resistant to permit sliding motion between the contacting surfaces of the two gratings. To minimize transducer losses due to beam divergence, the substrate thickness should be no more than a few tenths of a millimeter.

With regard to commercially available plane gratings, with grating surfaces sufficiently hard for this application, those gratings produced by Johannes Heidenhain GmbH for The Ealing Corporation are probably the most suitable. The Heidenhain gratings are produced by the patented "Diadur" process in which a hard metal is deposited upon a glass substrate. The metal is harder than Inconel and the glass is flat within 10 Newton rings. The standard thickness is 5 millimeters, which is much too thick for this application. All factors considered, it appears that no commercially available gratings can be made to function in this application using the original concept.

It appears that the only feasible means for producing suitable gratings at this time without extensive process development is to use conventional thin-film deposition techniques. Chromium is probably one of the better deposition materials because of its hardness and good adhesion properties.

Several different grating configurations may be used to convert a small mechanical motion (or strain) into a digitally-encoded measurement via fiber optic transmission lines.

Figure 7.3.3, illustrates the original and most basic concept. For an eight-bit digitally encoded measurement, the encoding elements would have eight separate tracks wherein the grating of each successive track would be twice as coarse as the previous. If transmissive, rather than reflective grating properties were used, the two gratings would be identical and, at least in theory, mechanical motion would be resolved into 256 levels and the measurement would be encoded in eight-bit straight binary. This approach, however, has an inherent practical limitation. Because several bits may change state at the same time, very large errors may appear if only very slight misalignment should occur between the two gratings, or if the transmission properties vary slightly from grating-to-grating, or if the decision elements in the following electronics exhibit slightly different threshold levels. This limitation is the reason why nearly all digital position encoders employ the Gray code in which only one bit changes at a time.

Figure 7.3.4 shows a pattern similar to that of Figure 7.3.3 except that the least-significant bit is offset by one-half bit period. If, with this pattern, the more significant bits are strobed and read only when the least significant bit changes state, then most of the objections to straight binary encoding are eliminated. A main problem with this scheme is that, upon turn-on, a complete position word cannot be read until there has been one change in the least-significant bit. Also, with a given limitation in the resolution capabilities of the thin-film processes, a single bit would necessarily be twice as large as in the straight binary or Gray codes due to the required half-bit offset. And an error of two bits may be encountered if the direction of strain motion were opposite the direction of the offset. No error is introduced if the strain and offset directions are the same.

AD-A059 016 BOEING AEROSPACE CO SEATTLE WA NAVY SYSTEMS AND ADVA--ETC F/G 14/2
FEASIBILITY DEMONSTRATION OF FIBER OPTIC DIGITAL STATUS MONITOR--ETC(U)
MAR 78 G E MILLER, T A LINDSAY N00019-77-C-0039
UNCLASSIFIED D296-10048-1 NL

2 OF 2
AD
A059016

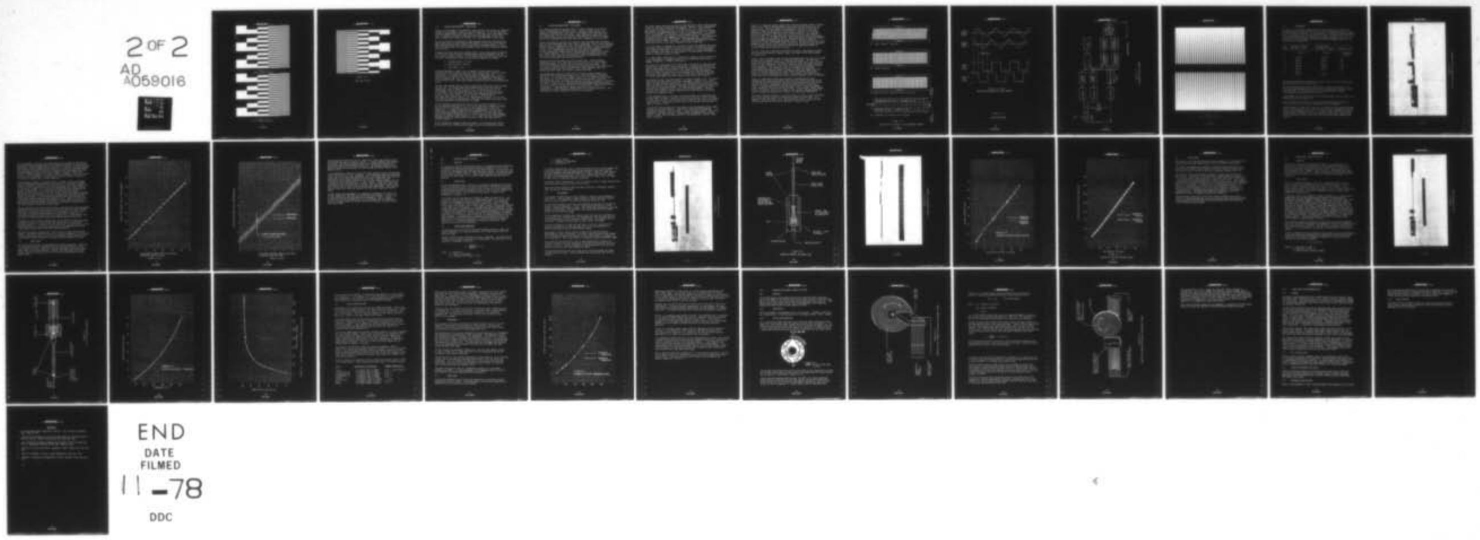

END
DATE
FILMED
11-78
DDC

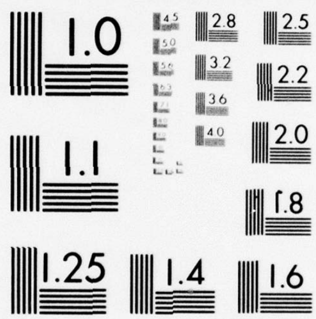

MICROCOPY RESOLUTION TEST CHART

NATIONAL BUREAU OF STANDARDS-1963-A

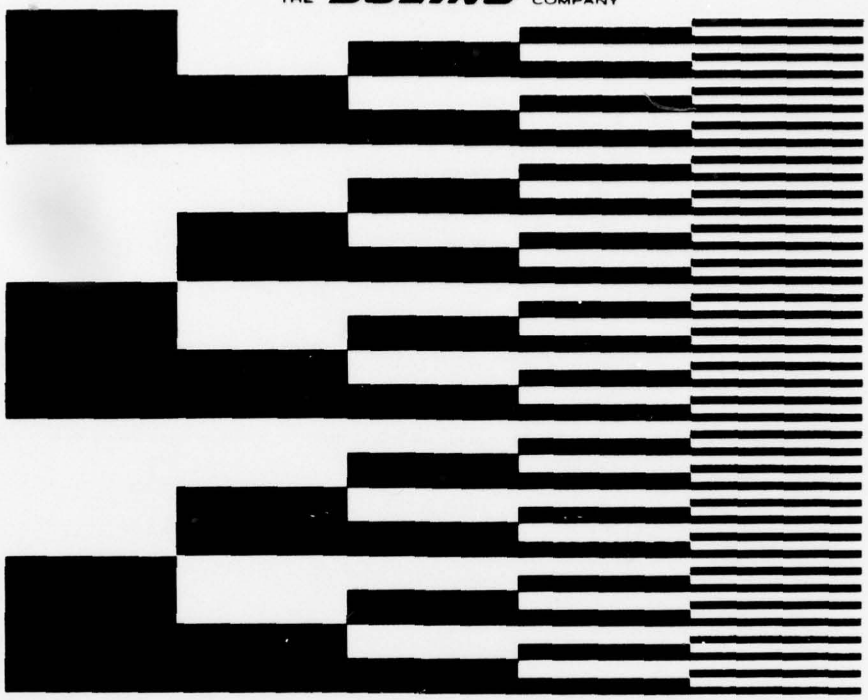

FIGURE 7.3.3
STRAIGHT BINARY ENCODING

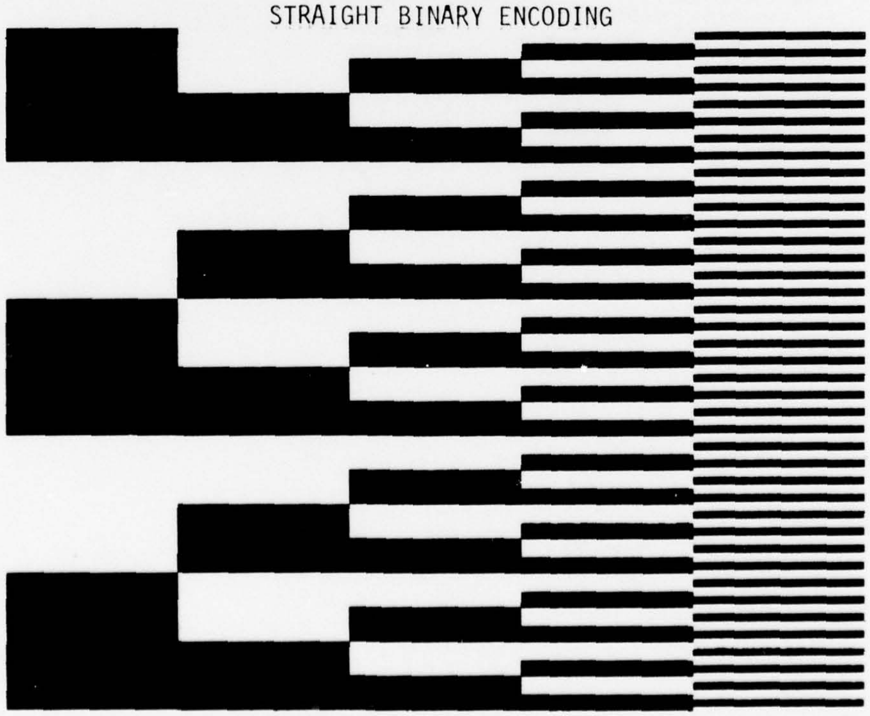

FIGURE 7.3.4
OFFSET BINARY ENCODING

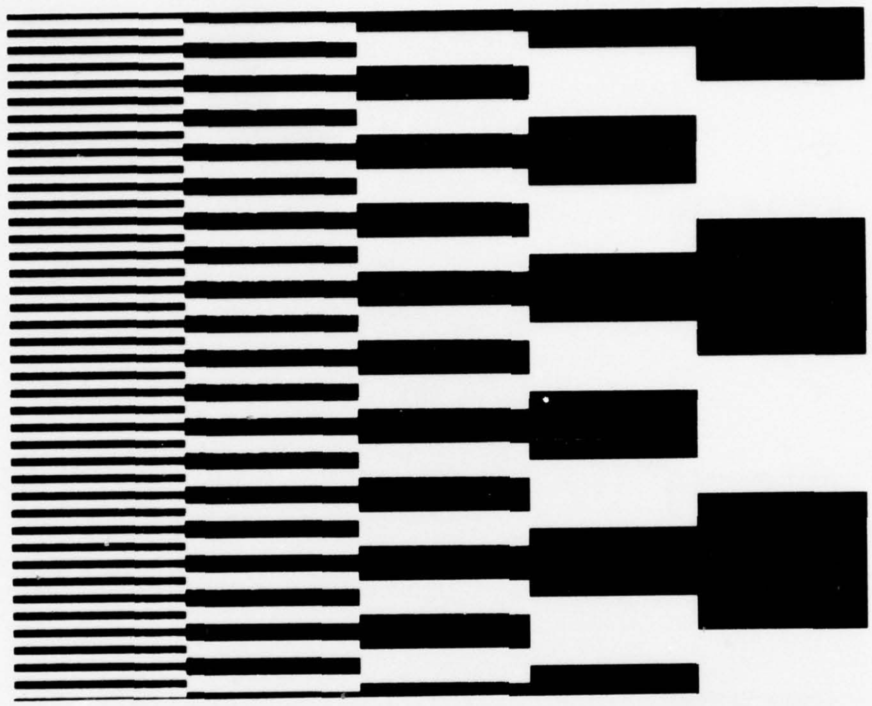

FIGURE 7.3.5

GRAY CODE PATTERN

7.3 DESIGN CONSIDERATIONS (Continued)

For any of the schemes to be effective, any given bit must be able to completely change its state within a single bit period of motion. It is also desirable to derive approximately equal quantities of light from each of the eight tracks. Thus, it becomes necessary to read the pattern through eight single slits, each no wider than a single bit period; i.e., the resolution of the system.

As the resolution of the pattern is made progressively finer, the excitation power density must be made progressively greater, or the track width must be made progressively wider, in order to provide a detectable signal. If the tracks are made wider, then the alignment of the slit with the pattern becomes more critical.

Alignment precision may be the limiting factor in the final system resolution. If the various codes are each examined under slight misalignment such that the system is one bit in error n track widths away from the least significant bit track, the potential errors for the various codes are as follows:

1. Straight binary - 2^n bits
2. Offset binary - 2^n bits
3. Gray code - 1 bit

The described angle is small, yet is capable of causing severe errors, primarily with the straight binary and offset binary codes. With all things considered, it is obvious that the Gray code is highly superior. It is significantly less sensitive to small angular misalignment, allows only one track to change state at a time (useful for error detection), introduces no directional errors, and allows maximum resolution with a given manufacturing limit.

The Gray code example shown in Figure 7.3.4(b) has the various tracks stacked side by side. To further reduce misalignment errors, the tracks may be stacked end to end as shown in Section 7.2. In the prior case, for no misalignment errors, the angle must be within 1 bit of accuracy across all of the tracks. With the end to end case, the accuracy must be held only across a single track width. Angular control is improved due to the longer total pattern length. The configuration of Figure 7.2.2 is the final pattern chosen for development. Note that the seventh and eighth tracks have been combined to reduce the overall length.

In the interest of maximizing the strain sensor resolution capabilities, it must be determined how small of a slit can be used from a theoretical standpoint as well as consideration made for the capabilities of thin-film technology. In a paper presented by Morse and Rubenstein, in which plane waves traveling through narrow slits are analyzed, it is shown that the transmitted energy through the slit is closely a function of simple geometry down to slit widths of approximately $d = \lambda/2$. There is little polarization, although diffraction would scatter a portion of the light away from the receiving fibers.

As slit widths are reduced to much less than $d = \lambda/2$, polarization effects become significant, thereby reducing power by half, and diffraction causes

7.3 DESIGN CONSIDERATIONS (Continued)

the intensity pattern to approach that of a half-cylinder, as all of the light is compressed into the zero order. However, further losses from geometrical considerations cease and it thus appears that there may be no true theoretical limit to slit widths. Some controversy does exist, but the article seems to say that some specified quantity of light will always be able to be gathered by the receiving fibers, regardless of slit width.

Within the realms of the thin-film industry, some extremely high resolution work has been performed using rather exotic techniques. With X-ray Lithography, where a resist is exposed by X-rays, line-spacings down to as low as 50 nm are claimed. Another technique uses electron beam scanning to expose the photo-resist, and is stated that line spacings near 100 nm are possible. By more conventional methods where a photographically reduced mask is used in a contact process, 1 to 2 micron patterns seem to approach the limit. Near ultra-violet light must be used and it should be monochromatic so as to minimize diffraction and dispersion effects.

Boeing's thin-film processes are of the latter type. Given a perfect photographic mask, it is felt that work as fine as 0.1 mil (2.54 micron) could be produced, but would require substantial time and effort. The limitation is centered around the exposing and developing of the photo-resist. Very precise control of the strength of the light, exposure times, and developing times render the process extremely sensitive.

The photographic reduction capabilities of Boeing are approximately the same as the thin-film process capabilities. The limitation is caused by the optics. A five inch focal length, f/#4.5 lens is claimed to be the best lens Boeing has, and it is essentially diffraction-limited. Using the Rayleigh criterion for resolving two objects, the lens is capable of resolution of .119 mil (3.02 micron). Some work has been performed very close to this limit but, normally, various vibrations hold the work to 0.25 mil (6.35 micron). Consequently, it was decided to design the strain sensor with 0.25 mil resolution as a good compromise between effort and ultimate resolution. The photographic plates available are accurate to 0.5 micron.

The strain sensor which was carried into the feasibility model stage presumes a need for absolute displacement measurement. However, strain measurements may be made on either a static or a dynamic basis. In a static strain measurement, the absolute distance, as well as changes in distance, between points of attachment is retained as a part of the measurement. In a dynamic strain measurement, the absolute distance between points of attachment is disregarded and only the changes in distance are retained. With conventional bonded grid strain gages, for example, the measurement must generally be considered dynamic unless some means is provided for unloading the structure under test so that a zero strain reference can be established.

If a strain gage is attached to a structure strictly to determine the strain introduced into that structure as the direct result of an applied stimulus, then a dynamic measurement is probably preferable to a static measurement since residual strain does not then appear in the measurement to produce an offset or otherwise confuse the data.

If a strain gage is applied to a temperature or pressure sensor, then static strain measurement is probably necessary since temperature and pressure change information is seldom of much value.

The reason for digressing at this point into a discussion of the distinction between static and dynamic strain measurement is because the selection of type of measurement has a profound effect on the configuration of the Fiber Optic Digital Strain Sensor which is the subject of this investigation. Because a dynamic strain sensor can be designed with patterns having only two tracks, the alignment is much less critical and it should be possible to achieve much higher resolution than with the static strain sensor.

One example of such a two-track pattern is shown in Figure 7.3.6. The sensor employs two periodic optical gratings, designated in Figure 7.3.6 as the lower and upper gratings respectively. The lower grating is split into two tracks "A" and "B" with the grating patterns on the two tracks displaced from each other by 90 spatial degrees. The upper grating, also has two tracks but which are aligned with each other with zero displacement. The two gratings have identical spatial frequencies and both consist of alternate opaque and transparent lines.

In the assembled sensor, the upper and lower gratings are aligned parallel to each other as shown in Figure 7.3.6(d) with two arrays of optical fibers on each side, one array in coincidence with track "A", and one in coincidence with track "B". The position of the fibers in the plane of the gratings is shown in Figure 7.3.6(c).

In operation, the gratings are illuminated by the interrogation fibers shown adjacent to the upper grating. Light that is transmitted through the transparent regions of both gratings is received by the response fibers shown adjacent to the lower grating. Although other arrangements are possible, Figure 7.3.6(d) shows the upper grating as the moving part, with all other parts stationary.

Figure 7.3.7 shows the optical power output from the response fibers of tracks A and B as a function of displacement of the upper grating relative to the lower grating. The displacement corresponding to a period of the optical response is equal to the period of the gratings. The use of two tracks separated by 90 spatial degrees provides sense information. If the upper grating is displaced to the right, the waveform of track 8 leads that of track A by 90^o. If the upper grating is displaced to the left, the waveform of track B lags that of track A by 90^o. When processed by suitable electronics, the periods may be counted from any given origin to provide a precise indication of total displacement from that origin. By utilizing the 90^o offset between the two tracks, a bidirectional counter may be made to sense direction of displacement and provide a precise indication of net displacement (or position) relative to the point of origin.

The basic electronics required to generate the optical interrogation signals and to process the optical response signals are shown in the block diagram of Figure 7.3.8.

A basic clock is divided by two to provide alternate drive to a pair of current switches which commutate a pair of light-emitting diodes. The two light sources provide optical interrogation through two fiber optic paths to tracks A and B of the transducer. All optical response signals from the transducer return through a third fiber optic path to a single optical detector such as a PIN photodiode. The resultant electrical responses are amplified, synchronously detected and lowpass filtered to remove the commutation rate. A pair of threshold detectors (or level detectors) provide logic-level outputs to drive a bidirectional counter. The counter is provided with a reset input which establishes the origin from which dynamic strain is measured.

The use of commutated (rather than constant) interrogation provides a chopped optical signal which permits the use of ac coupled circuitry within the receiver thereby eliminating zero-drift problems associated with direct-coupled circuitry. Commutation, combined with the effect of displaced tracks on one grating, also provide the receiver with a continuous dynamic signal regardless of position of the gratings. The continuous signal permits the use of automatic gain control (AGC) in the receiver, thereby making the overall system very tolerant of variations in optical-path attenuation.

The effect achieved in Figure 7.3.6 with a split grating can also be achieved with single gratings which are rotated with respect to each other. An example is shown in Figure 7.3.9. The pattern of Figure 7.3.9(b) has been displaced one grating line width from that of Figure 7.3.9(a).

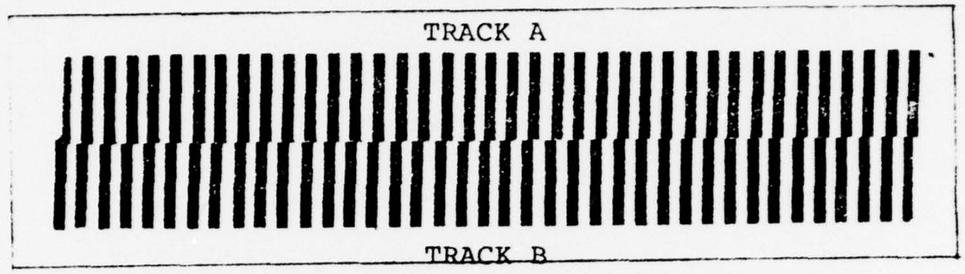

a) Lower (Split) Grating

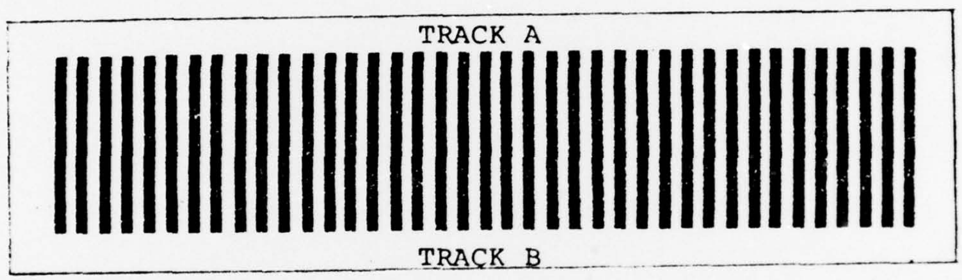

b) Upper Grating

c) Upper Grating Showing Fiber Locations

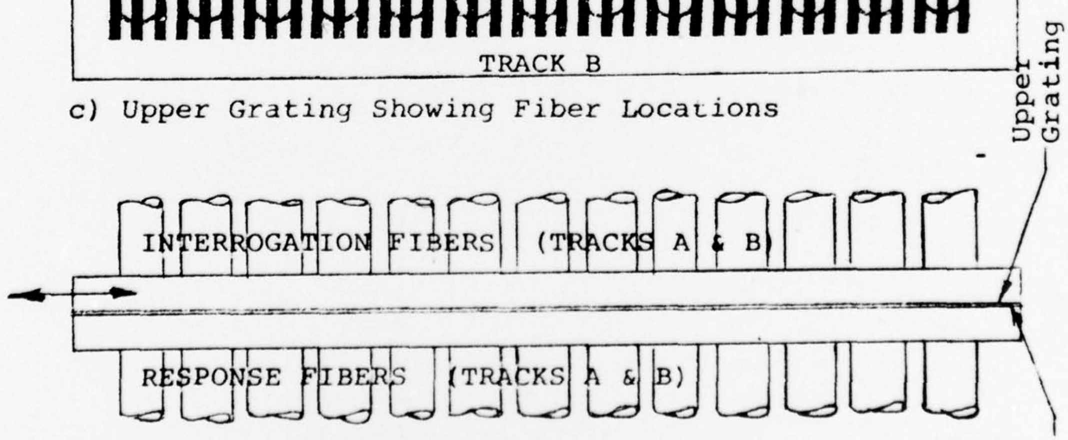

d) Assembly of Fibers and Gratings

FIGURE 7.3.6

FIBER OPTIC DYNAMIC DISPLACEMENT SENSOR

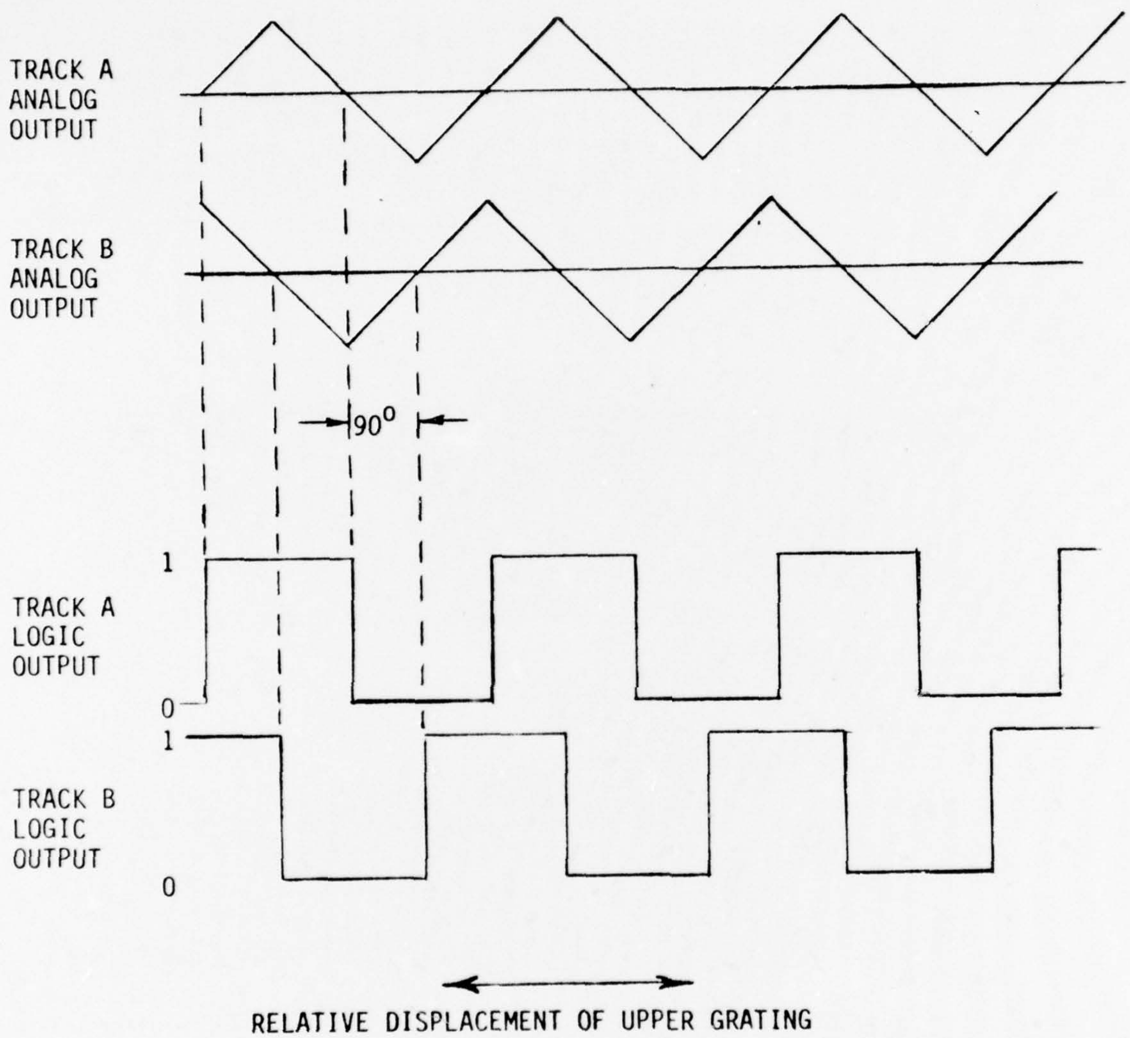

FIGURE 7.3.7

SENSOR WAVEFORMS

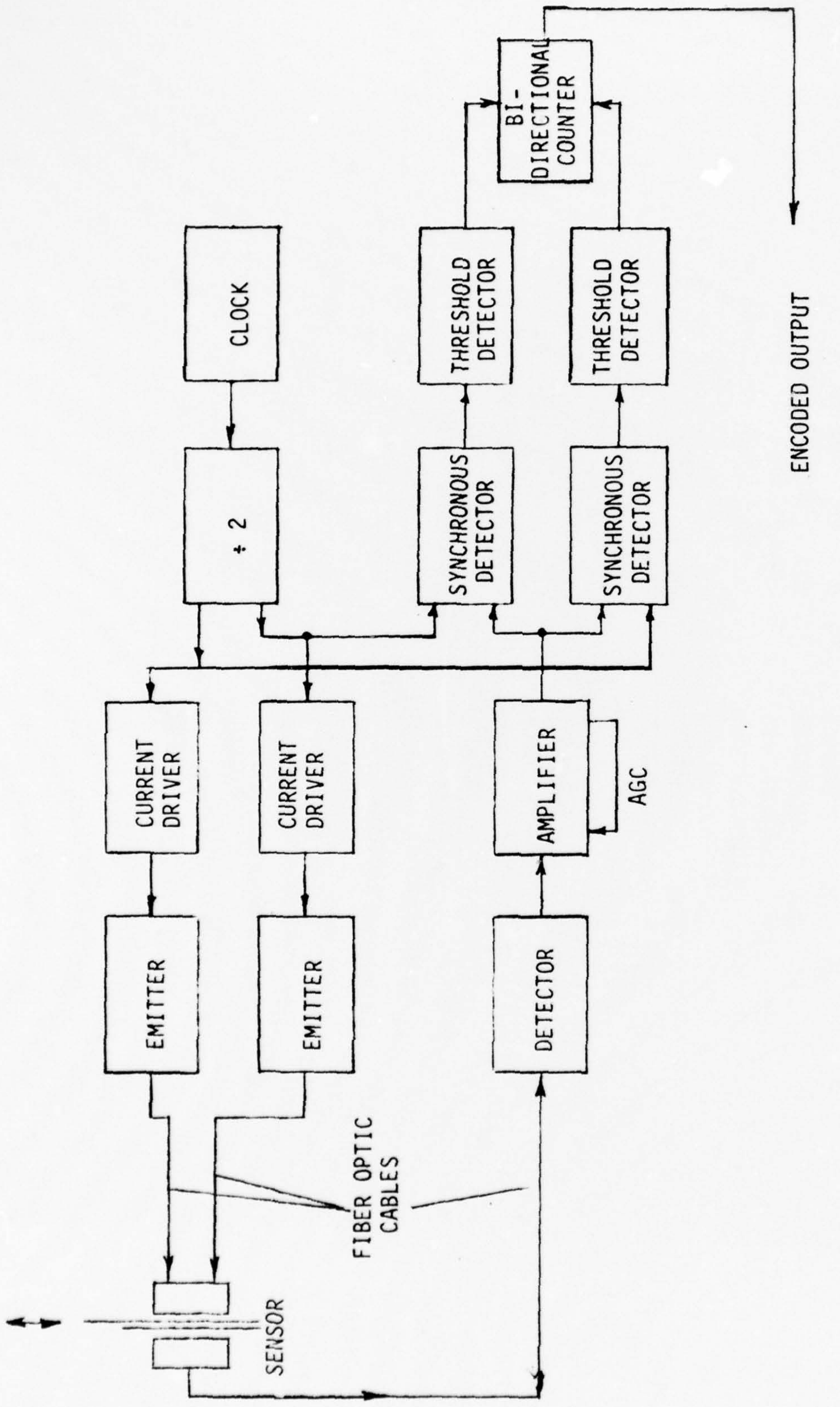

FIGURE 7.3.8
FUNCTIONAL BLOCK DIAGRAM

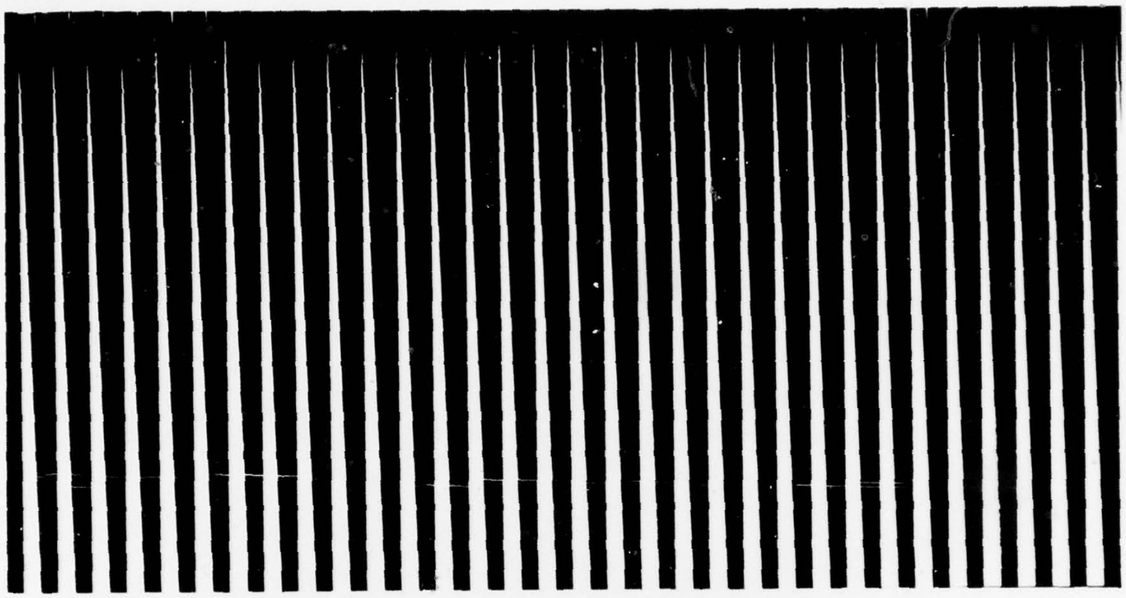

(a)

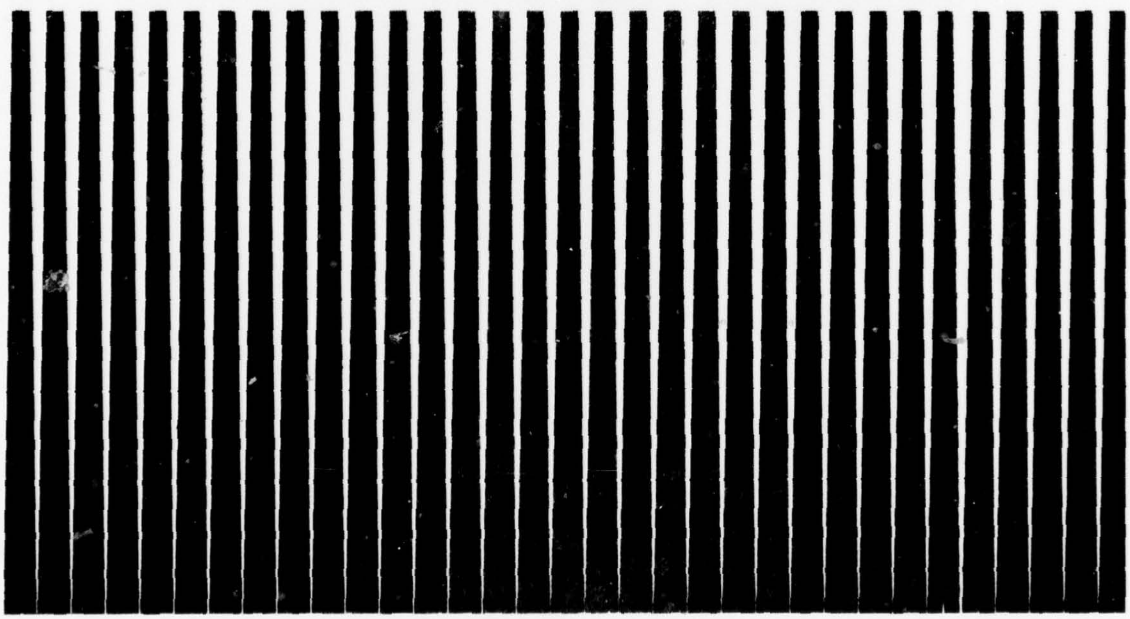

(b)

FIGURE 7.3.9
EFFECT OF ROTATED GRATINGS

7.4 PERFORMANCE

The small slit array and encoding plate for the TD-1105 Strain Sensor are required to have relative accuracies well within a single bit period in order to achieve design resolution. At the completion of the photo reduction process, each of the patterns was investigated for accuracy with the aid of a precision microscope (with a graticule) and micropositioners readable to 0.01 mil. A comparison of the two patterns was made to evaluate alignment precision, and the results are shown below.

Track Number	Viewing Slit Array Left Edge of Slit	Encoding Plate Left Edge of Pattern	Difference (mils)
1	0 (mils)	0 (mils)	0 (reference track)
2	70.09	70.09	0
3	140.08	140.10	+.02
4	210.10	210.11	+.01
5	280.06	280.10	+.04
6	350.15	350.11	-.04
7	420.13	-	-
8	436.15	436.15	0

The design resolution of the system is 0.25 mil and it is clear that the two elements match well within that value.

Because the alignment accuracies were held as closely as they were, it is a straightforward assumption that the individual tracks were of proper sizing, since they were all produced identically and everything was reduced simultaneously, thereby cancelling any errors.

A measurement for the seventh track of the encoding plate is missing due to its combination with the eighth track.

Also, the widths of individual slits were measured, and were found to be 0.25 mil to as close as could be determined by the instruments.

The photograph of Figure 7.4.1 shows the test setup for the assembled TD-1105 Sensor. A micrometer head was used to drive the sensor through its intended travel and was readable to 0.1 mil. An aluminum clamp connected the fixed section of the micrometer to the fixed portion of the sensor, and the small center rods were in direct end-to-end contact with each other under spring tension.

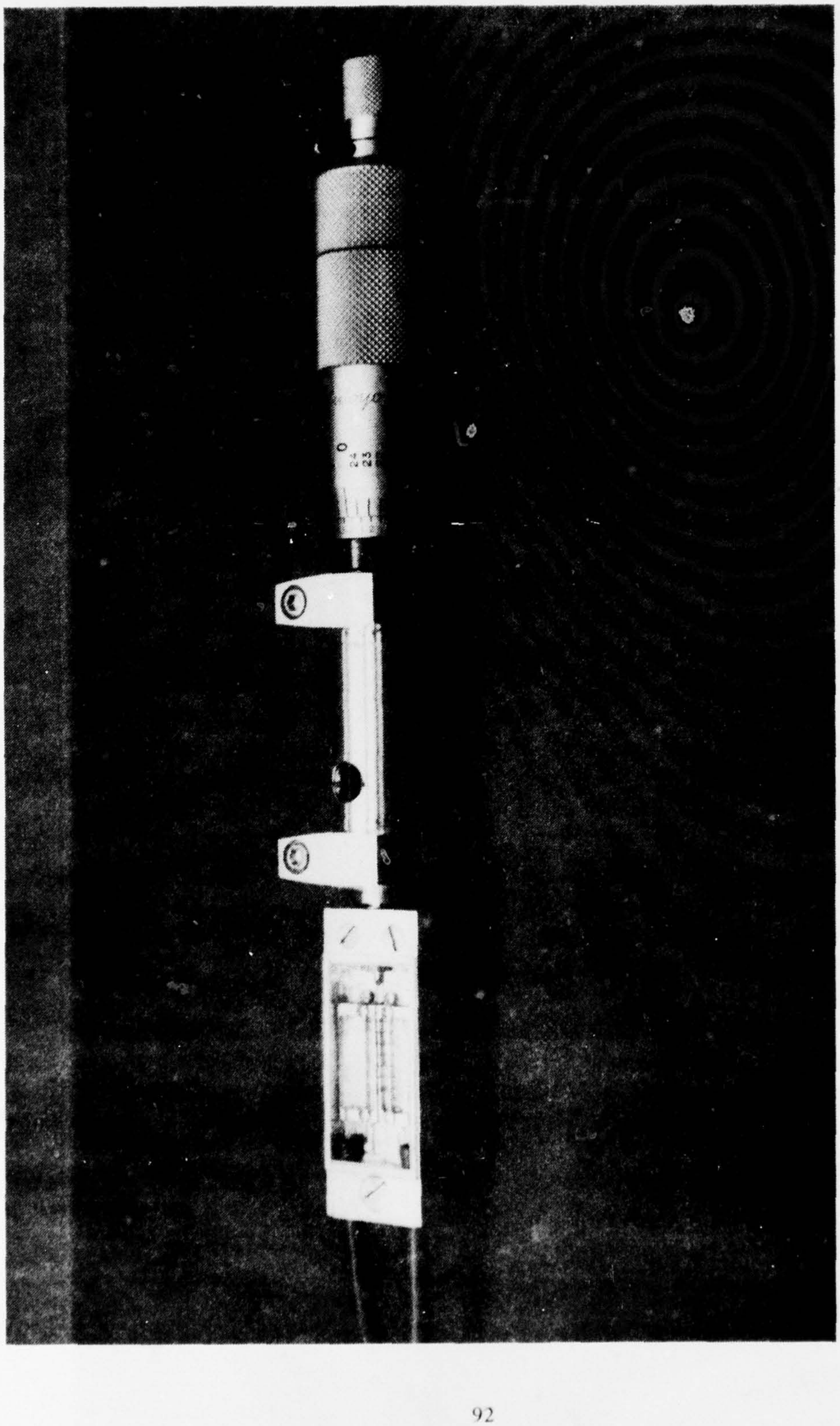

FIGURE 7.4.1
TD-1105 STRAIN SENSOR WITH TEST MICROMETER

For the purposes of testing, the coded output of the sensor was read from an oscilloscope detecting the output of the integrator section of the detection electronics. The micrometer was adjusted until a particular code was observed. Since the resolution contained four bits per mil of travel, the coded output was converted to decimal equivalents, divided by four and compared directly to the micrometer setting. The results appear in Figures 7.4.2(a) and 7.4.2(b). The data observed in Figure 7.4.2(a) were taken at 16-bit intervals across the entire pattern. A short range of bit-by-bit data is plotted in 7.4.2(b) for a better look at system accuracy.

The performance appears to be nearly ideal in Figure 7.4.2(a), and indeed, the points measured did not deviate more than 0.1 mil from their expected values. The plot of Figure 7.4.2(b) shows more error at various points, but all errors still remain within the ± 1 bit quantizing error limits inherent in any digital system. It is interesting to note than some tendencies are obvious in the results of 7.4.2(b) that are periodic with distance. Two explanations are possible; the first being is possible slight longitudinal offsets of some tracks relative to others although this has been previously shown to be minimal. A more probable explanation deals with the decision or threshold levels chosen for the different tracks. Ideally, the decision level should be halfway between the extremes for any given track, and any amplitude variation could lead to premature or retarded bit changes which in turn would produce the periodic effects shown.

The construction of the TD-1105 Strain Sensor involved single fiber procedures. Extreme patience and care are required to maintain control of the individual fibers but, in general, the process was very successful. In spite of the care taken, a few fibers were broken, and a few others did not line up precisely with their respective 0.25-mil viewing slits. Consequently, some variations in detected signal levels were present from track to track.

Although all tracks coupled abundant power to the detector, there was enough variation from track to track to make the setting of a single decision threshold difficult. If additional units were built and, particularly if any kind of production run were made, additional quality checkpoints would be established to ensure better uniformity between channels.

The feasibility model incorporates a small spring to return the actuating plunger. The spring required a force of 7.5 grams to compress it to mid-scale. In most applications, such a spring would be unnecessary and the only force involved would be that required to overcome the small amount of friction.

7.5 CONCLUSIONS

The TD-1105 Strain Sensor was determined to be highly successful. The 0.25 mil resolution design was indeed attained and with essentially no errors across the entire code. Some difficulty was realized in achieving uniform power levels in the eight channels. However, the sensor was still quite usable, and such difficulties could most likely be eliminated in any production model.

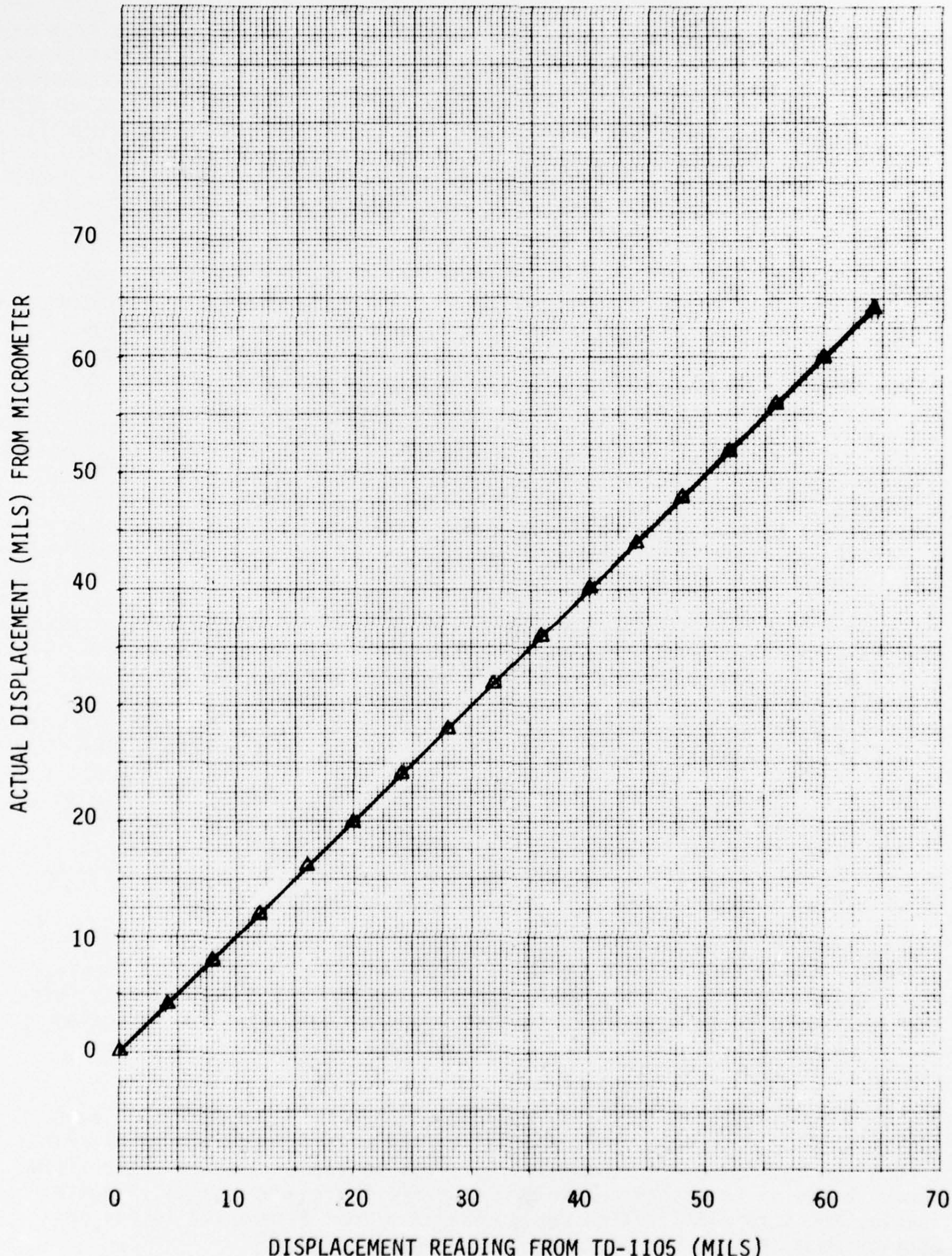
70
60
50
40
30
20
10
0
ACTUAL DISPLACEMENT (MILS) FROM MICROMETER
0
10
20
30
40
50
60
70
DISPLACEMENT READING FROM TD-1105 (MILS)
(CONVERTED FROM 8-BIT CODE)

FIGURE 7.4.2(a)

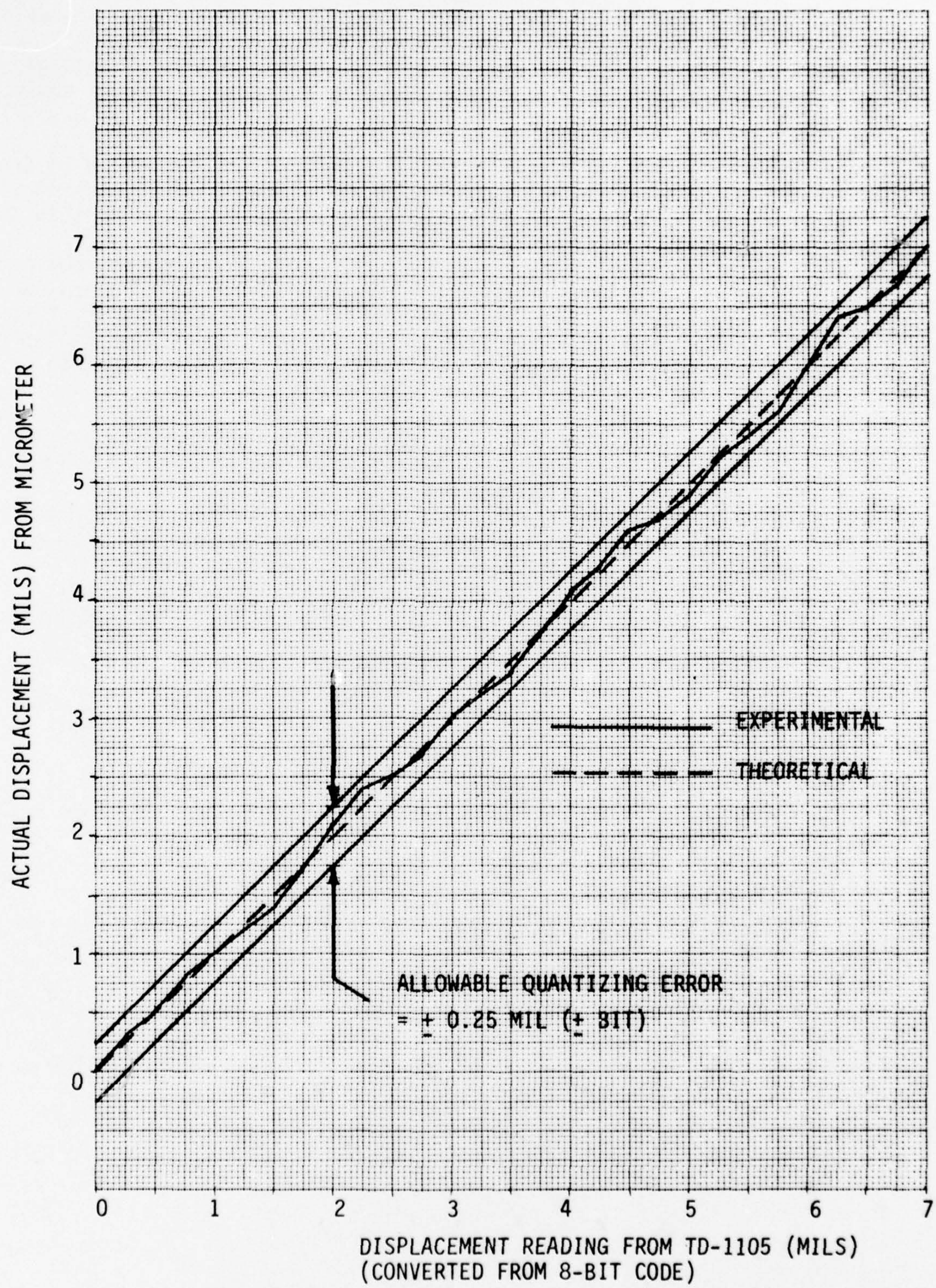
7
6
5
4
3
2
1
0
ACTUAL DISPLACEMENT (MILS) FROM MICROMETER
0
1
2
3
4
5
6
7
EXPERIMENTAL
THEORETICAL
ALLOWABLE QUANTIZING ERROR
= ± 0.25 MIL (± BIT)
DISPLACEMENT READING FROM TD-1105 (MILS)
(CONVERTED FROM 8-BIT CODE)

FIGURE 7.4.2(b)

The encoding plate and the 0.25 mil viewing slit arrays were found to have errors much less than a single bit period. It would therefore seem probable that Boeing could produce patterns even finer, perhaps achieving 0.1 mil resolution under well-controlled conditions. The ultimate capabilities of Boeing's facilities have perhaps not been reached and further efforts could prove fruitful.

It was mentioned in Section 7.3 that ultra high resolution work could be done with electron beam or x-ray lithography. Such techniques deserve considerable study, and it is likely that resolution near, or possibly even finer than the wavelengths of the light involved may be possible. Diffraction and polarization would become evident, as well as other effects perhaps, but the consequences need investigation as to their impact. Single fiber operation represents distinct possibilities, and thus, the total physical sizes, fiber optic cables, and all else could be substantially diminished. High radiance emitters would most likely be required for sufficient coupling of optical power.

Further studies and development are suggested to determine the effects of extreme temperature, humidity, and vibrational environments. At this time, no such testing has been performed and consequently, little is known. Differential expansion between the various components due to temperature may be a problem, especially between the glass substrates and the aluminum fiber optic heads.

8.0 PRESSURE SENSOR (TD-1106)

8.1 FUNCTION

The function of the TD-1106 Pressure Sensor is to demonstrate the feasibility of sensing and digitally encoding the relative pressure of a gas or fluid by means of an electrically-passive sensor which receives its excitation, and returns the measurement data, through fiber optic cables. The pressure range of the device is zero to 100 psi. When interfaced with the SR-1100 Scanner/Receiver, the data output is an eight-bit Gray-coded word proportional to pressure.

8.2 DESCRIPTION

The TD-1106 Pressure Sensor consists of a pressure-to-mechanical motion converter in combination with a TD-1105 Strain Sensor. The converter converts an applied pressure within the range of zero to 100 psi into a proportional linear mechanical motion of 0.064 inch, which is the full-scale range of the TD-1105 Strain Sensor. The TD-1106 Pressure Sensor is shown in the photograph of Figure 8.2.1.

A sectional view of the converter assembly is shown in Figure 8.2.2. Conversion of pressure into motion is accomplished by means of a small metal bellows which elongates with applied internal pressure. The elongation appears as a differential motion between a center rod, which is attached to one end of the bellows, and an outer sleeve, which is effectively attached to the other end of the bellows. A threaded plug permits adjustment of the conversion factor by applying added external pressure to the bellows through a light helical compression spring. The internal components of the converter are shown in Figure 8.2.3. The bellows was initially adjusted to elongate 0.065 inch for a pressure change of 100 psi by slightly reducing the outside major diameter. A measurement of elongation versus applied pressure was made using a precision dial indicator. A plot of this data is shown in Figure 8.2.4. As might be expected, the converter showed good linear characteristics with little hysteresis.

8.3 DESIGN CONSIDERATIONS

The bellows used in the TD-1106 Converter Assembly provides a simple yet verstile approach for converting pressure to a linear motion within the required ranges.

Another system that was considered involved a diaphragm. For simplicity of construction, an edge-fixed design was investigated. The deflection of the center of a diaphragm is given as:

$$y = \frac{3a^4(m^2-1)}{16Em^2t^3} \times P$$

where: y = deflection
a = radius of diaphragm
m = reciprocal of Poisson's ratio

E = Young's modulus
t = thickness of diaphragm
P = pressure of air

If a metal diaphragm were used, it would have had to be of a spring temper with a very high elastic limit in order to keep the device size small and not encounter permanent diaphragm deformation problems. Elgiloy, a metal popular for watch springs, has an elastic limit at or greater than 150 Ksi. With Elgiloy, it was determined that with a radius of 1.50 inches, and a thickness of .036 inch, all conditions would be satisfied.

Diaphragms of more common metals, such as stainless steel or copper-based alloys, would have been excessively large to do the job.

Rubber and certain plastics might have been usable for a diaphragm, however, their use was not investigated.

8.4 PERFORMANCE

The complete TD-1106 Pressure Sensor Assembly is shown in the photograph of Figure 8.2.1. The converter is shown coupled to the TD-1105 Strain Sensor, which was used to generate the pressure-sensitive eight-bit code.

For the test procedure, an air hose was connected to the base of the bellows through a pressure regulator. The air pressure was monitored by a high-quality, low-hysteresis pressure gage. The coupling was mechanically adjusted between the two sensors such that the strain sensor was set at the proper end of its travel at 0 psi gage.

The test began by increasing the pressure from 0 psi by 5 psi increments up to the upper limit of deflection. The procedure was then reversed, and the pressure decreased by 5 psi increments towards zero. The response time of the sensor, although not determined, was well within one second.

The plot of figure 8.4.1 shows the test data. The x-axis represents the pressure displayed by the pressure gage and the y-axis represents the decimal equivalent of the TD-1106 code word output.

The output is clearly quite linearly related to the applied pressure. Approximately 4 bits of hysteresis is evident along the entire range between the increasing and decreasing pressure cycles; which amounts to roughly 1.6 psi of variation. This is believed to be competitive with conventional gages.

The sensor ran off the 256-bit scale at approximately 98 psi during the pressure increase cycle and returned on scale during the decrease cycle at a pressure of 96 psi. Careful adjustment of spring pressure could have been made to correct the full-scale reading to 100 psi.

The observed hysteresis was most likely due to friction between the center rod and the outer sleeve. Teflon bushings were used to keep the friction minimal.

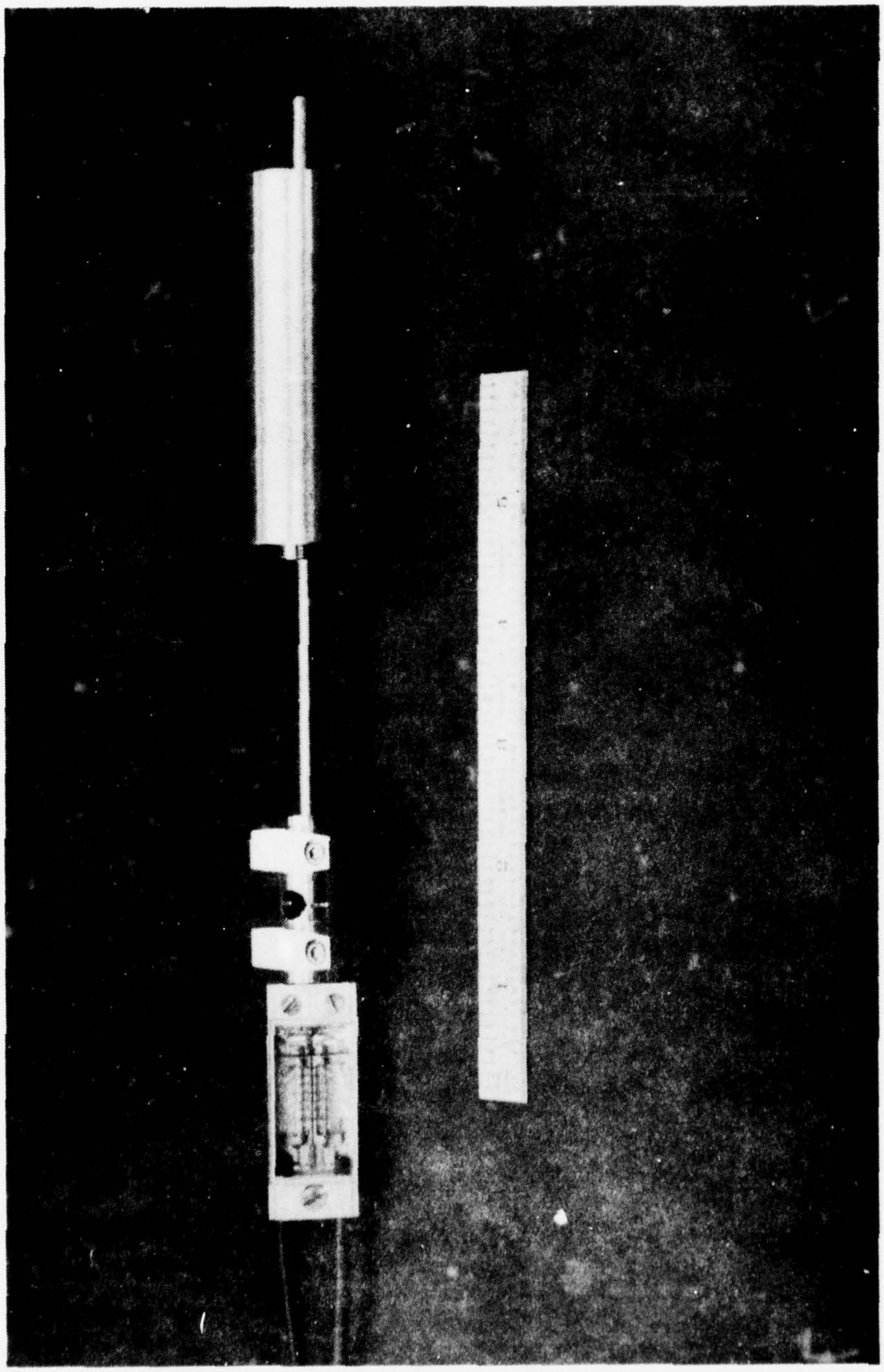

FIGURE 8.2.1
TD-1106 PRESSURE SENSOR

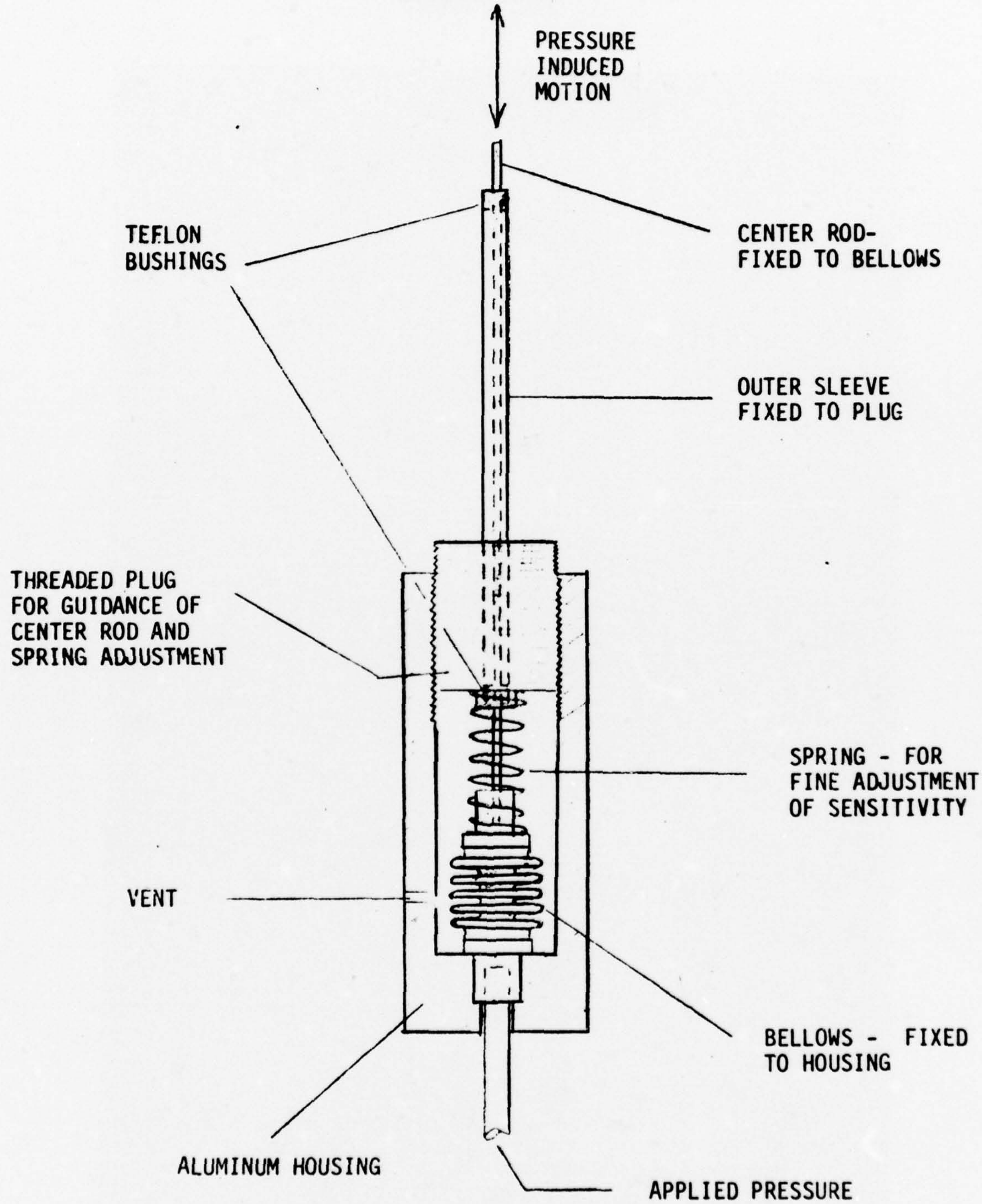

FIGURE 8.2.2

CONVERTER ASSEMBLY SECTIONAL VIEW

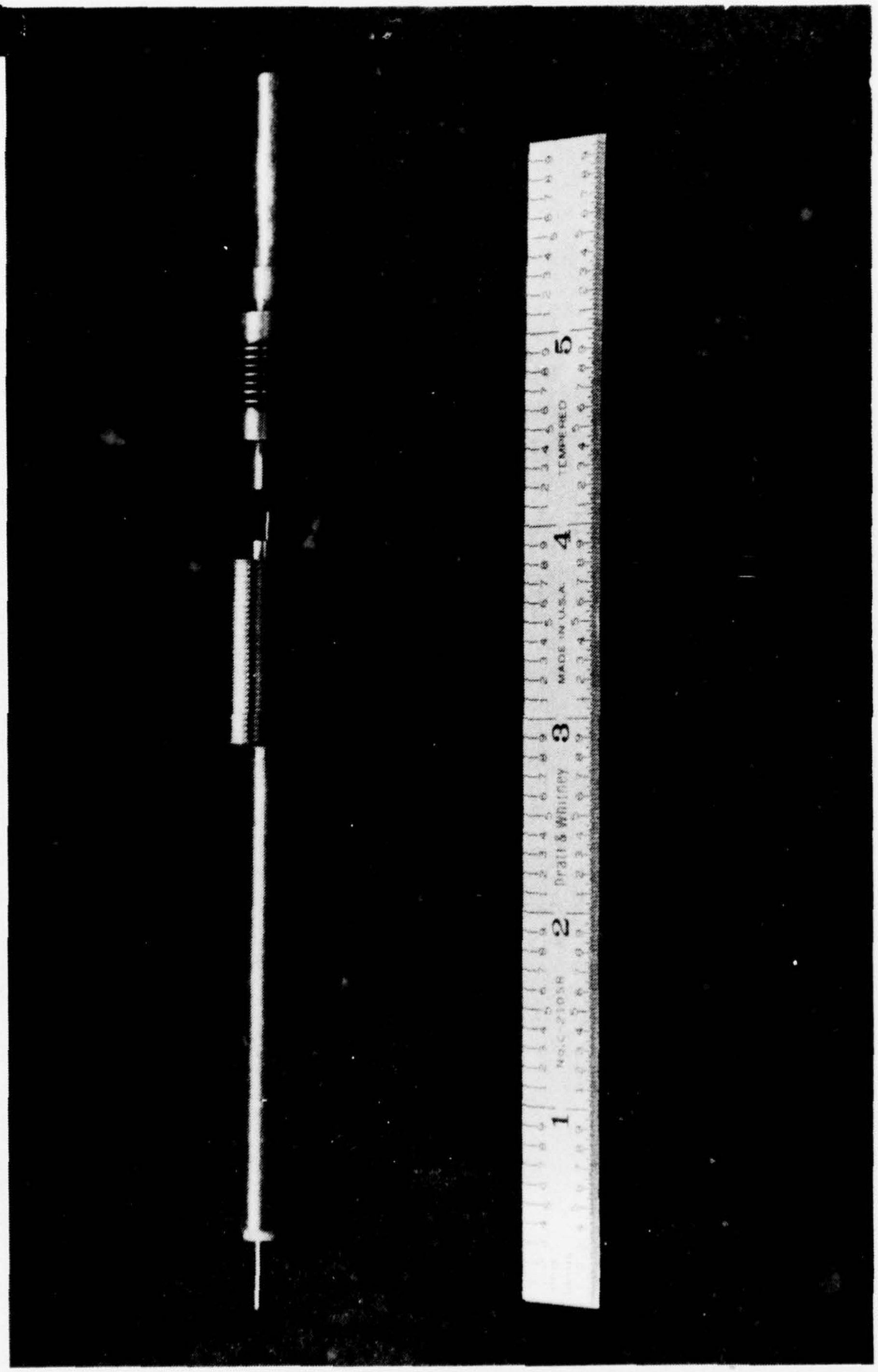

FIGURE 8.2.3
INTERNAL COMPONENTS OF CONVERTER

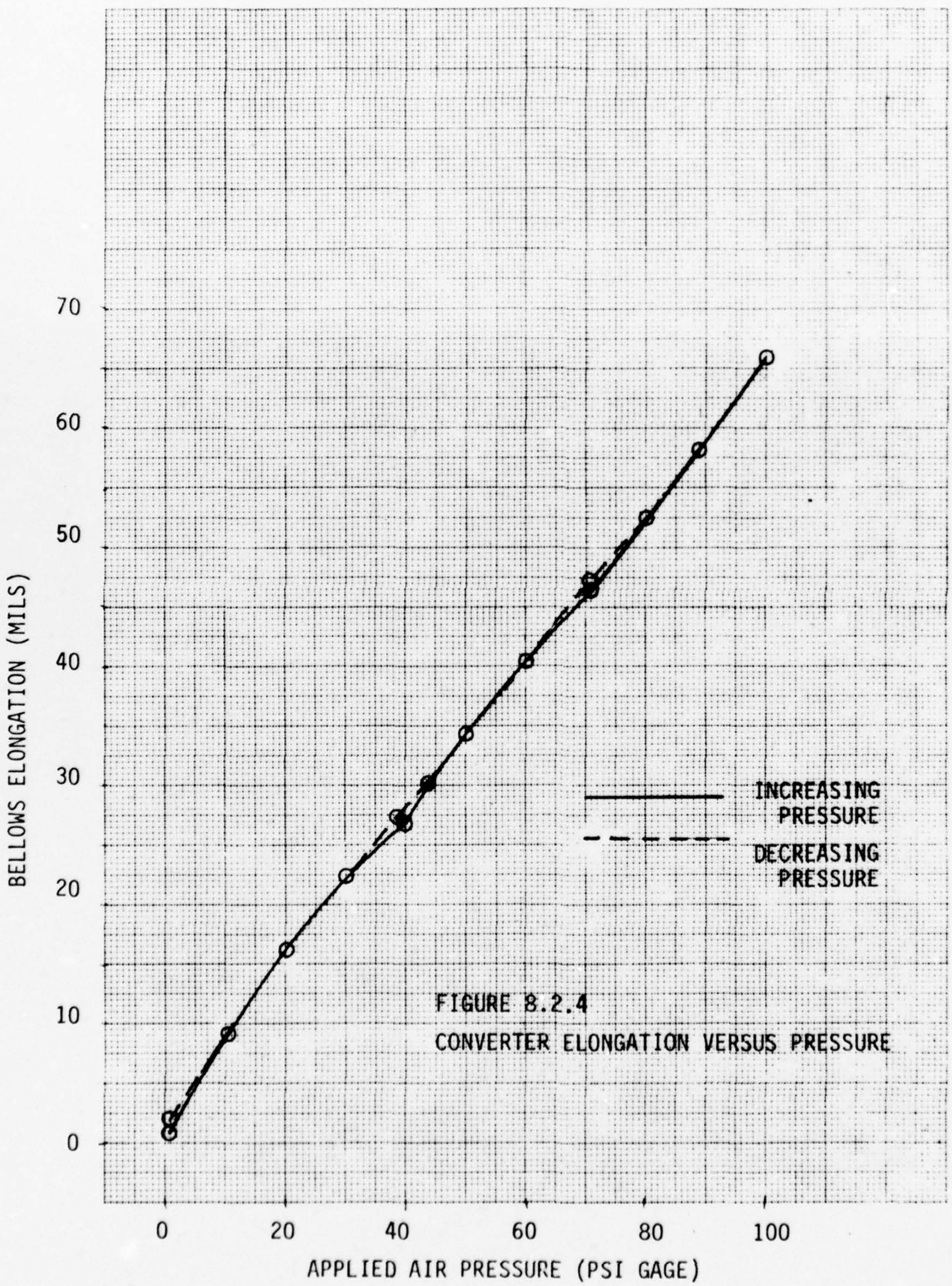

FIGURE 8.2.4
CONVERTER ELONGATION VERSUS PRESSURE

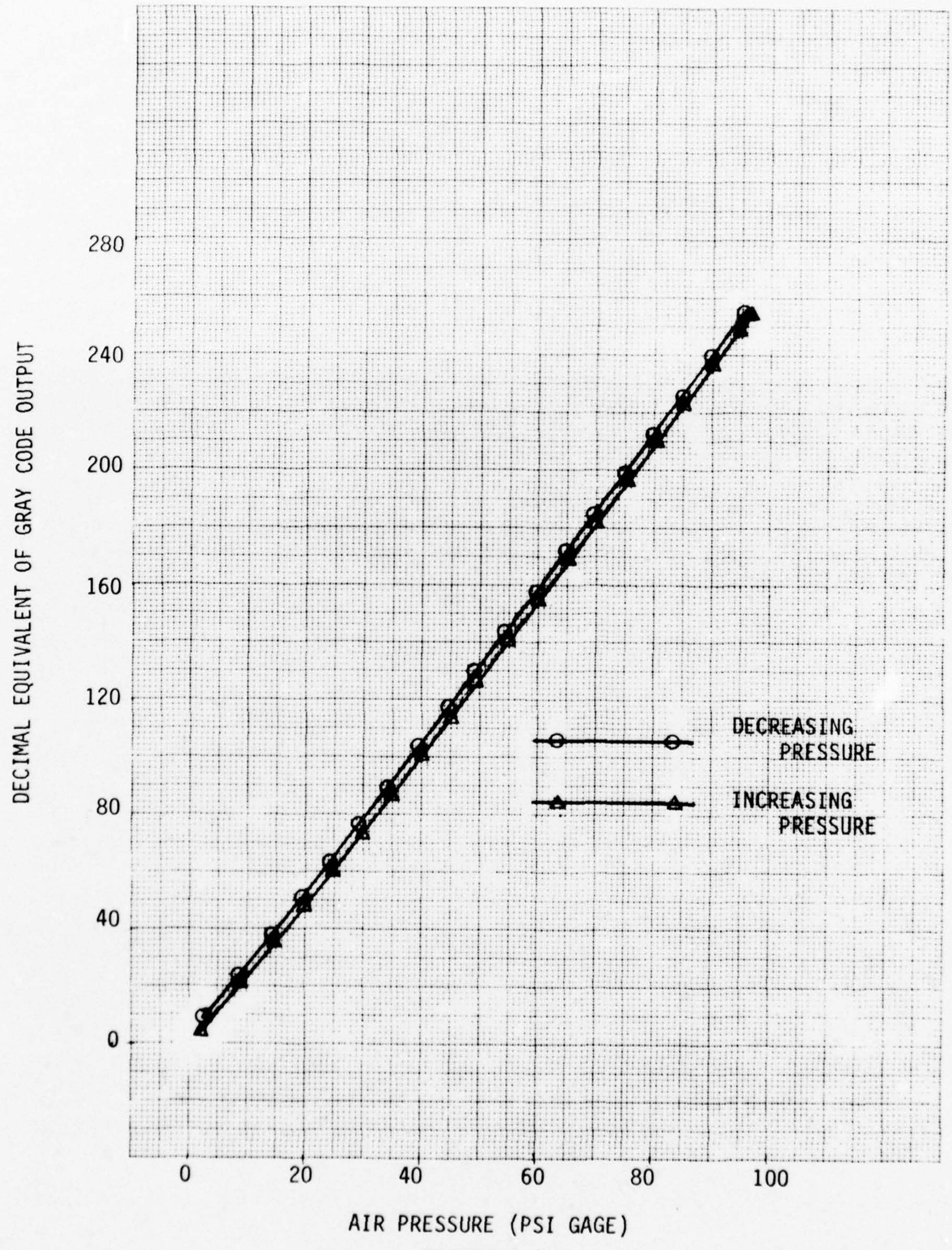

FIGURE 8.4.1

RESPONSE OF TD-1106 PRESSURE SENSOR

8.5 CONCLUSIONS

The feasibility of digitally sensing pressure by means of a fiber optically-coupled sensor has been demonstrated using the TD-1106 Pressure Sensor.

The concept of mechanically coupling a pressure-to-motion converter to a precision strain sensor allows sensors to be built covering a wide range of pressures by using a variety of bellows, diaphragms, Bourdon tubes, etc.

The converter used in the feasibility model is larger than desirable for two reasons: (1) because of the detachable linkage required to couple it to the strain sensor, and (2) because a relatively large travel (0.064 inch) is required to drive the present strain sensor to full scale. The linkage problem would be eliminated completely if the pressure sensor used a permanent dedicated strain sensor, in which case the encoding plate would be attached directly to the bellows or diaphragm with no intermediate linkage. In addition to reducing physical size, this could eliminate essentially all friction and all of the hysteresis except that inherent in the bellows or diaphragm itself. The device then might be considered for sensitive applications such as altimeters (with digital readout.)

Increasing the sensitivity of the strain sensor by methods discussed in Section 7.3 would decrease the size of the pressure sensor and would further reduce hysteresis and functional loading by reducing the motion required of the pressure-sensing element.

9.0 TEMPERATURE SENSOR (TD-1107)

9.1 FUNCTION

The function of the TD-1107 Temperature Sensor is to demonstrate the feasibility of sensing and digitally encoding temperature by means of an electrically-passive sensor which receives its excitation, and returns the measurement data, through fiber optic cables. The temperature range of the device is zero to 500^{o} F. When interfaced with the SR-1100 Scanner/Receiver, the data output is an eight-bit Gray-coded word proportional to temperature.

9.2 DESCRIPTION

The TD-1107 Temperature Sensor consists of a temperature-to-mechanical motion converter in combination with a TD-1105 Strain Sensor. The converter converts temperature within the range of zero to 500^{o} F into a linear mechanical motion of 0.064 inch, which is the full-scale range of the TD-1105 Strain Sensor. The TD-1107 Temperature Sensor is shown in the photograph of Figure 9.2.1.

A sectional view of the converter is shown in Figure 9.2.2. Conversion of temperature into the required mechanical motion is accomplished by differential expansion between a Teflon element and a stainless steel rod. One end of the Teflon element is attached to a stainless steel sleeve; the other end of the Teflon element is attached to a stainless steel rod which passes through the sleeve. Because the temperature coefficient of expansion of Teflon is much greater than that of stainless steel, relative motion occurs between the rod and the sleeve as a function of temperature. A threaded fitting on the end of the rod permits adjustment of scale factor by effectively changing the length of the Teflon element. The scale factor was adjusted to provide a relative motion of 0.064 inch for a temperature change of 500^{o} F. With this adjustment, the effective length of the Teflon element is approximately 1.5 inches.

The converter assembly was tested in an oven with a precision thermometer and a dial indicator to determine the temperature versus motion characteristic over the range of zero to 500^{o} F. The test data is shown in the plot of Figure 9.2.3. The nonlinear relationship is characteristic of the material Teflon.

A test to determine the time constant of the sensor was run by inserting the probe into a hot oven and measuring its deflection as a function of time. The results of the test, as plotted in Figure 9.2.4, show a curve that closely fits the familiar equation:

$$y = y'(1-e^{-t/\tau})$$

where: y = expansion at time = t
y' = expansion at time = ∞
τ = time constant of teflon element

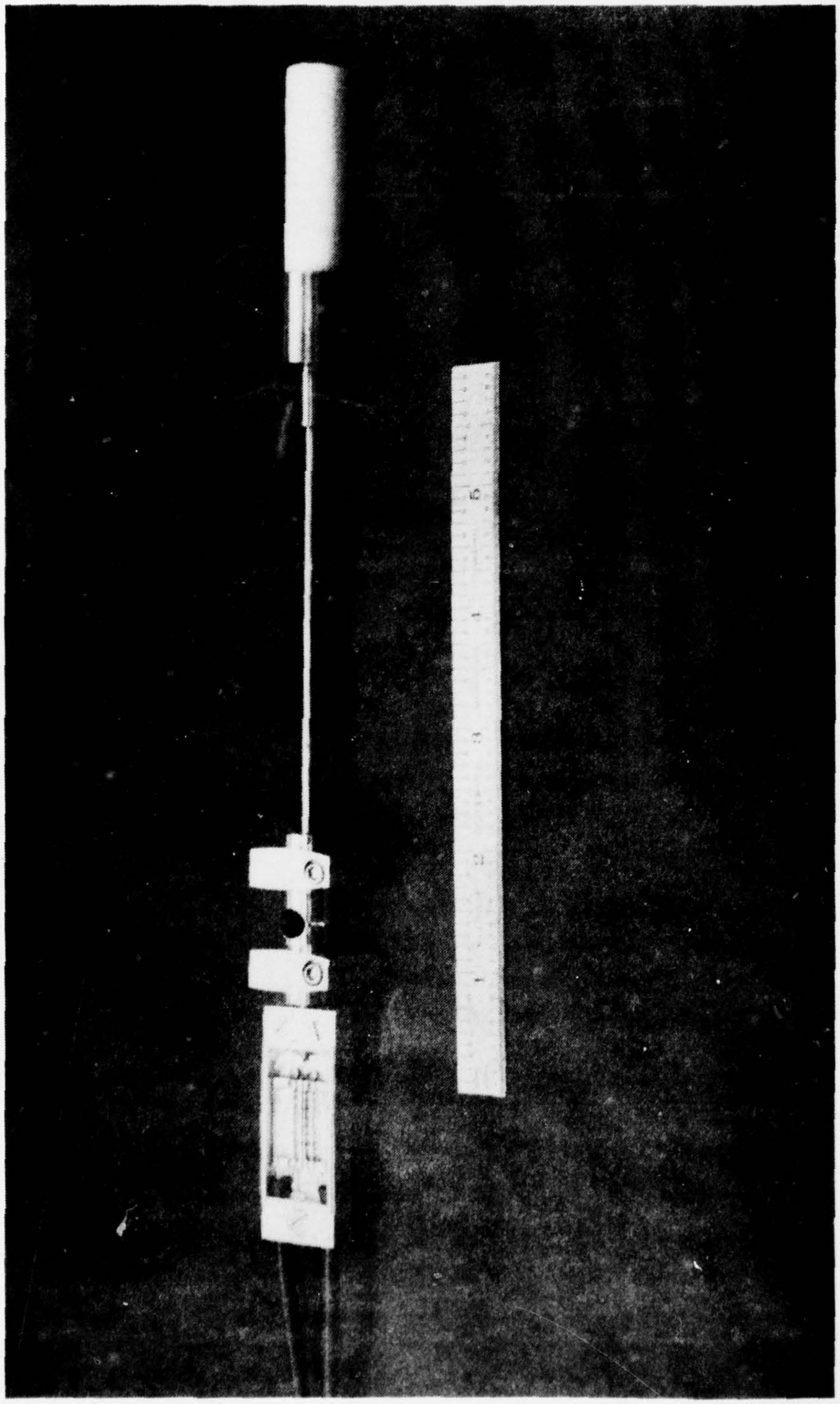

FIGURE 9.2.1
TD-1107 TEMPERATURE SENSOR

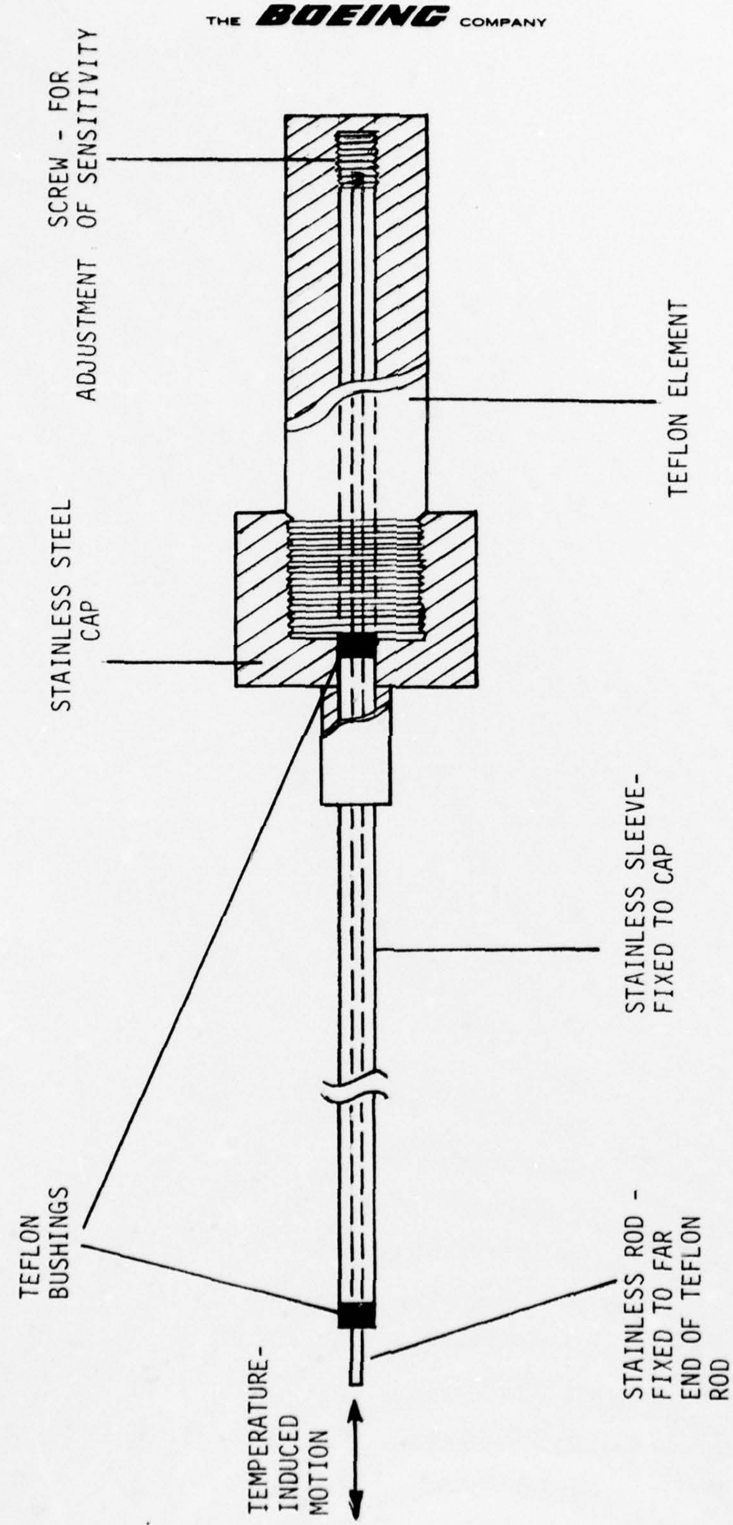

FIGURE 9.2.2
TD-1107 TEMPERATURE CONVERTER

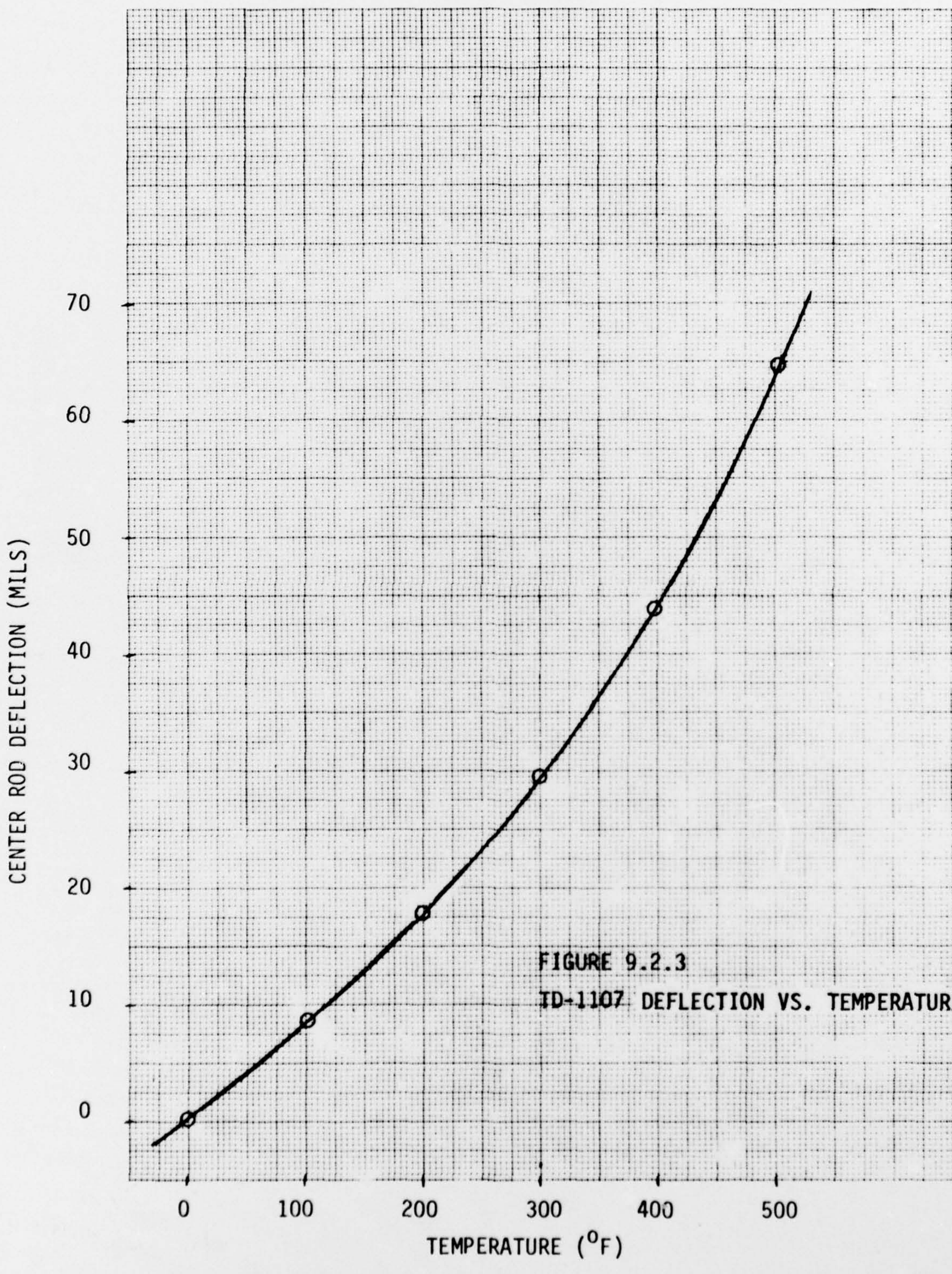

FIGURE 9.2.3
TD-1107 DEFLECTION VS. TEMPERATURE

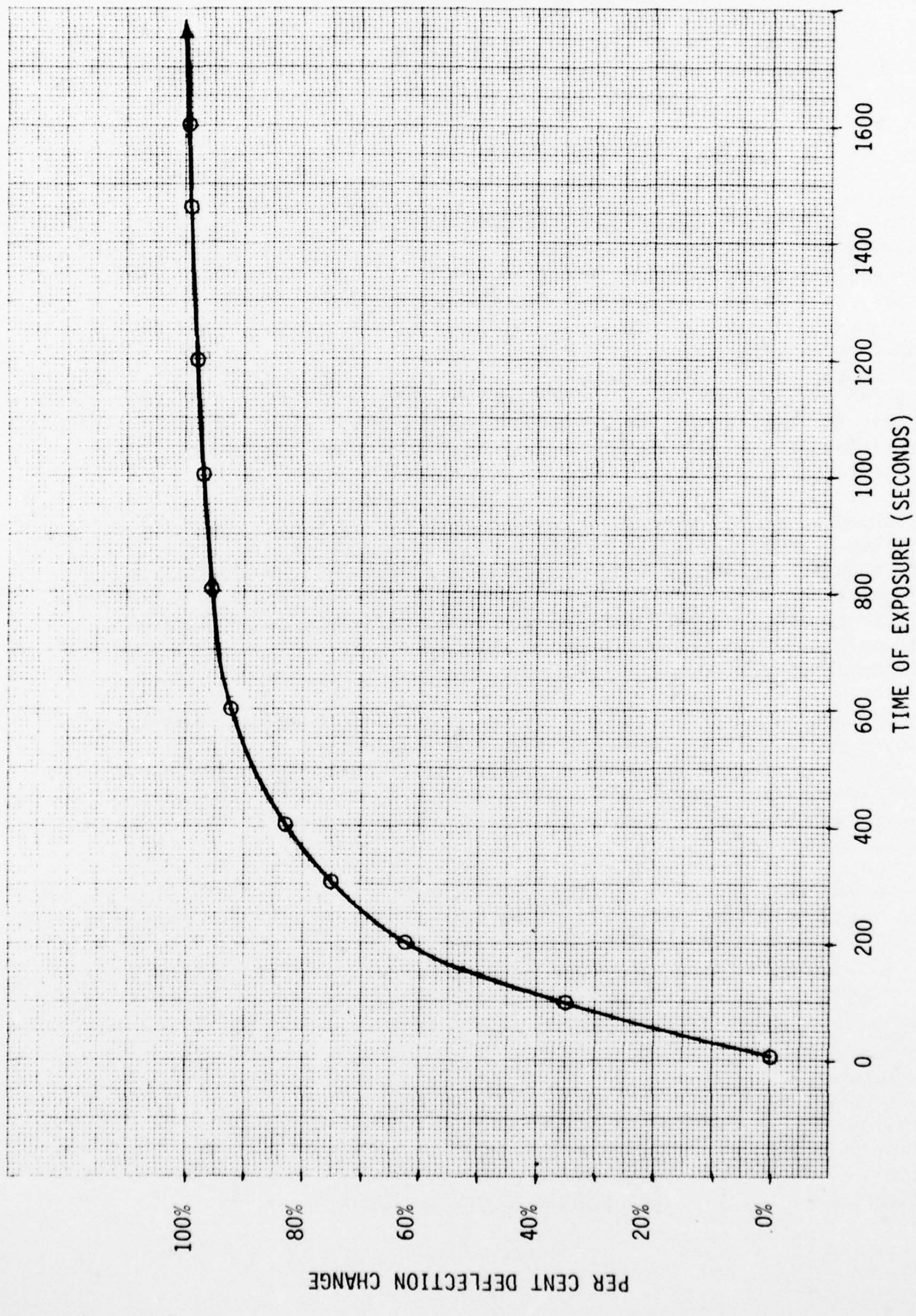

FIGURE 9.2.4 TIME RESPONSE OF TD-1107 TO THERMAL STEP FUNCTION

An approximate time constant, as determined experimentally, is 300 seconds, or five minutes. If 30 minutes, or six time constants, is allowed between test temperatures, the converter will undergo approximately 99.7% of its final contraction or expansion due to that temperature change.

9.3 DESIGN CONSIDERATIONS

Temperature can be converted to motion by a number of methods. Some of the more appropriate methods involve: the linear expansion properties of solids as a direct means, the properties of bi-metallic strips and the like, and gas-filled bellows. The first type was chosen for this purpose because of mechanical simplicity and good vibration resistance.

The encoded plates used in the strain sensor have a full scale travel of .064 inch. Considering the 500° F temperature range specified, the probe element must expand so as to change its length an average of 1.28×10^{-4} inches per degree F. The converter must be fabricated from materials which can tolerate the wide temperature range and should also exhibit low absorption and corrosion properties.

A survey of common materials available turned up Teflon as a viable candidate for the converter element. Metals, due to relatively low expansion, would all require excessive lengths to expand .064 inch over the temperature range, as would any of the ceramic or silicate materials. The average linear coefficient of expansion for Teflon was experimentally found to be approximately 150 ppm/°F. With such a value, the total length for the element would be roughly 1.5 inches.

The expansion of the outer sleeve and center rod elements, shown in Figure 9.2.1, should be negligible relative to Teflon so as to not introduce errors. The sleeve and rod should exhibit low thermal conductivity such that the extreme temperatures would not be felt by the tiny elements of the fiber optics sensor. They must also posess high structural strength, with metal being preferable.

There are several low expansion alloys available which would be well suited for the application. The following chart shows some of the better choices.

ALLOY	COEFFICIENT OF EXPANSION	THERMAL CONDUCTIVITY	
Invar	0.7 ppm/°F (0°F to 200°F)	7.74	Btu/ft^3/hr/°F
Lo-expansion 36	0.8 ppm/°F (0°F to 200°F)	6.12 (?)	"
Lo-expansion 39	1.22 ppm/°F (0°F to 400°F)	6.12	"
Lo-expansion 42	2.5 ppm/°F (0°F to 600°F)	6.12 (?)	"
Elgiloy	7.06 ppm/°F (0°F to 120°F)	7.21	"
Elinvar Extra	4.5 ppm/°F (-50°F to +150°F)	(?)	"
Nicol	7.06 ppm/°F (0°F to 120°F)	7.21 (?)	"
Nilvar	6.4 ppm/°F (400°F to 600°F)	7.75	"

Invar and the low-expansion alloys are largely iron and nickel alloys whereas the others may also contain cobalt, manganese, molybdenum, chromium, and other metals. Lo-expansion 39 would undoubtedly be the best choice for this particular application because of the wide temperature range of low expansion and the low coefficient of thermal conductivity. However, as with some of the other alloys, only selected shapes are available and special requests would have to be made. All of the alloys are machineable, and some are offered in various tempers.

Stainless steel was chosen for the center rod and the sleeve elements because of availability. The linear coefficient of stainless steel is approximately 9.3 ppm/^{o}F and its coefficient of thermal conductivity is around 10.0 Btu/hr/ft^{3}/^{o}F. The expansion coefficient is much less than that of the Teflon sensing element.

9.4 PERFORMANCE

For purposes of the test, the probe was inserted through a port in an oven capable of both cooling and heating with high accuracy. The probe was cooled to 0^{o}F and the coupling between the converter and the strain sensor was mechanically adjusted to set the temperature limit.

The temperature of the oven was monitored by a high-resolution dial thermometer and was adjusted in approximately 100^{o}F increments. The temperature sensor was allowed 30 minutes for response (as determined in Section 9.2), at which time the digital output signal was read from the electronics. The temperature was run up only to 490^{o}F (to minimize any chance of running off scale) during the temperature increase cycle. In preparation for the temperature decrease cycle, the temperature was increased in slight excess of 500^{o}F, and then brought gradually back down.

The test results are plotted in Figure 9.4.1, and the curve appears similar to that of Figure 9.2.3, except that the y-axis now represents the decimal equivalent of the optical code word.

The data points for the increase and decrease cycles appear to lie on identical curves, and it was therefore concluded that hysteresis for the sensor was negligible. It is of interest to note that, at the bottom of the decrease cycle (0^{o}F), the optical code word differed by only a single bit from the initial 0^{o}F setting for the increase cycle.

The sensor did run off scale at a temperature slightly less than 500^{o}F...... probably near 495^{o}F. A slight adjustment of the threaded screw to shorten the length of the teflon probe would cure the problem.

9.5 CONCLUSIONS

The TD-1107 Temperature Sensor proved the feasibility of digitally sensing temperature by optical means. The sensor appears to have good repeatability characteristics, and should be quite durable.

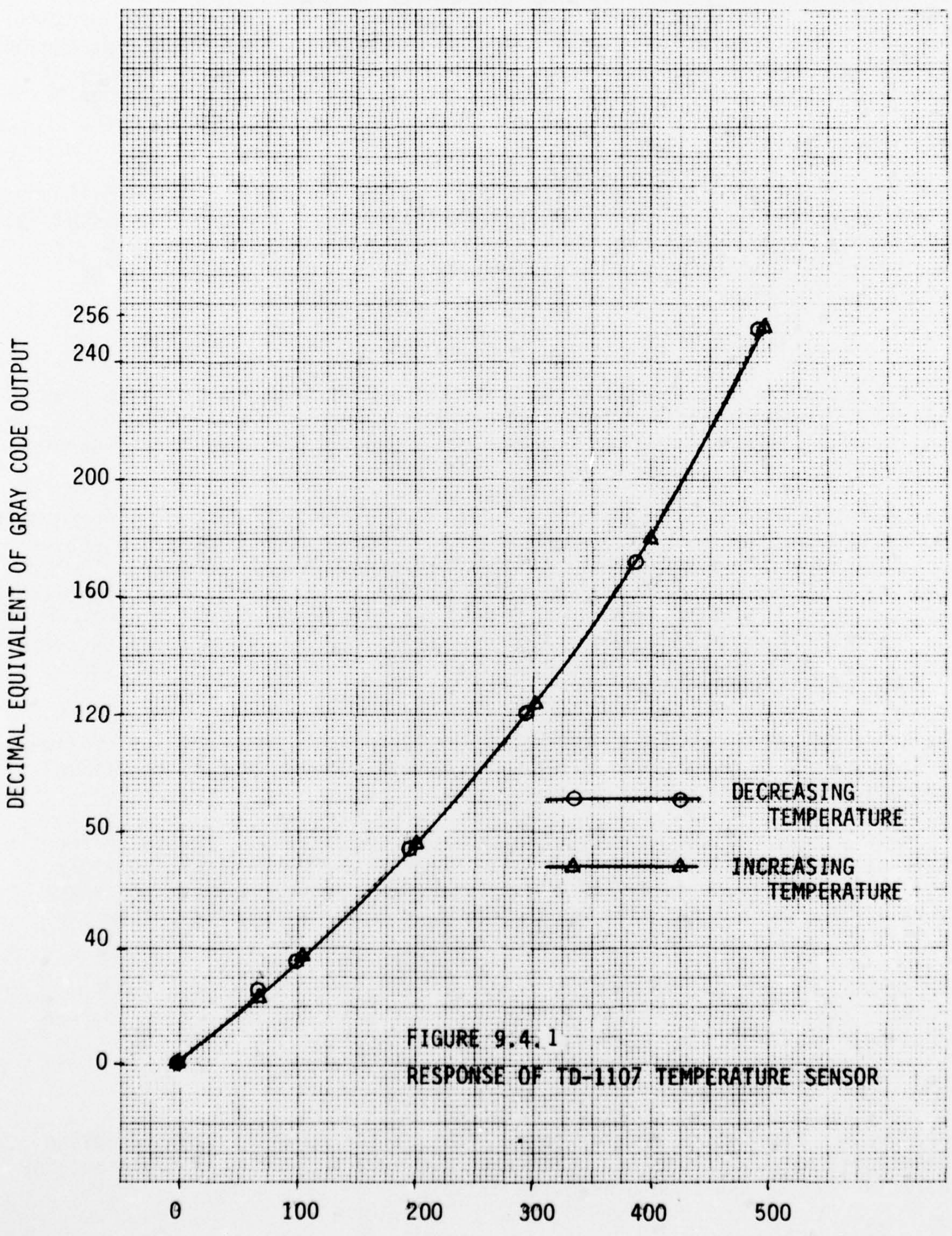

FIGURE 9.4.1
RESPONSE OF TD-1107 TEMPERATURE SENSOR

Temperature resolution of the sensor is, on the average, approximately 2^oF over a 500^oF range. The response range and or sensitivity of the sensor could be adjusted by varying the length of the teflon element, or by attaching it to a sensor similar to the TD-1105 Strain Sensor but of different resolution. If some of the techniques discussed in Chapter 7 could be used, resolution considerably finer than 1^oF could be realized.

Response time for the TD-1107 Sensor is quite slow, which may or may not be advantageous. If rapidly-changing temperatures are encountered, the probe would only show long term average temperatures, serving somewhat as a thermal "integrator". The probe should be quite insensitive to mechanical vibration.

Teflon is a reasonably good thermal insulator, and therefore time is required for the probe to attain thermal equilibrium. Response could be accelerated if the probe was made narrower and with thinner walls. It may also be worthwhile to investigate some other more exotic materials, or perhaps other methods such as bi-metallic deflection, which can be quite rapid and sensitive.

Teflon, as a sensing element, does offer the advantage of being chemically inactive in the presence of almost anything. Because of the ease with which data can be linearized in a digital system, the nonlinear expansion characteristic of Teflon is not necessarilly a bad feature.

If a temperature sensor were built using a dedicated strain sensor, most of the linkage of the feasibility model would be eliminated because the strain sensor could be attached directly to the sensing element - - - provided that the strain sensor could tolerate the temperature of the sensing element. The reduced mechanical loading would permit the use of a sensing element of small cross-sectional area and would thereby offer a response time constant much shorter that that of the feasibility model.

With a judicious selection of materials, it should also be possible to use the Strain Sensor itself as a temperature sensor over certain temperature ranges - particularly if the sensitivity of Strain Sensor were increased by the methods suggested in Section 7.3.

10.0 ANGULAR DISPLACEMENT SENSOR (TD-1108)

10.1 FUNCTION

The TD-1108 Angular Displacement Sensor would digitally sense rotational position by means of an electrically-passive optical sensor in much the same way as the TD-1102 Linear Displacement Sensor detected linear position. Fiber Optics cables would couple the SR-1100 Scanner/Receiver to an eight-bit encoded disc which would indicate angular position.

10.2 DESCRIPTION

The TD-1108 Angular Displacement Sensor was not built. Therefore, there can be no description. A brief discussion of conceptual designs follows, however.

10.3 DESIGN CONSIDERATIONS

For a feasibility study, the fiber optics head and cables used would be the same as for the TD-1102 Linear Displacement Sensor (refer to Chapter 4.) The coded disc would contain eight separate tracks (eight-bit encoding), would be a cyclic Gray Code as shown in the example of Figure 10.3.1, and would be of a deep-etched reflective nature as was the linear code for the linear sensor.

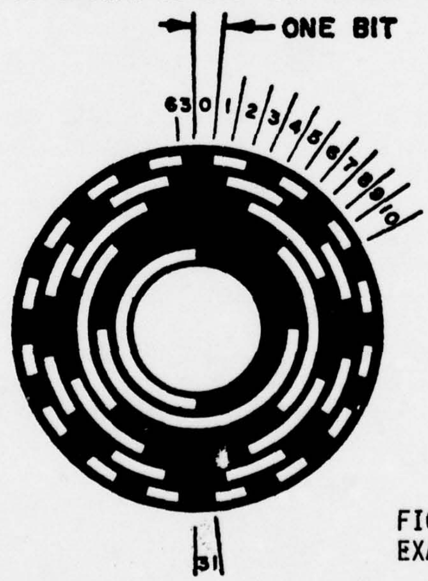

FIGURE 10.3.1
EXAMPLE OF CYCLIC GRAY CODE
(6 BIT)

The SR-1100 Scanner/Receiver would scan the eight tracks sequentially by means of the fiber optic cables and would detect the coded angle for proper display. The principle is illustrated in Figure 10.3.2.

Since eight-bit encoding would be used, the 360° or 2π radian rotational pattern would be resolved into 256 equal angles, each being $2\pi/256$ radians. To be accurate for such resolution, the edge of any mark or space must be within $\pm \frac{1}{2}$ bit of accuracy, or $\pm \pi/256$ radians from its exact position.

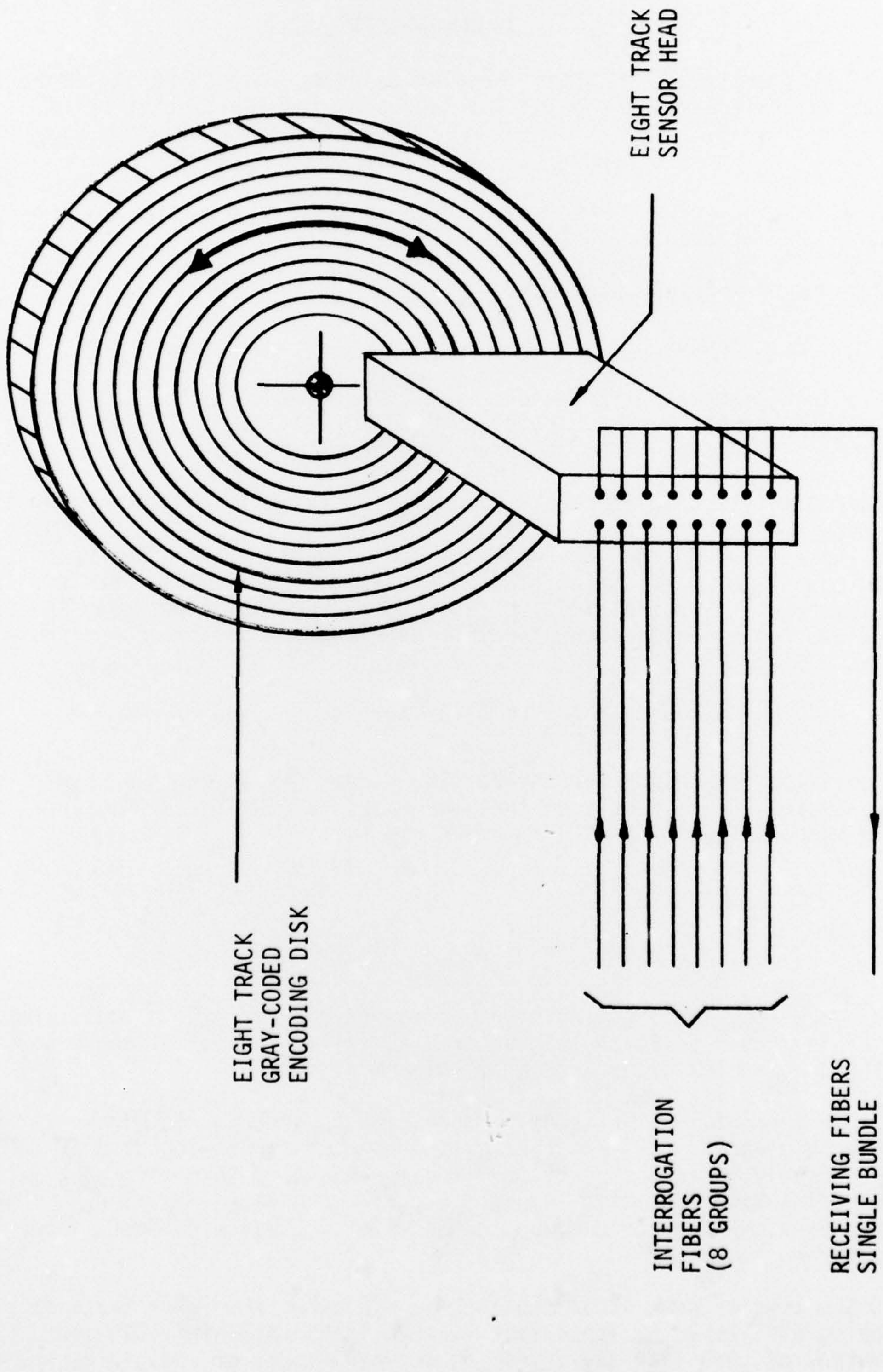

FIGURE 10.3.2

CONCEPTUAL BLOCK DIAGRAM OF ANGULAR DISPLACEMENT SENSOR

Since it is a circular pattern, angular tolerance can be converted to tangential tolerance by knowing the radius at that particular point.

$$B_T = r\ B_A \qquad \text{(for small angles)}$$

where: B_T = tangential tolerance

B_A = angular tolerance

r = radius

If a 3-inch diameter pattern were used, the required tangential accuracy of the outside of the outside track would be $\pm$ .0184 inch. The tolerance for the inside tracks would be decreased as the respective radii decreased.

Another limitation which requires mentioning involves the edge resolution of the reading head used for the linear transducer. Figure 4.3.2(b) demonstrates that the edge resolution was approximately .003 inch, or about one fiber diameter. This necessitates that no bit width can be less than .003 inch for any track. For the limiting case, where the individual bits are perfectly sized and rotationally accurate, the inner edge of the track must have a radius

$$r \geq \frac{.003}{2\pi/256} = 0.122 \text{ inch}$$

The total pattern width for the TD-1102 Linear Displacement Transducer was approximately 0.95 inch, such that the radius of the total rotational pattern would be 0.95 + 0.122 or 1.072 inches minimum.

In essence, the TD-1105 Strain Transducer of Chapter 7 is no more than a subminiature linear position transducer. A similar technology could be applied to the development of an angular displacement sensor.

One such concept involves single fibers and is sketched in Figure 10.3.3. Light would be coupled from the SR-1100 electronics through single fibers (per channel), guided through individual slits in a thin film mask, through an encoding disc sensitive to rotation, and into receiving fibers. The slits in the viewing mask could be on the order of 0.5 mil wide and a fiber diameter in length.

If 0.5 mil slits were used, the minimum radius of the inner track of the encoding disc would be approximately .020 inch. Allowing .025 inch, fiber diameters of .003 inch and a spacing between fibers of .003 inch, the radius of the entire pattern would be .073 inch.

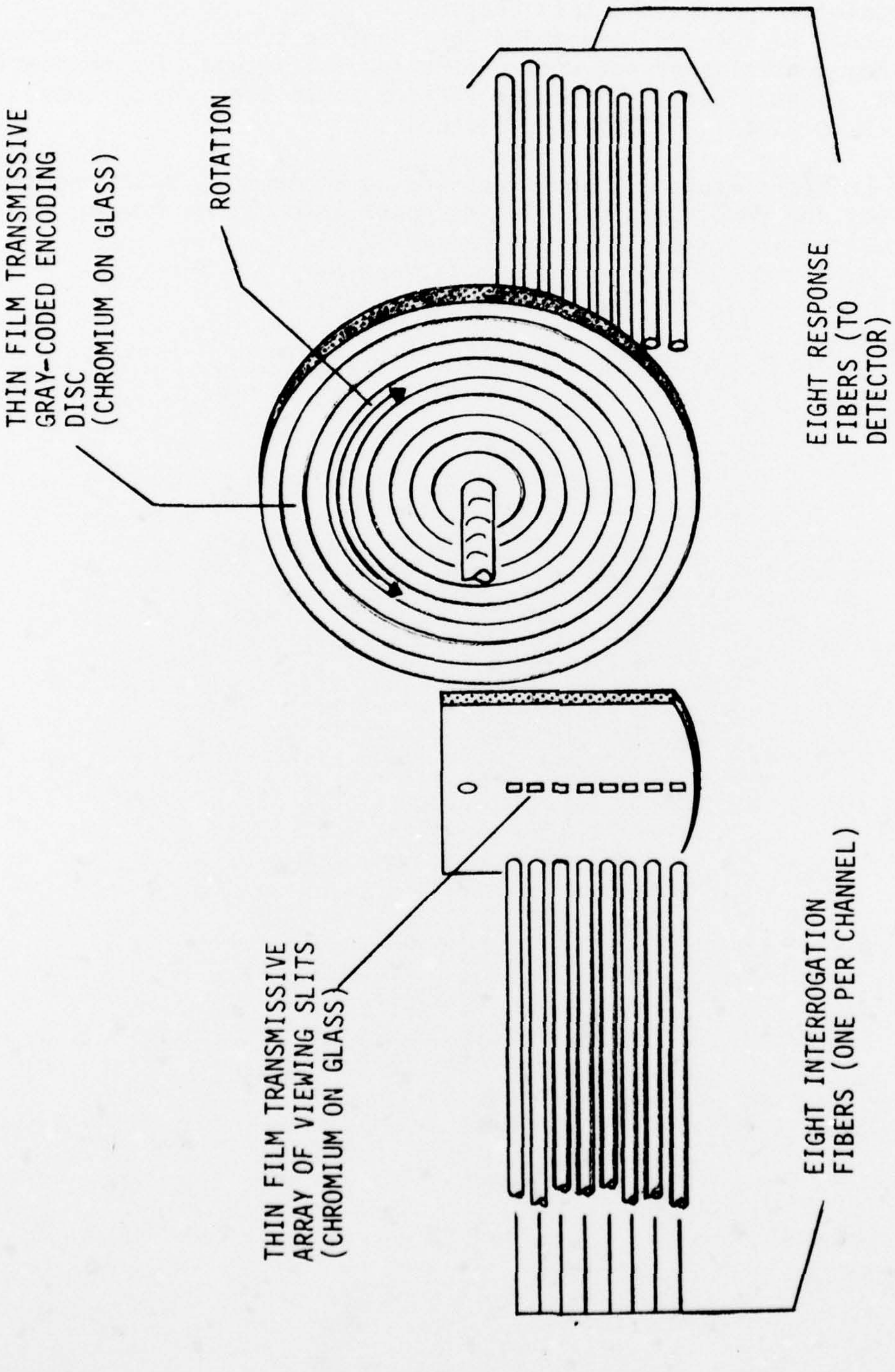

FIGURE 10.3.3

CONCEPTUAL SUBMINIATURE ANGULAR DISPLACEMENT SENSOR

The configuration of 10.3.3 shows the individual fibers arranged in a straight row. With such a scheme, low numerical aperture fibers would be required to minimize crosstalk within the viewing mask. The chromium on the two patterns would be face-to-face and light from one fiber could conceivably divert to an adjacent slit if not well controlled. It would also be possible to displace the eight fibers in a rotary fashion about the axis by some amount so as to completely isolate the channels.

High radiance emitters would also be suggested in conjunction with the single fibers to ensure the coupling of sufficient power through the system.

11.0 CONCLUSIONS AND RECOMMENDATIONS

11.1 GENERAL

All sensors investigated during this effort require that the response signal amplitude exceed a threshold value at the receiver in order to cause a change of binary state. This feature makes all of the devices vulnerable to changes in interrogation amplitude, fiber optic cable losses, sensor insertion losses, and receiver sensitivity.

Reliable field application of sensors employing these exact principles would require that the sensors either offfer extremely high on/off power ratios (so that threshold level would not be critical), or that tight tolerances be maintained on all of the parameters which affect the received signal power. It is felt that work needs to be done to maximize the on/off power ratios of these sensors. Alternate methods which place the data output signals elsewhere than in the pure amplitude domain should also be investigated as a possible solution to the problem. Frequency-shift keying, phase-shift keying, optical wavelength keying and correlation techniques --- or their equivalents --- should all be considered as possibilities.

High-radiance emitters and single-fiber transmission lines should be considered for many reasons. Increased signal power, reduced sensor size, improved signal uniformity, improved resolution, reduced cable size and weight and simplified sensor fabrication techniques are just a few of the advantages.

Any future effort should initially establish a fiber optic cable type and then proceed to design a prototype connector for the application --- possibly one with a circular array of interrogation fibers surrounding a core of response fiber(s). A circular array of emitters on a single header would provide an ideal interface for such a connector. Emitters with pigtail terminations could be considered an interim solution. The connector should preferably be small enough to be used also on the sensor itself.

11.2 FUEL (LIQUID) LEVEL

Alternate forms of sensor elements should be investigated in more detail for increased ruggednesss and reliability. Materials other than glass should be investigated for wetting properties. An experimental model designed for a specific application should be flight-tested in parallel with a conventional sensor to determine possible unforseen problems in a flight environment.

11.3 LINEAR DISPLACEMENT AND STRAIN

Alternate approaches should be investigated which might offfer sufficient sensitivity to be considered truly a "strain" sensor. Several alternate approaches have been considered but detailed investigation has been beyond the scope of this study.

11.3 TEMPERATURE AND PRESSURE

Sensors using dedicated "strain"-sensing elements which emphasize low friction

and low hysteresis should be built and tested to determine what performance and ranges can actually by realized under these conditions. Eventually, the design and fabrication of a complete air data or engine data package for flight evaluation would probably be a worthwhile effort.

11.4 EVENT COUNTING

The application of the optical probe as a means for measuring vibration, shaft runout, turbine blade irregularities and other incipient failure phenomena should be considered.

REFERENCES

1. "Electron Beam Pattern Generation," Nelson C. Yew, Industrial Research, Sept. 1976, Pg. 92.

2. "Fabrication Techniques for Surface Acoustic Waves and Thin-Film Optical Devices," Henry I. Smith, IEEE Journal, Oct. 1974, Pg. 1361.

3. "The Diffraction of Waves by Ribbons and by Slits," Philip M. Morse and Pearl J. Rubenstein, Physical Review, Dec. 1938, Pg. 895.

4. "Formulas for Stress and Strain," Raymond J. Roark, McGraw-Hill, New York, 1965.

5. "Materials Handbook," George S. Brady, McGraw-Hill, New York, 1971.

6. "Handbook of Engineering Fundamentals," Ovid W. Eshbach, Wiley, New York, 1975.